Silesian University of Technology

Degradation of selected drug used in COVID-19 therapy in the aquatic environment by means of solar light driven processes

By Humam Ahmed, M. Sc., M.Phil.

Supervisor: Prof. dr hab. inż. Ewa Felis

Doctoral Thesis in discipline “Environmental engineering, mining and energy”

Silesian University of Technology

Faculty of Energy and Environmental Engineering

Department of Environmental Biotechnology

Gliwice, Poland, 2025

Polish Title:

Degradacja wybranych leków stosowanych w terapii COVID-19 w środowisku wodnym za pomocą procesów inicjowanych światłem słonecznym

Keywords in Polish

Leki stosowane w terapii COVID-19, mikrozanieczyszczenia antropogeniczne, środowisko wodne, fotodegradacja, procesy inicjowane światłem słonecznym

Keywords in English

Drugs used in COVID-19 therapy, anthropogenic micropollutants, aquatic environment, photodegradation, solar light driven processes.

Dedicated to:

My Father, my support

My Mother, my strength

And

My Siblings, my power

PREFACE

This thesis is submitted as the fulfilment of the requirements for the degree “Doctor of Philosophy” at the Silesian University of Technology (SUT), Gliwice, Poland. The work was carried out at the Faculty of Energy and Environmental Engineering at the Department of Environmental Biotechnology, with Professor Ewa Felis as supervisor.

This work has been financed by the BKM i.e., the competition for funding research tasks for young scientists (RIE-7) research project funded by the Ministry of Science and Higher Education in Poland, for maintaining and developing research potential with the following grant numbers:

i. BKM-688/RIE7/2022 (08/070/BKM22/0018)
ii. BKM-664/RIE7/2023 (08/070/BKM23/0028)
iii. BKM-717/RIE7/2024 (08/070/BKM24/0035)

The author also expresses her gratitude for providing financial support.

Table of Contents

ACRONYMS……...……..9-11

Abstract……..12

Abstract in Polish……...…13

1. Chapter 1 – Literature Review…….……..…….... 14-28

1.1 Introduction……..... 14

1.2 Antivirals drugs – an emerging pollutants in aquatic environment…….…... 15

1.3 Advance Oxidation Process (AOPs)……...… 19

1.4 Mechanism of AOPs……..……. 20

1.5 Environmental benefits of AOPs……...…….. 21

1.6 Environmental disadvantages of AOPs……..…… 22

1.7 Mitigation Strategies for the Environmental Drawbacks of AOPs……..….... 22

1.8 Sustainable development goals (SDGs) impacted by AOPs ……..……..…23

1.9 Drugs used in this study……..……..... 24

1.9.1. Isoprinosine……..24

1.9.2. Ritonavir……..25

1.9.3. Remdesivir……..27

2. Chapter 2 – Research hypothesis, purpose and scope of thesis ...…….. 29 - 32

2.1 Hypothesis……..29

2.2 Scientific problem needs to be solved……....29

2.2.1. Effect of water matrices on degradation efficiency……..29

2.2.2. Optimization of photocatalytic conditions……..29

2.2.3. Degradation Kinetics and Mechanistic Understanding ……..30

2.3 Main goal of the research ……..…….....30

2.4 Specific aims and objectives of the study ……..……..…30

2.5 Scope of the thesis……...31

3. Chapter 3 – Materials and Methodology…….……... 33 - 45

3.1 Materials and chemicals…….……..…..33

3.2 Water matrices……..……..... 33

3.3 Experimental Methodology……..…….. 35

3.3.1. Preparation of standard solution of drugs used……..35

3.3.2. Determination of absorption maxima……..35

3.3.3 Preparation of calibration curve ……..36

3.3.4. Description of solar light reactor……38
3.3.5. Photolytic Studies……39
3.3.5.1. For Isoprinosine (IPN)……39
3.3.5.2. For Ritonavir (RTR)……39
3.3.5.3 For Remdesivir (REM)……40
3.3.6. Photocatalytic Studies……40
3.3.6.1. For Isoprinosine (IPN)……40
3.3.6.2. For Ritonavir (RTR)……40
3.3.6.3 For Remdesivir (REM)……41
3.3.7. Photodegradation assisted with H_2O_2 studies……41
3.3.8. Quantification method……41
3.3.9. Sorption studies ……42
3.3.10. Anion Profiling in Milli-Q, Tap, and Surface Waters via Ion Chromatography……42
3.3.11. Kinetic studies……43
4. Chapter – 4 Results and Discussion…….……..…..... 46 - 89
4.1 Results and discussion..……..46
4.1.1. Ion profiling of selected water matrices……46
4.1.2. Photolysis with sunlight ……49
4.1.3. Photocatalysis experiments ……54
4.1.3.1. Photocatalytic removal of isoprinosine ……..…..…… 54
4.1.3.2. Photocatalytic removal of ritonavir…….. 59
4.1.3.3. Photocatalytic removal of remdesivir……..….63
4.1.4. Sorption tests……69
4.1.5. Photolysis assisted with H_2O_2 ……74
4.1.6. Photocatalytic degradation of isoprinosine in the presence of selected anions ……70
4.1.6.1. Effect of SO_4^{-2} ions on degradation of IPN..……..... 70
4.1.6.2. Effect of Cl^- ions on degradation of IPN …..…….. 80
4.1.6.3. Effect of NO_3^- ions on degradation of IPN ……..…... 83
4.1.6.4. Effect of CO_3^{-2} ions on degradation of IPN ……... 84
4.1.7. Adsorption of RTR in the presence of selected anions ……..…....86
4.1.8. Solar-induced mineralization of organic matter in selected water samples……86

5. Chapter 5 – Summary and Conclusion……..…… 90 - 94

5.1 Summary…….…….90

5.1.1. Research contributions…….. 90

5.1.2. Key contributions..…….. 90

5.2 Conclusion……. 92

5.3 Novelty Statement……..…… 94

6. Chapter 6 – Future Research Direction……..... 95

6.1 Future work and recommendations…….……... 95

7. Chapter 7 – References……...…….....… 96 - 108

8. Chapter 8 – Supporting Information ……..… 109 - 126

9. List of Figures……..…….127

10. List of Tables……129

11. List of Publications…….....130

12. List of other scientific activities……...131

ACRONYMS

IPN – Isoprinosine

RTR – Ritonavir

REM – Remdesivir

MQW – Milli-Q Water

TW – Tap water

SW – Surface water

WWTPs – Wastewater Treatment Plants

AOPs – Advance Oxidation Processes

ACN – Acetonitrile

UV-HPLC – Ultraviolet High Performance Liquid Chromatography

TiO_2 – Titanium dioxide

ZnO – Zinc oxide

SnO_2 – Tin oxide

Ag-TiO_2 – Silver titanate

ZrO_2 – Zirconium dioxide

$BaTiO_3$ – Barium titanate

$BaWO_4$ – Barium tungstate

NaCl – Sodium chloride

Na_2SO_4 – Sodium sulfate

$CaCO_3$ – Calcium carbonate

$NaNO_3$ – Sodium nitrate

H_2O_2 – Hydrogen peroxide

Na_2CO_3 – Sodium Carbonate

HOCl – Hypochlorous acid

ClO^- – Hypochlorite/ Chloroxide

FA – Formic acid

DMSO – Dimethyl sulfoxide

IBP – Ibuprofen

TC – Tetracycline

pH – Power of Hydrogen

FDA – Food and Drug Administration

UNO – United Nation Organization

SDGs – Sustainable development goals

WHO – World Health Organization

HPTLC – High Performance Thin Layer Chromatography

HIV – Human immunodeficiency virus

COVID – Coronavirus disease

SARS-CoV-2 – Severe acute respiratory syndrome coronavirus 2

DNA – Deoxyribonucleic acid

LOMO – Lowest unoccupied molecular orbital

HOMO – Highest occupied molecular orbital

COD – Chemical oxygen demand

BOD – Biological oxidation demand

POPs – Persistent organic pollutants

LOQ – Limit of quantification

LOD – Limit of detection

PEC – Predicted environmental concentration

FTIR – Fourier Transform infrared spectroscopy

XPS – X-ray photoelectron spectroscopy

XRD – X-ray Diffraction

NMR – Nuclear magnetic resonance

UV – Ultra Violate

EU – European Union

OCT – Over the counter

B.S.T. – Black Standard Thermometer

rpm – Revolutions per minute

nm – Nanometer

RT – Retention time

KL – Langmuir constant

SSE – Sum of Squared Error

TOC – Total organic carbon

TC – Total Carbon

NPOC – Non-Purgeable Organic Carbon

TN – Total Nitrogen

TIC – Total Inorganic Carbon

IC – Ion chromatography

IUPAC – International Union of Pure and Applied Chemistry

DOM – Dissolved organic matter

Abstract

The outbreak of the COVID-19 pandemic in 2019 resulted in a substantial rise in the global use of pharmaceutical compounds, particularly antivirals used or repurposed for the treatment of the disease. During the early phase, no specific drugs were available for COVID-19 therapy, leading to the off-label use of existing medications, while later the accelerated development and approval of new antiviral agents raised concerns regarding their environmental persistence and fate. This doctoral research focused on investigating the solar-light-driven degradation of selected antiviral compounds such as isoprinosine (IPN), ritonavir (RTR), and remdesivir (REM) in aquatic environment. The study examined direct photolysis, photocatalytic processes, and H_2O_2-assisted photolysis under simulated solar irradiation to evaluate the effects of environmental and operational parameters such as water composition, light intensity, catalyst dosage, pollutant concentration, and reaction time on degradation efficiency. Experiments were conducted using three different water matrices; Milli-Q, tap, and surface water to simulate real environmental conditions. Various photocatalysts, including TiO_2 P25, ZnO, SnO_2, Ag–TiO_2, and the composite SnO_2:ZnO system, were tested to compare their degradation efficiency. The results showed that direct photolysis alone was largely ineffective due to the structural stability and low solar absorptivity of the studied compounds, whereas photocatalytic and H_2O_2-assisted processes significantly enhanced degradation rates. Among the catalysts, TiO_2 P25 and SnO_2:ZnO composites exhibited the highest photocatalytic activity under solar irradiation. The study further evaluated the role of water matrix components and specific anions such as Cl^-, SO_4^{2-}, and HCO^- in modulating the degradation process and assesses the applicability of sunlight-activated photocatalysis as a sustainable method for environmental purposes. Kinetic studies indicated that the degradation of IPN followed pseudo-first-order kinetics, RTR fitted the Langmuir–Hinshelwood adsorption model, and REM followed a two-phase adsorption–desorption dynamic model. The study demonstrated that water matrix composition and catalyst dosage strongly influenced overall degradation efficiency. These findings confirm that solar-assisted photocatalysis represents a sustainable and energy-efficient approach for mitigating antiviral contamination, offering novel insights into the environmental behavior and removal mechanisms of COVID-19-related pharmaceuticals in aquatic systems.

Streszczenie po polsku

Wybuch pandemii COVID-19 w 2019 roku spowodował znaczny wzrost globalnego zużycia farmaceutyków, zwłaszcza leków przeciwwirusowych lub ich modyfikacji w leczeniu tej choroby. We wczesnej fazie pandemii, nie było dostępnych celowanych leków do terapii COVID-19, co doprowadziło do stosowania istniejących już leków (w tym przeciwwirusowych), a później przyspieszony rozwój i zatwierdzanie nowych leków przeciwwirusowych. Wzbudziło to też obawy dotyczące ich trwałości i dalszych losów w środowisku. Eksperymenty w niniejszej pracy doktorskiej koncentrowały się na badaniu możliwej degradacji wybranych związków przeciwwirusowych, takich jak izoprynozyna (IPN), rytonawir (RTR) i remdesiwir (REM), pod wpływem światła słonecznego, w środowisku wodnym. W pracy analizowano fotolizę bezpośrednią, procesy fotokatalityczne oraz fotolizę wspomaganą H_2O_2 w warunkach symulowanego promieniowania słonecznego, aby ocenić wpływ parametrów środowiskowych i procesowych, takich jak: skład wody, natężenie światła, dawka katalizatora, stężenie zanieczyszczeń i czas reakcji, na efektywność procesu fotodegradacji tych leków. Eksperymenty prowadzono z użyciem trzech różnych matryc wodnych: wody super czystej, tzw. Milli-Q, wody wodociągowej i powierzchniowej, aby symulować rzeczywiste warunki środowiskowe. Przetestowano różne fotokatalizatory, w tym TiO_2 P25, ZnO, SnO_2, Ag–TiO_2 oraz kompozytowy układ SnO_2:ZnO, aby porównać ich efektywność w kontekście fotodegradacji badanych leków. Wyniki wykazały, że bezpośrednia fotoliza była w dużej mierze nieskuteczna ze względu na stabilność i niską absorpcję światła słonecznego przez badane leki, podczas gdy procesy fotokatalityczne i wspomagane H_2O_2 znacząco zwiększyły wydajność procesów fotodegradacji. Spośród badanych fotokatalizatorów, to TiO_2 P25 i SnO_2:ZnO wykazały najwyższą aktywność fotokatalityczną w świetle słonecznym. W badaniach oceniono dodatkowo wpływ składników matrycy wodnej i anionów, takich jak: Cl^-, SO_4^{2-} i HCO^- na efektywność wspomnianych procesów, a także oceniono przydatność fotokatalizy aktywowanej światłem słonecznym jako zrównoważonej metody w zastosowaniach środowiskowych. Wykazano także, że degradacja IPN przebiegała zgodnie z równaniem reakcji pseudopierwszego rzędu, usuwanie RTR zachodziło zgodnie z modelem Langmuira-Hinshelwooda, a usuwanie REM można było opisać dwufazowym dynamicznym modelem adsorpcji i desorpcji. Badania wykazały, skład matrycy wodnej i dawka katalizatora znacząco wpływały na ogólną efektywność degradacji badanych leków za pomocą światła słonecznego. Odkrycia te potwierdzają, że fotokataliza inicjowana światłem słonecznym stanowi zrównoważone i energooszczędne podejście do ograniczania skażenia środowiska lekami przeciwwirusowymi, oferując nowe spojrzenie na możliwości usuwania leków stosowanych w leczeniu COVID-19 w szeroko pojętym środowisku wodnym.

Chapter 1- Literature Review

1.1 Introduction

Water supports life and is a vital resource for living organisms. It plays a key role in maintaining ecological balance and fostering the well-being of people and industrial activities. The Earth is made up of approximately 71% water and serves multiple purposes such as agricultural production, industrial and domestic use, as well as energy generation (Igor A. Shiklomanov, 2000; Jha & Schmidt, 2021). In addition, water also serves as a critical driver of social and cultural innovations and is globally recognized as symbol of rejuvenation and growth (Anderson et al., 2019; Emile et al., 2022).

Even though water stands as one of the most abundant resources on this planet. However, fresh, clean, and drinkable water continues to grow as a limited resource. Roughly 2.5% of the water on Earth is freshwater, and about 69% of freshwater is in glaciers and icebergs (Singh & Narayan, 2023). Water pollution caused by over-population, climate change, and unsustainable practices worldwide poses a significant threat to freshwater resources, further challenging its management and thus affecting public health and the ecosystem (Issakhov et al., 2021; Y. Liu et al., 2021).

One of the potential sources of water pollution is effluent from dye and pharmaceutical industries, hospital and households. With the COVID-19 pandemic, there has been an increased reliance on drugs to treat the disease, which has led to large amounts of these drugs entering the water bodies either in their original form or partially broken down (H. Ahmed & Felis, 2023; Biswas et al., 2021; Gwenzi, Selvasembian, & Offiong, 2022; Swati et al., 2011). Even though the pandemic is over, experts believe the SARS-CoV-2 virus has become endemic and will constantly be a need for these drugs as they continue to have periodic effects, like the flu, indicates that the community must get used to living with the virus forever (Sawicka et al., 2022). Moreover, the treatments for the infection will always be in demand, leading to the continuous release of these drugs into the environment.

Therefore, the treatment of pharmaceutical pollutants like antivirals, antibiotics, or even anti-inflammatories in the aquatic environment is uppermost because the world continues to experience a dire issue of having access to safe drinking water and proper sanitation (Eryildiz, Yavuzturk Gul, et al., 2022; Pal et al., 2022; Silva et al., 2022). As it is, these and other factors are linked to universal development targets and meeting the need for equity

(Obaideen et al., 2022). The economic value of water is significantly higher than its current usage. It includes measures to increase and sustain food supply, stimulate economic development, improve public health, and tackle environmental problems (Dawood et al., 2021). Also, it is essential to understand the importance of water in constructing a sustainable future by solving water-related problems through good management and innovative approaches. Therefore, searching for new solutions or improvement of already existing in the field of improving water quality or techniques for its purification in terms of drug residues, while meeting the criteria of sustainable development, seems to be crucial for the entire society.

1.2 Antiviral drugs – an emerging pollutants in aquatic environment

The frequent use of antiviral drugs in human and veterinary medicine is one of the main contributors to their presence in the environment, especially in aquatic environments (Ncube et al., 2018; Vardanyan & Hruby, 2016; R. Wang et al., 2023). These drugs are used to treat viral infections, such as influenza, HIV, hepatitis, and COVID-19 (Frediansyah et al., 2021; Tompa et al., 2021). Nonetheless, their resistance and incomplete removal in traditional wastewater treatment plants (WWTPs) make them significant environmental contaminants (Yao et al., 2021). Therefore, their presence in water bodies poses serious threats to the environment, health and development of living organisms.

Although numerous studies have examined the occurrence and fate of pharmaceuticals in the aquatic environment, most of this research has focused on commonly used drugs such as antibiotics, analgesics, and anti-inflammatory agents and others (H. Ahmed & Felis, 2023a; Heberer, 2002; Mansouri et al., 2021a). However, antiviral drugs particularly those introduced or extensively used during the COVID-19 pandemic remain far less studied. Data on their environmental concentrations, persistence, and degradation pathways are still limited, and their potential ecological and human health impacts are not fully understood. Table 1 presents the reported concentrations of various antiviral drugs detected in broadly understood aquatic environment. These data highlight the persistence of antiviral compounds, including those used in the treatment of COVID-19, in surface water, wastewater, and groundwater systems across several regions.

Table.1. Reported concentrations of drugs in the broadly understood aquatic environment

Drugs	Therapeutic use	Water matrix	Concentration	Region	References
Remdesivir	COVID-19	Wastewater/ river water	8.0 - 90 ng/L	USA/ Spain	(Voigt & Jaeger, 2025)
Favipirivir		Wastewater	24 – 97 µg/L	Turkey	(Eryildiz-Yesir et al., 2024)
Lopinavir	Antiretroviral (HIV/COVID-19)	Wastewater	28 – 140 ng/L	Spain	(Domingo-Echaburu et al., 2022a)
Ritonavir		Surface water	58 – 92 ng/L	Spain	(Domínguez-García et al., 2023)
Azithromycin	Antibiotic/COVID-19 supported therapy	Wastewater/ surface water	145 – 188 µg/L	India	(Kalugendo et al., 2025)
Chloroquine	Antimalarial/ COVID-19 supported therapy	Surface water	22 – 87 ng/L	Nigeria	(Morales-Paredes et al., 2022)
Hydroxychloroquine		River water	35 – 150 ng/L	India	(Srivastava & Reddy, 2022)
Ribavirin	Antiviral (Hepatitis, COVID-19 candidate)	Waste water	98 – 314 ng/L	China	(Q. Liu et al., 2022)
Oseltamivir	Antiviral (Influenza, sometime used in COVID-19	River water/ sewage discharge	12.0 – 290 ng/L	Japan	(Ghosh et al., 2010)

Antiviral drugs enter the aquatic environment through several pathways (Figure 1), including domestic wastewater, hospital effluents, pharmaceutical industry discharges, and

agricultural runoff (Heberer, 2002; Nannou et al., 2020; K. Wang et al., 2021). It has been studied that antiviral drugs undergo physical, biological and chemical changes in the aquatic environment. These drugs and their metabolites enter the water via urine and faeces of the patients in hospitals and day care centres, and these pollutants are persistently resilient to degradation (Choudhury et al., 2024; Thi et al., 2021).

The behaviour and fate of antiviral drugs on environment based on several factors: for example, bioaccumulation, sorption to sediments, persistency and degradation pathways (P. Gupta & Rani, 2024). According to the reported research, the antiviral drugs such as oseltamivir, acyclovir and remdesivir used to treat influenza, herpes infection and COVID-19, respectively, are particularly resistant to degradation and have been detected in both surface and groundwater due to their stability (H. Ahmed & Felis, 2023b; Gwenzi, Selvasembian, Offiong, et al., 2022). Another study reported that some antiviral drugs can degrade through photodegradation i.e. sunlight exposure, hydrolysis and microbial action (Jaya P. Ambhore et al., 2021; R. Wang et al., 2024). In some cases, antiviral drugs bind to sediments or organic matter in aquatic environments, extending their environmental impact.

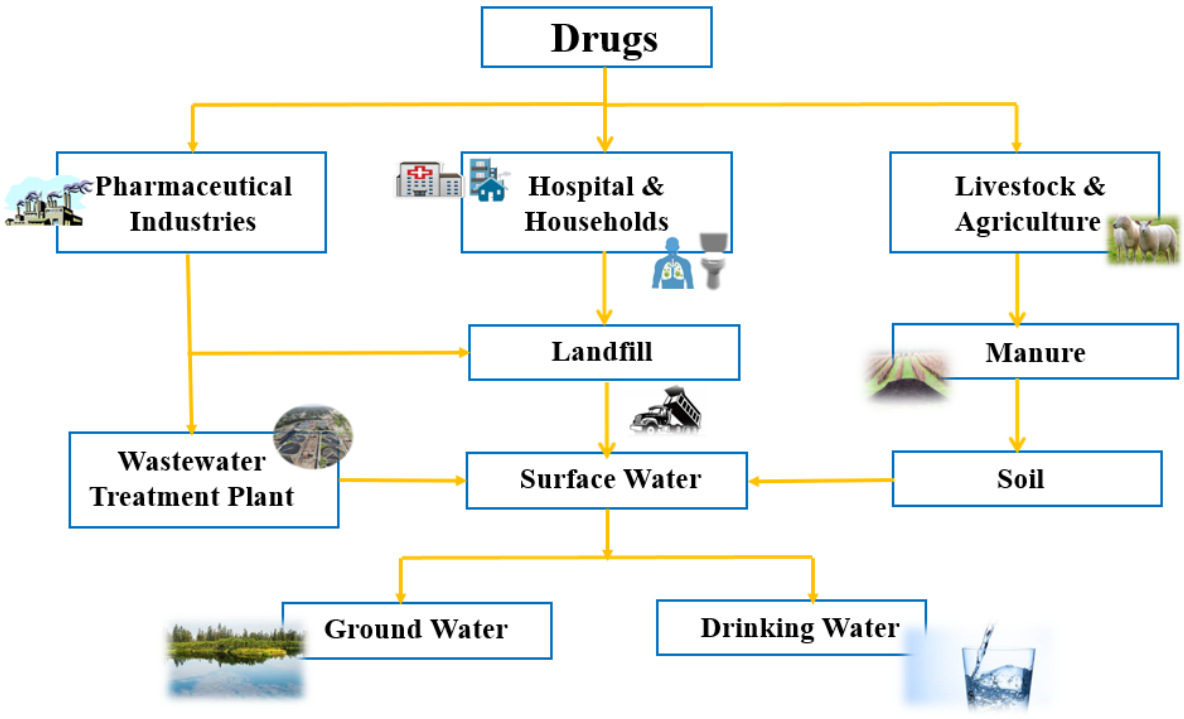

Figure 1. Routes of drugs release into the aquatic environment

Antiviral drugs in water bodies not only poses serious consequences to public health but also to the aquatic ecosystems. It can affect the growth, reproduction, and metabolism of aquatic organisms such as fish, invertebrates, and algae at low levels. Also, they can accumulate in fish, algae, and other aquatic organisms, potentially disrupting their biological functions. According to the reported research, ribavirin and ritonavir (RTR) both shows acute toxicity in *B. calyciflorus* (11.3 mg/L) and in *C. dubia* (2.0 mg/L), respectively. The oxidative stress and DNA damage caused by RTR and ribavirin in *C. dubia* was found to be 0.001 µg/L and1.0 µg/L respectively (Nugnes et al., 2024).

Similarly, antiviral drugs may also influence the important microbial populations in aquatic environment which is essential for maintaining ecosystem balance. They can participate in the growth of drug-resistance microorganisms, i.e., viruses and bacteria, resulting in infections harder to treat in both humans and animals due to prolonged exposure. Researchers successfully isolated the antiviral-resistant *E.coli* and *B. cereus* mutants when exposed to Zidovudine antiviral drug used to treat HIV infection (Wallace et al., 2023). Ames mutagenicity test: an important bioassay for determining the mutagenic substances by exposing them to the bacteria was performed by the researcher and results showed that TA 100 strain of *S. typhimurium* bacterial exhibited positive response to lamivudine (Omotola et al., 2021). In contrast to potential human health risks, the detected concentrations in drinking water are usually low, and long-term exposure to antiviral residues raises concerns about chronic health effects (Papagiannaki et al., 2022).

There are several methods for removing drugs pollutants from aquatic environment, including conventional water treatment processes such as coagulation, flocculation, sedimentation, sand filtration, disinfection, fluoridation, activated carbon treatment, and reverse osmosis (Bera et al., 2022; Chai et al., 2021; S. Gupta et al., 2024; Hong & Editors, 2021.; Qiu et al., 2022). These traditional techniques are effective in eliminating solids, organic matter, and sometimes nutrients, they often fall short in efficiently removing various types of anthropogenic micropollutants. To tackle the issue of drug contaminants in aquatic environments, advanced techniques, such as advanced oxidation processes (AOPs), are increasingly being adopted.

1.3 Advanced Oxidation Processes

The degradation of drug pollutants by advanced oxidation processes (AOPs) has gained popularity in the discipline of research in environmental science, especially water treatment (Dong et al., 2022). Antiviral drugs, which are commonly used to battle viral infections like influenza, HIV, hepatitis, and, more recently, COVID-19, have in the recent past been detected as micropollutants in water bodies such as surface water, groundwater, and wastewater (Domingo-Echaburu et al., 2022b; Eryildiz, Ozgun, et al., 2022). These drugs are released either as an unchanged substance or as active metabolites and enter wastewater systems, where they stay longer because of the greater stability and resistance to conventional treatment techniques (Zinicovscaia, 2016). The appearance of these toxic anthropogenic materials in the environment is considered a major risk, such as the possible development of drug-resistant pathogens and exposure to harmful problems for aquatic ecosystems.

AOPs are reliable techniques for the degradation of complex and stable organic substances and consequently provide a feasible solution to relevant issues. These techniques can remove active pharmaceutical contaminants because they produce very reactive species, non-selective and easily generated powerful oxidizing agents, known as hydroxyl radicals (•OH), capable of converting these compounds into smaller, less hazardous molecules (Albiter et al., 2015; Zhou et al., 2015a; Zhu et al., 2019). Many types of techniques are demonstrated by AOPs such as UV-H_2O_2, Fenton process, ozonation, sonolysis, photolysis, photocatalysis, etc. (Figure 2). These methods are especially advantageous in pharmaceuticals, where they can attack a specific range of chemical structures with little selectivity (Priyadarshini et al., 2022).

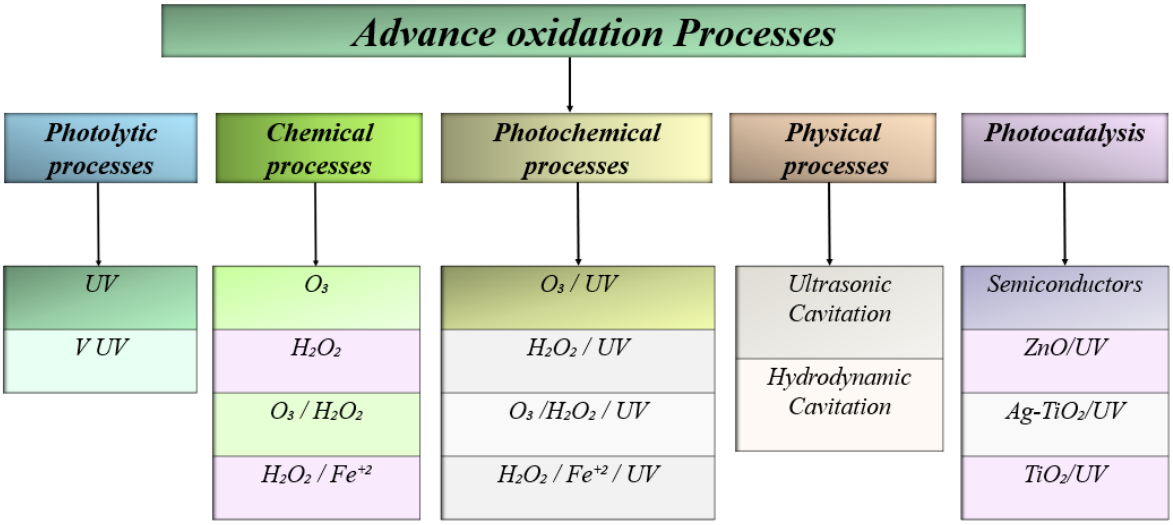

Figure 2. Selected types of AOPs

1.4 Mechanism of AOPs

This process that involves the formation of •OH ions; a reactive oxygen species for the treatment of organic pollutants such as drugs from the effluents. The key property of free radicals is their high redox potential which can easily oxidize pollutant molecules by reducing themselves (Jin et al., 2011; Miklos et al., 2018a, 2018b; J. M. Poyatos et al., 2009; Khan et al., 2023; Saravanan et al., 2022). These radicals are fundamental in initiating the AOPs. They are easily generated and non-selective and can mineralize toxic pollutants into harmless simple substances, such as carbon dioxide (CO_2) and water molecules (H_2O). The oxidation process initiated due to the presence of one unpaired electron, when the solar light is passed, and an electron transition occurs from LOMO to HOMO level. Hydroxyl radical ($HO^{\bullet}$), alkoxyl radical ($RO^{\bullet}$), superoxide anion radical ($O_2^{\bullet}$) are some examples of the radicals generated due to the electron transition in the presence of light source. Among these radicals, •OH is quick to react with organic contaminants. This attack involves the removal of hydrogen from the OH group to interact with different radicals by electron transfer. For example, with the help of oxygen molecules or electron transfer, peroxyl radicals ($RO_2^{\bullet}$) are formed. Results in the generation of intermediate species and the contamination is mineralized by making non-toxic by products (Coha et al., 2021; Giwa et al., 2021). For the reaction to occur the key point considered is the affinity of the organic compounds to the oxidant. Figure 3 represents the photocatalysis process as an example of AOPs.

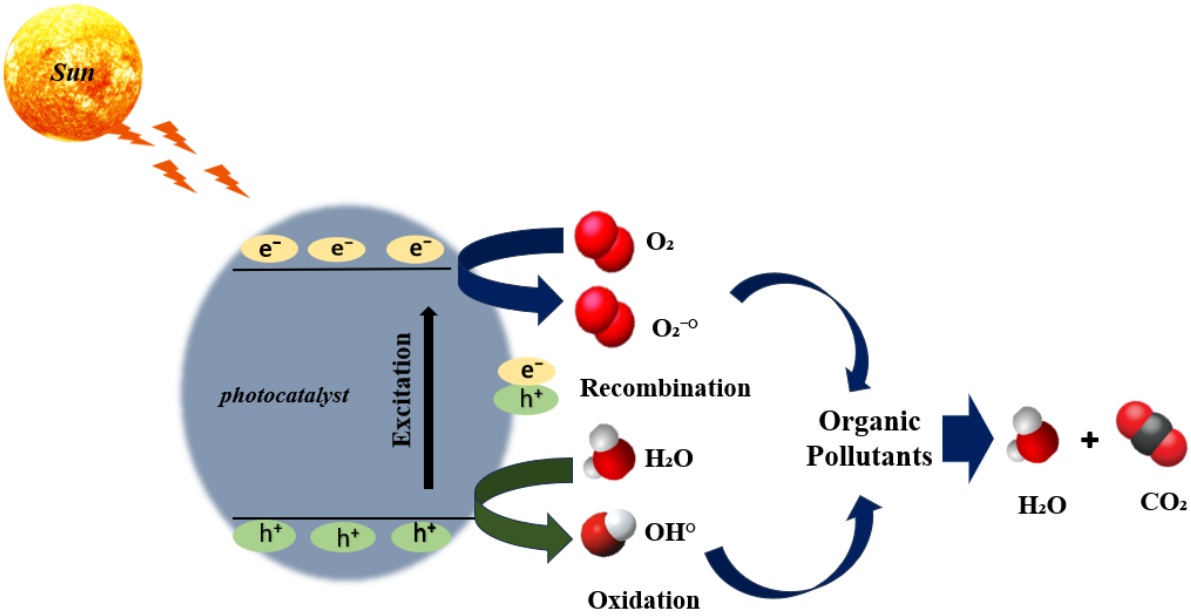

Figure 3. Mechanism of photocatalysis as an example of AOPs

1.5 Environmental benefits of AOPs

The importance of Advanced Oxidation Processes (AOPs) in the environment, especially in wastewater treatment, is tremendous. These are the processes, that are effective in the removal of persistent organic pollutants from water, which most often fail to be treated by traditional treatment methods. Removal of pollutants by AOPs leads to a decrease in chemical oxygen demand (COD) and biological oxygen demand (BOD) (Babu Ponnusami et al., 2023). These processes improve the drinking water quality by eliminating microorganisms, including viruses and bacteria, as well as other pathogens that might be present (Y. di Chen et al., 2021). Apart from improving water quality and reducing odour, these methods detoxify waste waters. They also reduce dependency on toxic disinfectants and reduce chemical coagulant requirement, which may create harmful by-products at the end of the treatment (Pandian et al., 2022).

AOPs have huge potential in utilizing wastewater for use in agricultural and industrial reused schemes, thus saving possible water resources, and are extremely environmental-friendly and sustainable as they use sources such as solar energy, ozone, hydrogen peroxide, or UV light, thereby minimizing dependence on fossil fuels (M'Arimi et al., 2020). Additionally, AOPs produce very little sludge or secondary waste, which makes them a low waste option for treatment. By improving wastewater treatment and reducing pollutants,

AOPs play a crucial role in combating climate change by preventing harmful greenhouse gas emissions, including methane released from untreated sewage (Kang et al., 2020a). They can also directly help to reduce nutrient runoff contributing to the harmful algal blooms and lessen their impact on climate change (Mohan et al., 2022).

1.6 Environmental Disadvantages of AOPs

Although AOPs are widely recognised for their outstanding ability to degrade persistent organic pollutants, their application presents several environmental drawbacks that limit their long-term sustainability. The generation of non-selective reactive oxygen species, while essential for the breakdown of contaminants, frequently results in the formation of intermediate oxidation products that may exhibit greater toxicity, mobility, or persistence than the original compounds (de Sousa Filho et al., 2019; J. Li et al., 2017; Shi et al., 2023). A prominent example is the formation of bromate, a potential carcinogen, during the ozonation of bromide-containing waters (Aljundi, 2011). Furthermore, many AOPs are characterised by high energy and chemical consumption, largely due to the continuous generation of oxidants such as H_2O_2 and O_3 and the dependence on UV irradiation (Dhamorikar et al., 2024). This dependence on intensive inputs contributes to an increased carbon footprint and resource depletion, which undermines their environmental efficiency (X. Chen et al., 2019; Kang et al., 2020b). Processes such as Fenton and photo-Fenton reactions also produce iron hydroxide sludge, creating challenges for disposal and posing risks of secondary contamination if not properly managed (Grassi et al., 2020; Kavitha & Palanivelu, 2004). Additionally, incomplete mineralisation can lead to the accumulation of partially oxidised intermediates that may interfere with downstream biological treatments (Garrido et al., 2007). Overall, these limitations underscore the need for a critical assessment of AOPs within a life-cycle perspective to ensure their application aligns with sustainable environmental management principles. However, these processes are very promising from the point of view of removing refractive compounds and anthropogenic pollution from the environment.

1.7 Mitigation Strategies for the Environmental Drawbacks of AOPs

To overcome the environmental challenges associated with AOPs, recent research has increasingly focused on developing more sustainable and integrated treatment approaches. The hybridisation of AOPs with biological or physicochemical processes has emerged as an

effective strategy, allowing for the partial oxidation of complex contaminants followed by microbial degradation of the resulting intermediates (Ganzenko et al., 2014; Nidheesh et al., 2022). This combination not only enhances overall treatment efficiency but also reduces energy consumption and toxic by-product formation. The adoption of green oxidants and catalysts, such as bio-derived H_2O_2 and natural mineral-based or carbon-doped heterogeneous catalysts, has further demonstrated promise in reducing sludge production and metal leaching (Matbiangthew Shadap & Sakunthala Ayyasamy, 2025). Moreover, the integration of renewable energy sources, including solar-driven photocatalysis and UV-assisted systems powered by photovoltaic energy, can substantially lower the operational carbon footprint of AOP applications (H. Ahmed et al., 2025a; Y. di Chen et al., 2021). Advances in process optimisation, through real-time monitoring, computational modelling, and control of radical generation efficiency, are also crucial in minimising reagent use and improving process selectivity. Ultimately, the transition towards sustainable AOP systems requires not only technological innovation but also the incorporation of life-cycle assessments, energy recovery mechanisms, and environmental risk evaluations (Omotola et al., 2021; Yang et al., 2024). Such an approach ensures that AOP implementation contributes meaningfully to the advancement of circular and low-impact water treatment technologies.

1.8 Sustainable development goals (SDGs) impacted by AOPs

The AOPs play an important role in achieving sustainable water management, pollution control, and climate resilience by degrading harmful contaminants. AOPs align with multiple UN SDGs and contribute to a healthier planet and a more sustainable future (United Nations, 2025). For example, SDG 6, which is related to *"Clean Water and Sanitation,"* entails that AOPs remove persistent organic pollutants (POPs), and pharmaceuticals that conventional treatment cannot handle, ensuring safe drinking water. They assist in wastewater treatment and reuse, reducing shortage of water and contamination, as well as preventing waterborne diseases by eliminating pathogens, bacteria, and viruses. AOPs are also connected to SDG 12 *"Responsible Consumption and Production"* which encourages sustainable water management by enabling wastewater reuse, reducing reliance on harmful chemicals in water treatment, and minimizing secondary waste production, making pollution control more efficient.

According to SDG 14: *"Life Below Water,"* AOPs prevent chemical pollution in oceans, rivers, and lakes by degrading harmful contaminants before discharge, reducing

eutrophication and algal blooms caused by nutrient-rich industrial wastewater, and protecting aquatic biodiversity from toxic pollutants and microplastics. In addition, they can also relate to SDG 13, which addresses *"Climate Action,"* dealing with the reduction of greenhouse gas emissions from untreated wastewater (e.g., methane from sewage), preventing environmental degradation that contributes to climate-related water crises, and supporting climate resilience by improving water security and quality, as well as with SDG 9 *"Industry, Innovation, and Infrastructure"* which promotes eco-friendly wastewater treatment technologies in industries, encourages innovation in green chemistry and sustainable engineering, and assists industries in meeting environmental regulations and reducing their ecological footprint.

1.9 Drugs used in this study

During the COVID-19 pandemic, several approved and unapproved drugs were used predominantly by hospitals, households, and healthcare units. Those drugs are either antiviral, antibacterial, or antifungal. The overuse of these drugs contaminates the water bodies. Later, the FDA approved some antiviral medicines to treat the COVID-19 infection: for example, isoprinosine (IPN), ritonavir (RTR), and remdesivir (REM). In this study, the photodegradation of the above-mentioned drugs has been assessed using Advanced Oxidation Processes (AOPs). Although some of the selected drugs did not receive clearly positive recommendations from FDA, the tests presented in the doctoral thesis were conducted during the pandemic and the short-post pandemic period, therefore drugs that aroused particular interest of the FDA as drugs useful in the treatment of COVID-19 were tested.

1.9.1. Isoprinosine

Isoprinosine, known also as inosine pranobex, is an antiviral and immunostimulant drug. Although this drug is not an officially approved drug in the treatment of COVID-19, some physicians have recommended this drug for the treatment of COVID-19 in an outpatient setting, and additionally, some publications indicate the potential of this drug in the therapy of COVID-19 (Beran et al., 2021). It is legal in over 70 countries throughout the world. In many countries, inosine pranobex-based medications are only accessible on prescription; however, in Poland, these preparations are available over the counter (OTC). As a result of it, the consumption of IPN has increased significantly during the past few years. In the treatment of more severe cases, IPN was also used, although in combination with other

medications (Jayanthi et al., 2022). IPN residues that are not metabolized can end up in the environment, which could lead to anthropogenic contamination. Table 2 shows the properties of IPN used in this study.

Table.2. Physicochemical properties of Isoprinosine

	Physicochemical properties of selected drug
IUPAC name	4-acetamidobenzoic acid;9-[(2R,3R,4S,5R)-3,4-dihydroxy-5 -(hydroxymethyl)oxolan-2-yl]-1H-purin-6 one;1(dimethylamino)propan-2-ol
Molecular Formula	$C_{52}H_{78}N_{10}O_{17}$
Molecular mass	1115.5 g/mol
Formulation	A crystalline solid
Colour	White to Off-White
λ max	260 nm
Solubility	DMSO (Slightly Heated), Methanol (Slightly, Heated, Sonicated), Water (Slightly).
Structure	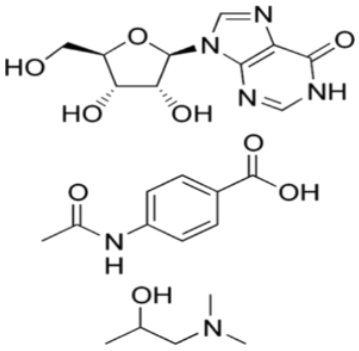

1.9.2. Ritonavir

Ritonavir (RTR) is an oral antiviral drug that has been found to be highly effective in treating COVID-19 when combined with other medications and approved for use in the EU (Vitiello & Ferrara, 2022). It is typically prescribed for individuals who do not require extra oxygen and are at a higher risk of developing severe COVID-19. In many countries including

Poland, RTR is only accessible on prescription. According to the guidelines, RTR has been proposed to be the best option for most eligible patients due to its therapeutic advantages, convenience of administration, and lower risk of side effects. In April 2022, the WHO first suggested RTR to treat COVID-19. Later, Pfizer created Paxlovid, an anti-COVID medication that contains a mixture of two antiviral agents, i.e. nirmatrelvir and ritonavir to treat COVID-19 (Steve Chaplin, 2022). Nevertheless, Paxlovid is unavailable for use as a test compound currently. Thus, RTR was chosen for this study to quantify its presence in the aquatic environment using processes driven by solar light. Table 3 shows the physicochemical properties of RTR used in this study.

Table.3. Physicochemical properties of Ritonavir

	Physicochemical properties of selected drug
IUPAC name	1,3-thiazol-5-ylmethyl *N*-[(2*S*,3*S*,5*S*)-3-hydroxy-5-[[(2*S*)-3-methyl-2-[[methyl-[(2-propan-2-yl-1,3-thiazol-4-yl)methyl]carbamoyl]amino]butanoyl]amino]-1,6-diphenylhexan-2-yl]carbamate
Molecular Formula	$C_{37}H_{48}N_6O_5S_2$
Molecular mass	720.9 g/mol
Formulation	A crystalline solid
Colour	White to light tan powder
λ max	248 nm
Solubility	Practically insoluble in water, Freely soluble in methanol and ethanol.
Structure	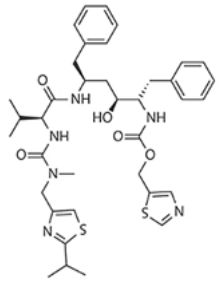

1.9.3. Remdesivir

Remdesivir (REM) is a broad-spectrum antiviral medication which is originally used to treat hepatitis C (Huda R. Taha et al., 2021). REM is the first treatment for COVID-19 to be approved by the US Food and Drug Administration (FDA). In November 2020, the FDA issued an emergency use authorization (EU) for the combination of baricitinib with REM, for the treatment of suspected or laboratory confirmed COVID-19 in hospitalized people two years of age or older requiring supplemental oxygen, invasive mechanical ventilation (A. B. Ahmed et al., 2022). In EU, REM is indicated for the treatment of COVID-19 in adults, who do not require supplemental oxygen and adolescents with pneumonia requiring supplemental oxygen and are at increased risk of progressing to severe COVID-19 (Alexandra Chera & Antoanela Tanca, 2022). The following are the properties of REM listed in Table 4.

Table.4. Physicochemical properties of Remdesivir

	Physicochemical properties of selected drug
IUPAC name	2-ethylbutyl (2*S*)-2-[[[(2*R*,3*S*,4*R*,5*R*)-5-(4-aminopyrrolo[2,1-f][1,2,4]triazin-7-yl)-5-cyano-3,4-dihydroxyoxolan-2-yl]methoxy-phenoxyphosphoryl]amino]propanoate.
Molecular Formula	$C_{27}H_{35}N_6O_8P$
Molecular mass	602.6 g/mol
Formulation	A crystalline solid
Colour	White powder
λ max	246 nm
Solubility	Practically insoluble in water, Freely soluble in methanol and ethanol.
Structure	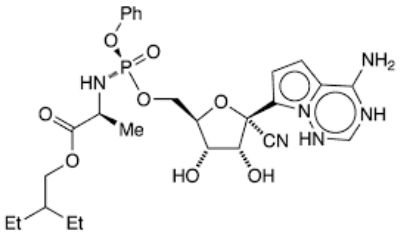

Chapter 2 - Research hypothesis, purpose and scope of thesis

2.1 Hypothesis

Taking into account the literature review from Chapter 1, the following research hypothesis was put forward:

> **H1.** The degradation efficiency of COVID-19-related pharmaceutical compounds in aquatic environments can be significantly enhanced through solar-light-driven photocatalysis, with performance strongly influenced by photocatalyst type, water matrix composition, and operational parameters.

2.2 Scientific problems need to be solved

According to the hypothesis as described above, the following scientific problems that need to be addressed:

2.2.1. Effect of water matrices on degradation efficiency.

Problem: The complexity of real water matrices (e.g. pH, ions) interferes with photocatalytic activity.

Research Question: How do specific matrix components (e.g., bicarbonates, chlorides, humic substances) affect the generation and activity of reactive species?

2.2.2. Optimization of photocatalytic conditions.

Problem: The effectiveness of photocatalytic degradation is influenced by several factors, such as pH, catalyst dosage, light intensity, and pollutant concentration, all of which must be optimized for each specific drug.

Research Question: Which photocatalyst (or combination) provides the highest efficiency for a given drug? What physicochemical properties (bandgap, surface area, crystallinity) correlate with activity?

2.2.3. Degradation Kinetics and Mechanistic Understanding

Problem: Lack of robust kinetic models that accurately describe photocatalytic degradation under environmental conditions.

Research Question: Which kinetic model best fits the observed degradation (e.g., pseudo-first-order, Langmuir-Hinshelwood, and others)?

Solving these problems will provide a comprehensive understanding of how to use solar-light-driven photocatalysis to degrade COVID-19-related drugs effectively in different aquatic environments.

2.3 Main goal of the research

The main goal of this research is to investigate the photodegradation behavior of selected COVID-19 pharmaceutical compounds in aquatic environments under sunlight and artificial light exposure, in the absence and presence of photocatalysts as substances supporting the degradation process of the tested drugs. The study aims to evaluate the effects of various environmental and operational parameters such as catalyst dosage, pollutant concentration, and water matrix composition on degradation efficiency. It further compares the photocatalytic performance of different catalysts (e.g., TiO_2, ZnO, SnO_2, Ag-TiO_2, and mixed systems like SnO_2:ZnO) and the degradation kinetics using appropriate kinetic models. Ultimately, the research seeks to advance understanding of solar light driven photocatalysis as an effective and sustainable approach for removing pharmaceutical pollutants from the aquatic environment.

2.4 Specific Aims and Objectives of the Study

To ensure environmental safety and sustainability in the removal of COVID-19 drugs, the specific aims and objectives of the study are outlined below:

i. To assess the susceptibility to degradation of selected drugs used in the treatment of COVID-19 in the broadly understood aquatic environment, using processes initiated by (artificial) sunlight.

ii. To determine the impact of selected aquatic matrix parameters on the efficiency of degradation of these drugs.

iii. Study the impact of real water matrices (e.g., salts, organic matter, inorganic anions) on degradation efficiency.

iv. Assessment of the selected photocatalysts "as tools" supporting the decomposition of selected drugs in the aquatic environment by means of solar-light driven photocatalysis.

v. Investigate the influence of operational parameters such as catalyst dose, pollutant concentration, and reaction time.

vi. Comparing the performance of various photocatalysts (e.g., TiO_2, ZnO, SnO_2, Ag-TiO_2 etc.).

vii. To evaluate the degradation kinetics of selected drugs under varying photocatalytic conditions (e.g., pH, light intensity, catalyst dosage). Compare the degradation efficiencies of single photocatalysts with combined ones such as SnO_2:ZnO).

viii. Study the degradation efficiency of different pharmaceutical drugs under controlled laboratory conditions.

ix. Model the degradation kinetics using common models like first-order, pseudo-second-order, or Langmuir adsorption kinetics and others.

2.5 Scope of the Thesis

This thesis is structured into eight comprehensive chapters, each focusing on different aspects of the research.

Chapter One serves as an introductory overview, presenting an in-depth examination of the factors that impact the photocatalytic degradation of various antiviral drugs. It also outlines the broader literature review.

Chapter Two articulates the specific aims and objectives of the research, main goal of the research, detailing the hypotheses that guide the investigation. This chapter clarifies the significance of studying the degradation of antiviral drugs, particularly their widespread use

during the COVID-19 pandemic. It also outlines the scope of the thesis as well as the scientific problem derived from the aims and objectives.

Chapter Three provides a thorough explanation of the methodologies employed to investigate the degradation processes of selected antiviral drugs prescribed for COVID-19 treatment. This includes descriptions of the experimental setup, the photocatalytic techniques used, and the parameters measured during the degradation studies.

Chapter Four presents an extensive discussion and analysis of the results obtained from the experiments. It examines the effectiveness of different photocatalysts and conditions on the degradation rates of the antiviral drugs, interpreting the implications of these findings for both pharmaceutical and environmental applications.

Chapter Five marks the inspiring summary and conclusion of this research journey followed by novelty of the research.

Chapter Six opens the door to future directions of the research, paving the way for continued exploration and discovery.

Chapter Seven compiles a comprehensive list of references, ensuring that all sources cited throughout the thesis are properly acknowledged and provide readers with further resources for exploration.

Finally, ***Chapter Eight*** provides the screenshot of HPLC display as supporting information of this research.

Chapter 3 - Materials and Methodology

3.1 Materials and Chemicals

The following materials were used in this study: pure analytical standards of isoprinosine (IPN), ritonavir (RTR), and remdesivir (REM), (Cayman Chemicals, Poland); acetic acid and sodium acetate for an acetate buffer (pH 5.0); 99% formic acid; analytical grade acetonitrile (ACN); and methanol (POCH S.A., Poland). Additionally, 99.9% pure TiO_2 P25 supplied by (Degussa Germany), ZnO, SnO_2, ZrO_2, and $BaWO_4$ were utilized as commercial photocatalyst, along with the ionic compounds NaCl, Na_2SO_4, $CaCO_3$, and $NaNO_3$ were used as a source of anions, all of them were purchased from Sigma-Aldrich. $AgTiO_2$ and $BaTiO_3$ were synthesized in the laboratory and used as photocatalysts in this study. Finally, a 12% v/v solution of H_2O_2 was obtained from Avantor, Poland.

3.2 Water matrices

In this study, three types of water matrices were employed: Milli-Q water (MQW), tap water (TW), and surface water (SW). MQW was sourced from the Synergy® Water Purification System (Merck, Germany), demonstrating a resistivity of 18.2 MΩ·cm at 25 °C and a conductivity of ≤ 5 µS (Tang et al., 2024). MQW served as a reference matrix, providing an ideal and impurity-free medium to assess the intrinsic photocatalytic activity of each catalyst without external interference. TW samples were collected from the Biotechnology Centre at the Silesian University of Technology. It represents typical domestic or treated water containing moderate concentrations of dissolved salts and minerals, allowing assessment of the impact of common inorganic ions such as chloride, sulfate, calcium, and magnesium. SW samples were sourced from the Ostropka river in Gliwice during both the summer and winter seasons (Figure 4). It was used to simulate real environmental conditions where organic matter, suspended solids, and various ions are present. The selection of these three matrices enabled a comprehensive understanding of the degradation behavior of antiviral drugs under both controlled and environmentally relevant conditions.

a.  b. 

Figure 4. Ostropka river, a.) winter season, b.) summer season

The three water matrices used in this study differed in composition to represent a range of aquatic environments. The basic physicochemical characteristics of the three water matrices used in this study are summarized in Table 5. Milli-Q water (MQW) served as an impurity-free reference matrix, while tap water (TW) and surface water (SW) represented increasingly complex environments containing natural ions and organic matter.

Table.5. Physicochemical properties of selected water matrices

Parameter	Milli-Q water	Tap water	Surface water
Source/Origin	Merck Germany	SUT	Ostropka River
Resistivity/Conductivity	18.2 MΩ·cm/≤ 5 µS	500 – 600 µS. cm^{-1}	300 – 400 µS. cm^{-1}
pH	~7.0	7.2 – 7.5	6.8 – 7.2
Major Cations	–	Ca^{2+}, Mg^{2+}, Na^{+}	Ca^{2+}, Mg^{2+}, Na^{+}, K^{+}
Major Anions	–	Cl^{-}, SO_4^{2-}, HCO_3^{-}	Cl^{-}, SO_4^{2-}, NO_3^{-}, HCO_3^{-}
Organic matter content	–	Low	Moderate
Suspended solids	–	Negligible	Present
Purpose of study	Control matrix for ideal laboratory condition	Represented treated domestic water	Represented natural environmental condition

3.3 Experimental methodology

3.3.1. Preparation of standard solutions of drugs used

The standard solution of drug 2.0 mg/L of IPN prepared by dissolving 2.0 mg of IPN into 100 ml of MQ water, for RTR, about 4.0 mg/L of RTR dissolved into 1000 ml of MQ water, sonicated for 2 hours at 30 °C with 800 rpm and transferred to the volumetric flask and was stirred overnight to dissolve the compound. RTR partially dissolved in water. For REM, about 1.0 mg/L of REM dissolved in 10.0 ml methanol. All these solutions were labelled as stock and refrigerated for further use. To prepare the working solutions, 2.0 mg/L for IPN and RTR and 1.0 mg/L (REM) were prepared by diluting 200 mL standard solutions in MQW, TW, and SW, respectively, to appropriate concentrations immediately before use.

3.3.2. Determination of absorption maxima

To determine the λ max of the selected drugs IPN, RTR, and REM, wavelengths for each drug were measured using a UV/Vis spectrophotometer using stock solutions. The data showed that IPN exhibited maximum absorption at a wavelength of 260 nm, RTR at 248 nm, and REM at 246 nm, as illustrated in Figures 5a, 5b, and 5c, respectively. The UV–visible absorption spectra of each drug (10 mg/L) were measured under three storage conditions: freshly prepared, refrigerated, and frozen. The purpose was to assess the influence of storage conditions on their spectral properties. Remarkably, the spectra obtained under all three conditions exhibited identical absorption maxima, suggesting that storage temperature has no appreciable effect on the optical stability of the studied drugs.

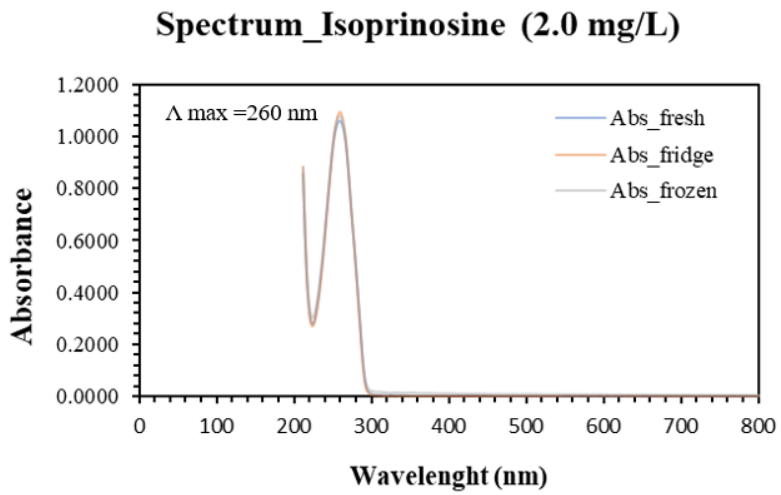

Figure. 5a. Spectrum of anti- COVID drug IPN

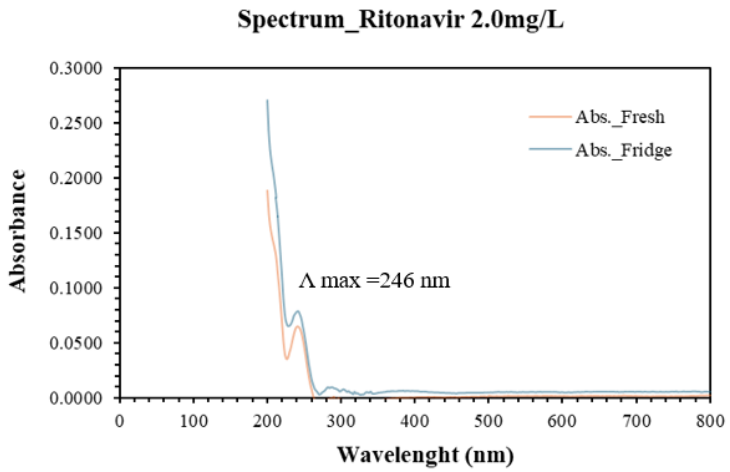

Figure. 5b. Spectrum of anti- COVID drug RTR

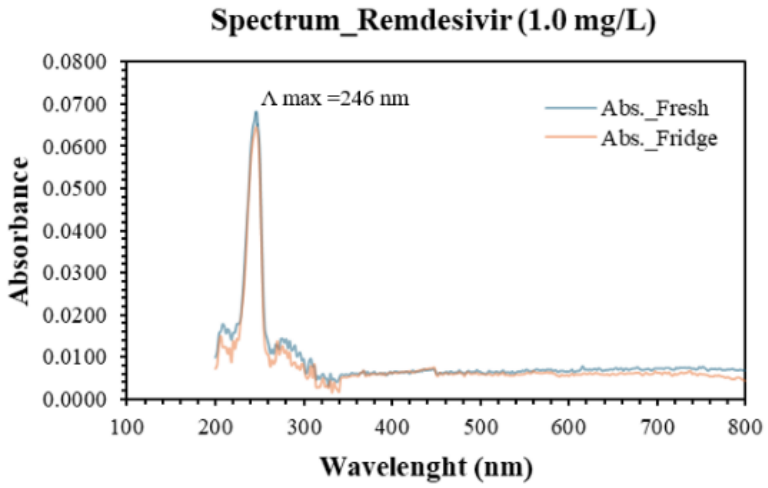

Figure. 5c. Spectrum of anti- COVID drug REM

3.3.3. Preparation of calibration curve

The solutions were prepared with precise known concentrations to create calibration curves for each drug. To prepared calibration curves, high performance liquid chromatography (HPLC) coupled with an ultraviolet light (UV) variable detector. (UltiMate 3000 system; Dionex Corporation, Sunnyvale, CA, USA) was employed. The samples were filtered by using MCEMF-Millipore® Membrane Filters with 0.22 µm pore size (Merck, Germany). The chromatographic separation was performed using a C18 Hypersil™ Gold column (250 mm x 4.6 mm; pore size: 5 mm) (Thermo Scientific, Polygen, Poland). For IPN, the mobile phase consisted of an ACN and MQ water in a ratio of 60:40 (v/v), in case of RTR, acetate

buffer (pH 5.0) and ACN in ratio of 30:70 (v\v), and for REM, ACN and 0.1% of formic acid solution (FA) in a ratio of 55:45 (v/v) with the retention time (RT) of IPN (5.0 ± 0.5 min), RTR (8.0 ± 0.5 min), and REM (9.0 ± 0.5 min) under the specified conditions. The limit of quantification (LOQ) of studied antiviral was equal to 0.2 mg/ L. It was established as the first lowest calibration point of their calibration curves (linear regression, $R^2 > 0.98$). The wavelength used for the analysis were 260, 248, and 246 nm for IPN, RTR, and REM, respectively. The data was evaluated using Dionex Chromeleon™ 6.8 software. Following curves illustrate the concentration-response relationship and are shown in Figures 6a, 6b, and 6c, each corresponding to a specific drug.

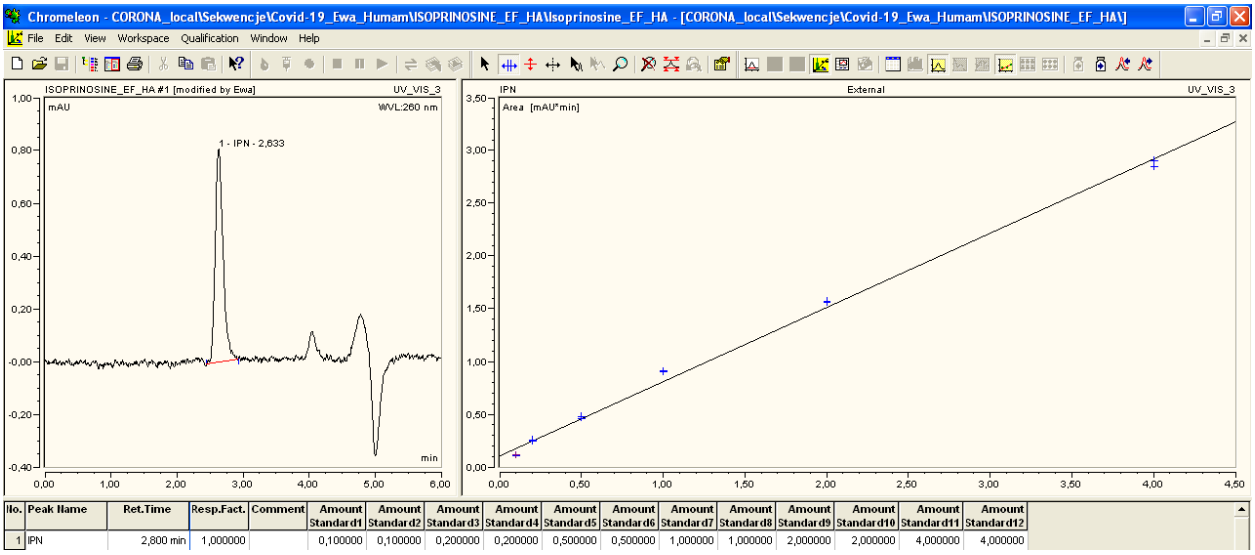

Figure. 6a. Calibration curve of isoprinosine. (y = 0.7045x + 0.1042; R^2 = 99.58%)

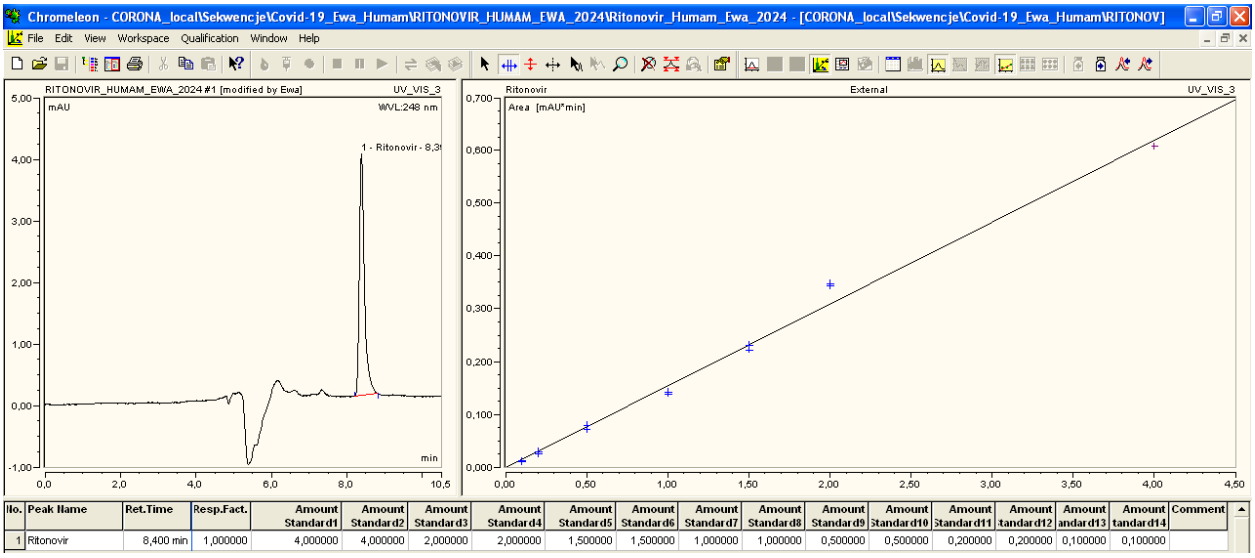

Figure. 6b. Calibration curve of ritonavir. (y = 0.1548x + 0.0000; R^2= 99.36%)

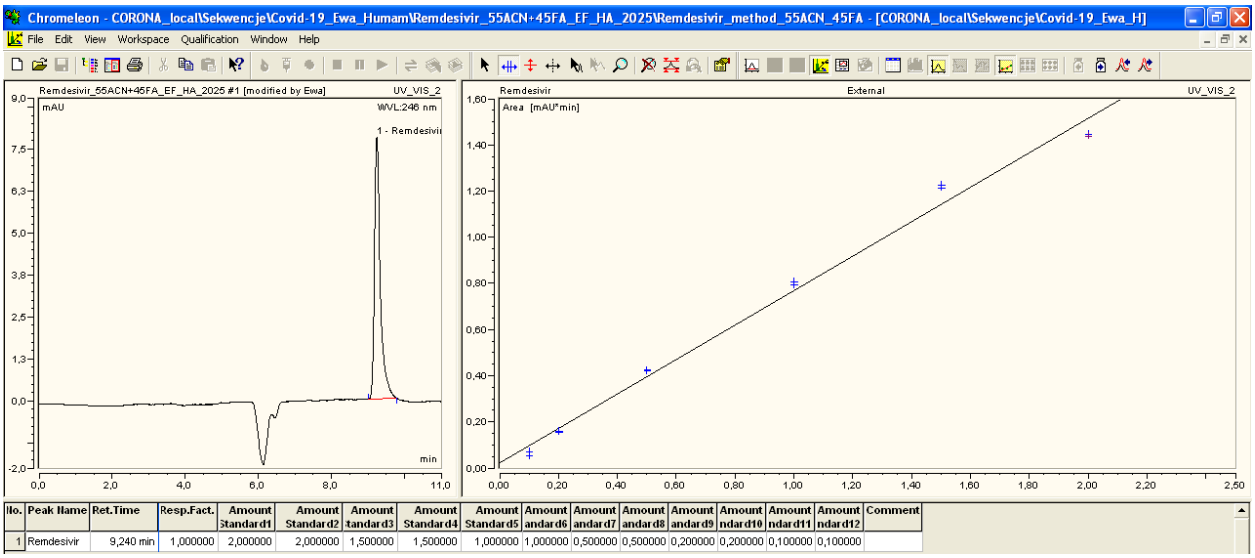

Figure. 6c. Calibration curve of remdesivir (y = 0.7458x + 0.0247; R^2 = 99.08%)

3.3.4. Description of solar light reactor

The research focused on the degradation of selected anti-COVID drugs using artificial solar light and was carried out in the Solar-box 1500e System, manufactured by Co.fo.me.gra in Italy as shown in figure 7. This advanced system comprises a 1500W polychromatic Xenon lamp that releases electromagnetic radiation. The radiation passes through a long-lasting soda-lime glass filter, providing natural outdoor exposure conditions. The filtered xenon light's spectral power distribution is closest to the sun, providing a similar environment to conduct research. The radiant heat emitted by the Xenon Lamp is continuously controlled

and monitored by a built-in B.S.T. (Black Standard Thermometer). The internal temperature of the system was maintained at 35 ± 2 °C. All the experiment were performed using solar irradiance 500 W/m^2.

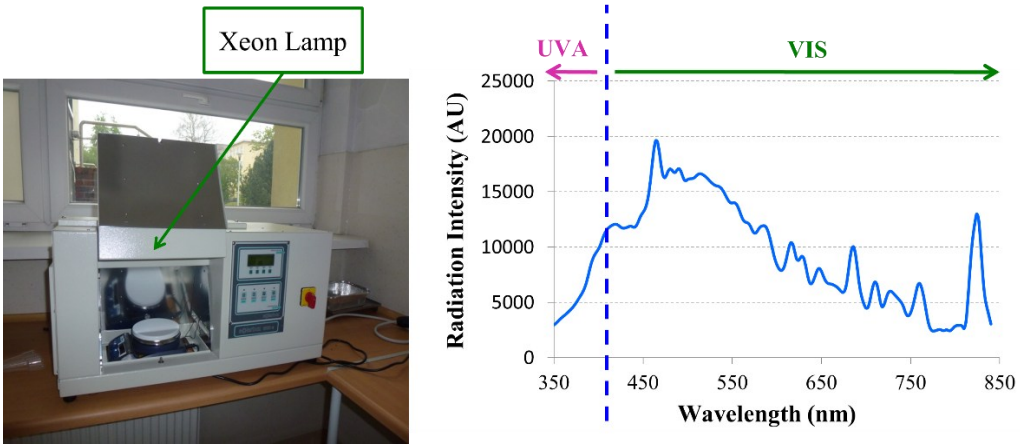

Figure. 7. Solar box System 1500 photoreactor and xenon lamp emission spectrum at light irradiance 500 W/m^2

3.3.5. Photolytic studies

3.3.5.1. For Isoprinosine (IPN)

For the photolysis experiment, approximately 200 mL of an aqueous solution of IPN was transferred into a glass beaker from working standard of concentration 2.0 mg/L and placed on a magnetic stirrer inside the Solar Box system. The sample was exposed to simulated solar irradiation with an intensity of 500 W/m^2 for 120 minutes under continuous stirring. Aliquots were collected at predetermined time intervals of 0, 10, 20, 30, 45, 60, 90, and 120 minutes, both before and after irradiation. The mass of the sample solution was monitored using an analytical balance to account for any evaporation losses during the experiment. The experiment was repeated in three selected water matrices i.e., MQW,TW, and SW, respectively.

3.3.5.2. For Ritonavir (RTR)

For RTR photolysis, 200 mL of a 2.0 mg/L aqueous solution was irradiated in a Solar Box system (500 W/m^2) for 120 minutes under continuous stirring. Samples were taken at 0 –120 minutes intervals, and the solution mass was monitored with an analytical balance to correct for evaporation. The experiment was conducted in three different water matrices, namely Milli-Q water (MQW), tap water (TW), and surface water (SW), respectively.

3.3.5.3. For Remdesivir (REM)

For the photolysis study of REM, about 200 mL of an aqueous solution was prepared from a working standard with a concentration of 1.0 mg/L. The solution was placed in a glass beaker and positioned on a magnetic stirrer inside the Solar Box system. It was then subjected to simulated solar irradiation at an intensity of 500 W/m² for a total duration of 120 minutes, while being continuously stirred to maintain uniform exposure. Samples were collected at specified time intervals of 0, 10, 20, 30, 45, 60, 90, and 120 minutes, both before and after irradiation. The mass of the solution was carefully measured using an analytical balance to compensate for any evaporation losses during the experiment. The experiment was repeated using three selected water matrices: MQW, TW, and SW, to evaluate the effect of water composition on degradation behaviour.

3.3.6. Photocatalytic studies

3.3.6.1. For Isoprinosine (IPN)

The photocatalytic degradation of IPN (2.0 mg/L), were studied in three selected environmental matrices i.e., MQW, TW, and SW. Seven different semiconductors for example, TiO_2 P25, ZnO, ZrO_2, $BaWO_4$, Ag-TiO_2, $BaTiO_3$, and SnO_2 were used in this work. Among the photocatalysts used, Ag-TiO_2 and $BaTiO_3$ were synthesized by fellow researchers as part of separate projects; therefore, their capabilities to degrade the selected drugs were evaluated in this study. The remaining photocatalysts were commercially available materials. Each photocatalyst was tested at different dosages, 5.0 mg/L (TiO_2 P25 and ZnO only), 10.0 mg/L and 20.0 mg/L, under solar light irradiance of 500 W/m^2. About 200 ml of the sample in each water matrices were transferred to the beaker and placed on the magnetic stirrer inside the solar box. Samples were collected time intervals of 0, 10, 20, 30, 45, 60, 90, and 120 minutes, both before and after irradiation. The mass of the solution was carefully measured using an analytical balance to compensate for any evaporation losses during the experiment.

3.3.6.2. For Ritonavir (RTR)

For the photodegradation of RTR, approximately 200 mL of the sample solution was transferred into a beaker to obtain a concentration of 2.0 mg/L. Based on the results obtained from the IPN experiments, the three most effective photocatalysts, TiO_2-P25, ZnO, and SnO_2:ZnO (2:1) were selected for RTR degradation. The combined use of SnO_2:ZnO was

intended to enhance the photocatalytic activity of SnO_2, as SnO_2 alone exhibited limited degradation efficiency. The prepared solution was placed on a magnetic stirrer inside the Solar Box system and irradiated under simulated solar light at an intensity of 500 W/m^2 for 120 minutes, with continuous stirring to ensure homogeneous exposure. Samples were withdrawn at specific time intervals of 0, 10, 20, 30, 45, 60, 90, and 120 minutes, both before and after irradiation. The mass of the solution was monitored using an analytical balance to account for any evaporation losses. The experiment was repeated using three selected water matrices (MQW, TW, and SW) to assess the influence of water composition on the degradation behavior of RTR.

3.3.6.3. For Remdesivir (REM)

For the photodegradation of REM, a 200 mL aqueous solution with a concentration of 1.0 mg/L was prepared and placed in a glass beaker inside the Solar Box system. Based on prior IPN and RTR results, the three most efficient photocatalysts, TiO_2-P25, and ZnO were selected for this study. The sample was exposed to simulated solar irradiation (500 W/m$_2$) for 120 minutes under continuous stirring. Aliquots were collected at 0, 10, 20, 30, 45, 60, 90, and 120 minutes, and the solution mass was checked using an analytical balance to correct for evaporation. The experiment was performed in three water matrices (MQW, TW, and SW) to evaluate the effect of water quality on REM degradation.

3.3.7. Photodegradation assisted with H_2O_2 studies

In the case of photodegradation assisted with H_2O_2, the studies were carried out with a selected concentration of H_2O_2; 125 µL (108.8 mg/L), 250 µL (217.5 mg/L), and 500 µL (435 mg/L) and with a specific dose 2.0 mg/200 mL of each drug (IPN, RTR, REM) with continues stirring using magnetic stirrer. These doses are reasonable and environmentally acceptable for lab-scale AOP studies, especially for tough pollutants like antiviral drugs. All the above-mentioned experiments were performed in duplicate. All these experimental parameters have already been published in our own publication (H. Ahmed et al., 2025b).

3.3.8. Quantification method

The quantification of selected drugs was carried out by high performance liquid chromatography (HPLC) coupled with an ultraviolet light (UV) variable detector. (UltiMate 3000 system; Dionex Corporation, Sunnyvale, CA, USA). The samples were filtered by

using MCEMF-Millipore® Membrane Filters with 0.22 µm pore size (Merck, Germany). The chromatographic separation was performed using a C18 Hypersil™ Gold column (250 mm x 4.6 mm; pore size: 5 mm) (Thermo Scientific, Polygen, Poland). For IPN, the mobile phase consisted of an ACN and MQ water in a ratio of 60:40 (v/v), in case of RTR, acetate buffer (pH 5.0) and ACN in ratio of 30:70 (v\v), and for REM, ACN and 0.1% of formic acid solution (FA) in a ratio of 55:45 (v/v) with the retention time (RT) of IPN (5.0 ± 0.5 min), RTR (8.0 ± 0.5 min), and REM (9.0 ± 0.5 min) under the specified conditions. The limit of quantification (LOQ) of studied antiviral was equal to 0.2 mg/ L. It was established as the first lowest calibration point of their calibration curves (linear regression, $R^2 > 0.98$). The wavelength used for the analysis were 260, 248, and 246 nm for IPN, RTR, and REM, respectively. The data was evaluated using Dionex Chromeleon™ 6.8 software.

3.3.9. Sorption studies

To investigate the adsorption isotherms of the selected pharmaceuticals pollutant on selected photocatalysts surface, an aqueous stock solution of each drug was prepared at a concentration of 500 mg/L. The stock solutions were diluted with MQW and TW respectively to obtain the concentration of 200 mg/L of the investigated pollutant. The experiments were conducted in the beakers securely covered with aluminum foil to limit the potential exposure of the samples to sunlight. The samples were stirred continuously during the experiment using magnetic stirrer. Next, the samples were taken out from the beaker after the time intervals between 10 to 120 minutes and then filtered using MCEMF-Millipore® Membrane Filters with 0.22 µm pore size (Merck, Germany). The concentrations of each drug in the liquid phase were determined by means of HPLC-UV. The tests were performed in duplicates.

3.3.10. Anion Profiling in Milli-Q, Tap, and Surface Waters via Ion Chromatography

Ion chromatography (IC) was performed using a Dionex Aquion Ion Chromatography System (Thermo Fisher Scientific, USA) equipped with an IonPac AS23 analytical column and an AG23 guard column, coupled with a suppressed conductivity detector. The system was operated under isocratic conditions following standard U.S. EPA protocols. A sodium carbonate solution (0.5 M) was used as the eluent at a constant flow rate of 1.0 mL/min. The total runtime per sample was 25 minutes, with well-resolved anion peaks observed within this retention window. Environmental water samples including MQW, TW, and SW were filtered through 0.45 µm membrane filters to eliminate suspended solids prior to injection.

An injection volume of 25 µL was used for all analyses via autosampler. Calibration was conducted using certified multi-anion standards across a linear concentration range (R^2 > 0.999), and ultra-pure water served as both a procedural blank and baseline reference. Method performance was further validated using quality control spikes, confirming accuracy and instrumental precision.

3.3.11. Kinetic studies

To investigate the kinetics studies of photolysis and photolysis assisted with H_2O_2, and photocatalysis (IPN only), removal of selected drugs using selected photocatalysts used in this study, the pseudo-first-order kinetics method is used with all the experimental data obtained from degradation of selected drugs. This method relies on the concentration of the reactant in a chemical reaction. The linear form of the pseudo-first-order equation is given below:

$$\frac{C}{C_0} = exp^{-kt.t} \qquad (1)$$

where: C and C_0 are the drugs amount adsorbed at equilibrium and at time t, respectively (mg/g), kt is a rate constant (min^{-1}), obtained from the slope of the graph C/C_0 vs time (min). The half-life of the reaction is determined by the following equation:

$$\frac{1}{2}t = \frac{ln\,2}{kt} \qquad (2)$$

The half-life of a chemical reaction refers to the duration it takes to remove 50% of a selected pollutant through photolytic or photocatalytic processes (½t, min). It is a crucial parameter for understanding the efficiency of these reactions in environmental applications. For the analysis and calculation of pseudo-first-order kinetics, all necessary computations are calculated using the SAP Interactive Excel application. This method allows for precise tracking and assessment of pollutant degradation over time, providing valuable insights into the reaction dynamics and effectiveness of the treatment process. Given that the primary factor influencing the degradation of solar light over time is cumulative energy, we can substitute cumulative energy (QUV) for time (t) in the pseudo-first-order reaction, leading to the following equation:

$$\ln\left(\frac{C_t}{C_0}\right) = -k_{UV}Q_{UV} \qquad (3)$$

where k_{UV} (L kJ^{-1}) is the pseudo-first-order rate constant of selected drugs photocatalysis considering the value of cumulative energy, wherein the cumulative energy (Q_{UV}) (kJ L^{-1}) is calculated as:

$$Q_{UV,n+1} = Q_{UV,n} + \overline{UV}_{G,n+1} \cdot \frac{A_i}{V_t} \cdot \frac{\Delta t_n}{1000};\ \Delta t_n = t_{n+1} - t_n \qquad (4)$$

Where $Q_{UV,n+1,}$ and $Q_{UV,n}$ are the cumulative UV energy per volume unit of the treated medium at times *n* and *n-1*, respectively (kJ L^{-1}); $\overline{UV}_{G,n+1}$ is the average incident solar UV irradiance measured in time interval Δt_n (W m^{-2}); A_i is the irradiated area (m^2); V_t is the total volume of the treated medium (L) and Δt_n is the time interval between consecutive samples (s).

In case of RTR, the experimental results showed the strong adsorption. According to the observations, Langmuir isotherm model was chosen to calculate the amount of drug adsorbed on the selected photocatalysts surface using following equation:

$$q_e = (C_o - C_e) \times V/m \qquad (5)$$

Where, 'q_e' is amount of drug adsorbed per unit mass of photocatalysts used (mg/g) , 'C_o' is initial concentration of the drug (before adding photocatalysts) and 'C_e' is a concentration of the drug in the solution at time t (after adsorption), 'V' is volume of the solution (L), and 'm' is an amount of catalyst used (g). To characterize the adsorption equilibrium, Langmuir adsorption isotherms model was used (Equation 6):

$$\frac{1}{q_e} = \frac{1}{q_{max}} + \frac{1}{q\,max\,k_L c_e} \qquad (6)$$

Where: qe is amount of drug adsorbed at equilibrium (mg/g), Ce is equilibrium concentration of drug in solution (mg/L), q_{max} is a maximum adsorption capacity (mg/g), and KL = Langmuir constant.

In case of the REM, a simplified two-phase adsorption–desorption kinetic model was applied to approximate the early-stage behavior. The kinetic behavior of the adsorption–desorption process was described using a two-phase reversible model, governed by the equation:

$$\theta(t) = \frac{Kads}{Kads - Kdes} \times (1 - e^{-(Kads + Kdes) \times t}) \qquad (7)$$

Where: θ(t) is the fraction of the surface covered (adsorbed fraction) at time (t), kads. is the adsorption rate constant (min^{-1}), kdes. is the desorption rate constant (min^{-1}), t is the time in minutes, and ($k_{ads} + k_{des}$) is the total kinetic rate constant. The term $\frac{Kads}{Kads-Kdes}$ represents the equilibrium surface coverage (i.e., maximum achievable θ at steady state). The percent adsorption and desorption using this model in theory and real environment was calculated using following equations:

$$\% \text{ Adsorption } = \frac{\text{Kads}}{\text{Kads}-\text{Kdes}} \times 100 \quad (8)$$

$$\% \text{ Desorption } = \frac{\text{Kdes}}{\text{Kt}} \times 100 \quad (9)$$

Equations 8 and 9 represented the percent adsorption and desorption theoretically. Where kt is total kinetic constant i.e., (kdes + kads). In case of real environmental condition (experimental), (Equations 10 & 11) the percentage adsorption and desorption were calculated as follows:

$$\% \text{ Adsorption } = \frac{C_o - Ct_a}{C_o} \times 100 \quad (10)$$

$$\% \text{ Desorption } = \frac{Ct_f - Ct_i}{C_o} \times 100 \quad (11)$$

Where, C_o is the initial concentration, Ct_a is a concentration at time where adsorption occurs or started, Ct_f is a concentration at time 120 min i.e., desorption final time or maximum desorption, and Ct_i is a concentration at times, where desorption has started.

Chapter 4 – Results and Discussion

4.1 Results and discussion

4.1.1. Ion profiling of selected water matrices

Ion chromatography (IC) was employed as an initial diagnostic tool to assess the anionic composition of three distinct water matrices: MQW, TW, and SW. This profiling was critical for establishing the ionic background prior to the application of treatment processes such as photolysis and photocatalysis. Table 6 shows the comparative summary of ions in all selected water matrices.

The chromatogram of MQW revealed a very low background conductivity with minimal ionic presence, as expected from ultra-purified laboratory-grade water. Small peaks for chloride (6.137 min), nitrate (10.271 min), and sulfate (16.091 min) were detected at trace levels, indicating possible minor system contamination or residual baseline ions. The early unknown minor peak signal close to baseline could correspond to trace contamination or a low-level inorganic acid as shown in figure 8a.

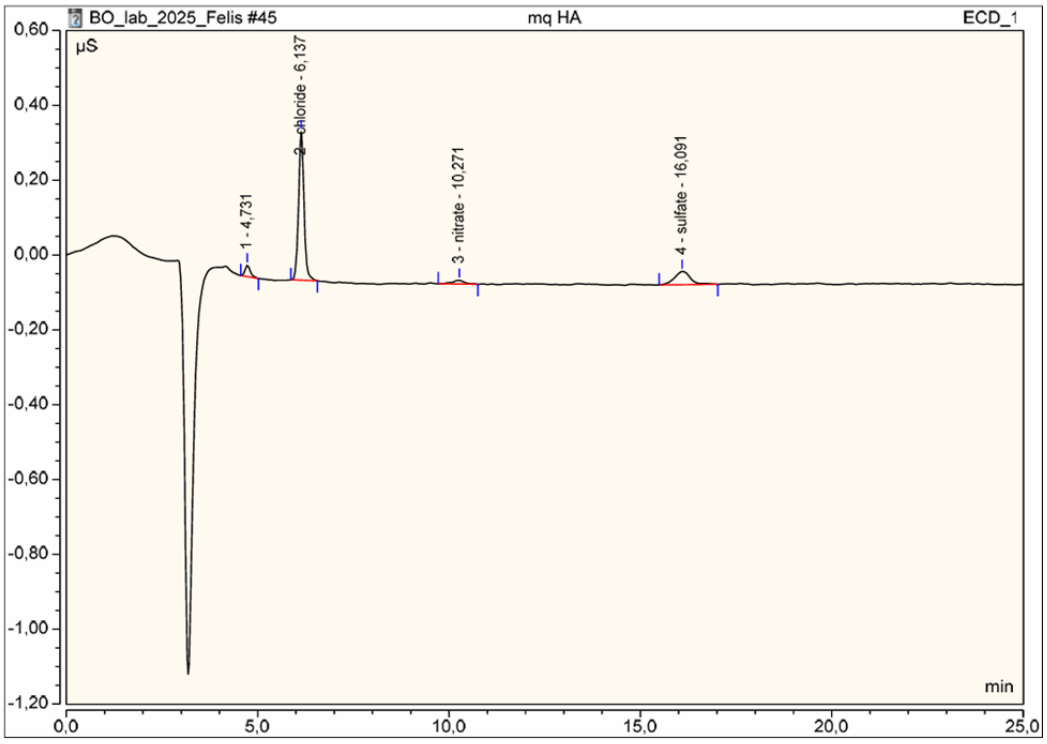

Figure. 8a. Ion profiling in MQW using Ion chromatography

MQW is designed to be ion-free (18.2 MΩ·cm resistivity), the detection of these anions suggests minor background contamination, likely introduced during sample handling or storage. The most prominent ion, chloride, is common due to its presence in lab environments. Sulfate and nitrate appear in trace amounts, with all signals well below 0.6 µS, confirming the high purity of water and the sensitivity of the IC system. No significant peaks are observed beyond 20 minutes, indicating an absence of late-eluting high-molecular-weight or multivalent anions in this sample.

Table.6. Comparative anionic summary of all selected water matrices using ion chromatography

		Selected Water Matrices		
Ions	**Retention Time (min)**	**Milli-Q water**	**Tap water**	**Surface water**
Fluoride	4.1	–	✓	✓
Unknown/Acetate	4.7	✓	✓	✓
Chloride	6.1	✓	✓✓✓	✓✓✓
Nitrite	7.3	–	✓	✓
Bromide	9.0	–	✓	✓
Nitrate	10.2	✓	✓✓	✓✓
Unknown/Organic Acid	13.3	–	–	✓
Sulfate	16.0	✓	✓✓	✓✓

✓: Low/Trace, ✓✓: Moderate, ✓✓✓: High, – : Not detectable

In case of TW, multiple anionic species was observed, indicating a complex but typical ionic profile. The conductivity response is significantly higher compared to Milli-Q water, confirming the presence of a broader and more concentrated ion spectrum. According to figure 8b, a dominant chloride peak (6.160 min)confirming chloride as the most abundant anion in this sample, which may arise from source water mineral content or due to municipal treatment. Other prominent anions included fluoride (4.100 min), nitrite (7.284 min), bromide (8.977 min), nitrate (10.207 min), and sulfate (15.934 min). The presence of fluoride

suggests fluoridation for public health, while nitrate and nitrite point to possible agricultural or urban runoff influence. The varied anion spectrum reflects both intentional water treatment and environmental input, offering insight into potential scavengers or competing species in oxidative treatments.

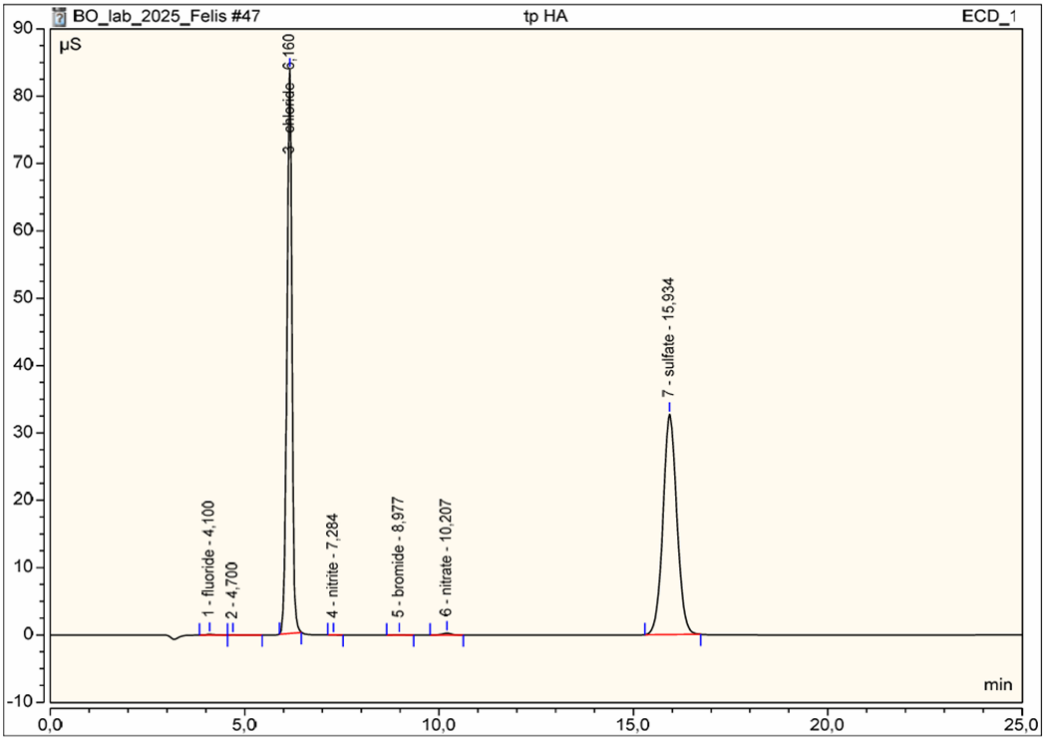

Figure. 8b. Ion profiling in TW using Ion chromatography

In case of SW, a prominent chloride peak (6.167 min) was accompanied by notable sulfate (15.971 min) and nitrate (10.221 min) peaks as shown in figure 8c. Trace levels of fluoride (4.124 min), nitrite (7.304 min), and bromide (8.994 min) were also observed. Interestingly, an additional unidentified peak at 13.314 min may indicate the presence of naturally occurring organic acid anions, a quality of SW influenced by biological activity and organic matter degradation. Compared to TW, the surface water exhibited broader baseline noise and additional minor peaks, reinforcing its susceptibility to both natural and anthropogenic inputs.

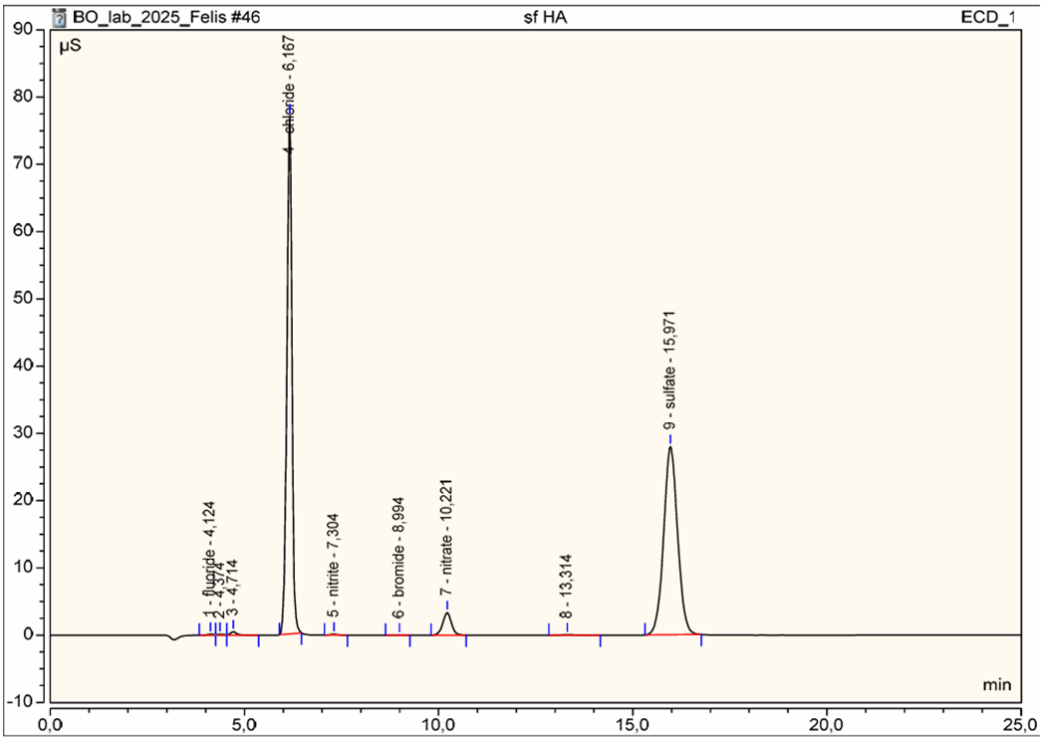

Figure. 8C. Ion profiling in SW using Ion chromatography

4.1.2. Photolysis with sunlight

Photolysis is a crucial process in the degradation of drugs. During this process, pharmaceutical compounds break down when exposed to solar light. The underlying chemistry involves the excitation of electrons, which absorb energy from sunlight. These excited electrons then cause the compounds to break down either through oxidation or by breaking chemical bonds. This results in the formation of photoproducts, which can be active, inactive, or harmless.

The studies have been performed in three different water matrices (MQW, TW, and SW) to check the degradation efficiency of selected antiviral drugs (IPN, RTR, and REM) in the presence of sunlight at a concentration of 2.0 mg/L with an irradiance of 500 W/m². As illustrated in Figure. 9a, the photolysis of IPN, a complex of acetaminobenzoic acid, dimethylaminoisopropanol, and inosine in a 3:3:1 ratio (1115.23 g/mol) in three different water matrices, were observed. The finding shows that after 60 mins of exposure to light irradiance 500W/m², IPN was only degraded by 9%, in MQ water. However, in the case of environmental matrices (TW) and (SW), the removal rate of isoprinosine was 14% and 8% after 120 mins, respectively, indicating that in environmental conditions, IPN will not

undergo further changes. The findings presented here partially build upon our previous publication (H. Ahmed & Felis, 2024).

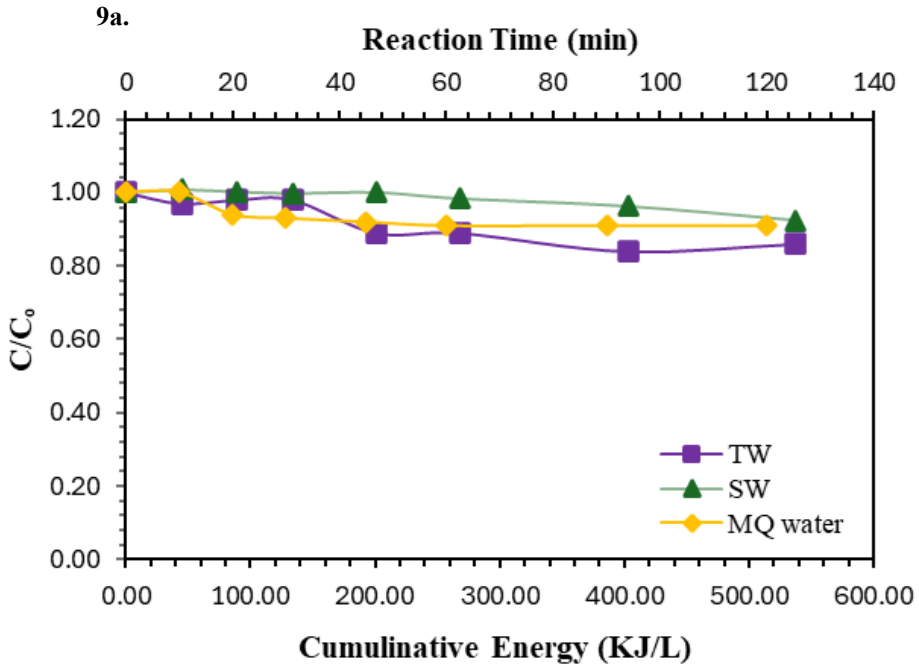

Figure. 9a. Photo-degradation of anti- COVID drug IPN in aquatic matrices

According to predicted environmental concentration (PEC), IPN should be removed, with an efficiency of >80% (Tobólska et al., 2018). However, the limited experimental data does not provide sufficient evidence to support this claim. According to the study findings, the photodegradation rate constant for IPN removal from TW is higher than that of MQW and SW and the slight decomposition of IPN under solar light indicates that it will not undergo further changes in environmental conditions.

Subsequently, the same experiment was conducted using another selected drug, RTR, a protease inhibitor employed in COVID-19. The removal efficiency of RTR was investigated in three different water matrices: MQ water, known for its high purity, TW and SW. The findings, represented in Figure 9b, reveal that under the solar light irradiance (500 W/m^2), RTR showed inadequate degradation of only 15% within 90 minutes in MQ water. In the TW sample, the degradation rate increased to 38% with a reaction time of 120 minutes. While in the SW sample, the concentration of RTR degraded significantly, 51%, with a reaction time of 120 min. The findings presented here partially build upon our previous publication (H. Ahmed et al., 2025b) These results suggest that, under typical environmental conditions, RTR degraded significantly in SW only and may not further degrade beyond this point.

While the photodegradation of RTR in natural waters may decrease its persistence in the environment, there is a concern about the potential formation of photoproducts and their ecological or toxicological effects on aquatic organisms. The toxic effects of the selected drug, RTR, on freshwater organisms are significant. RTR is toxic at concentrations in the tens of mg/L (Nugnes et al., 2024).

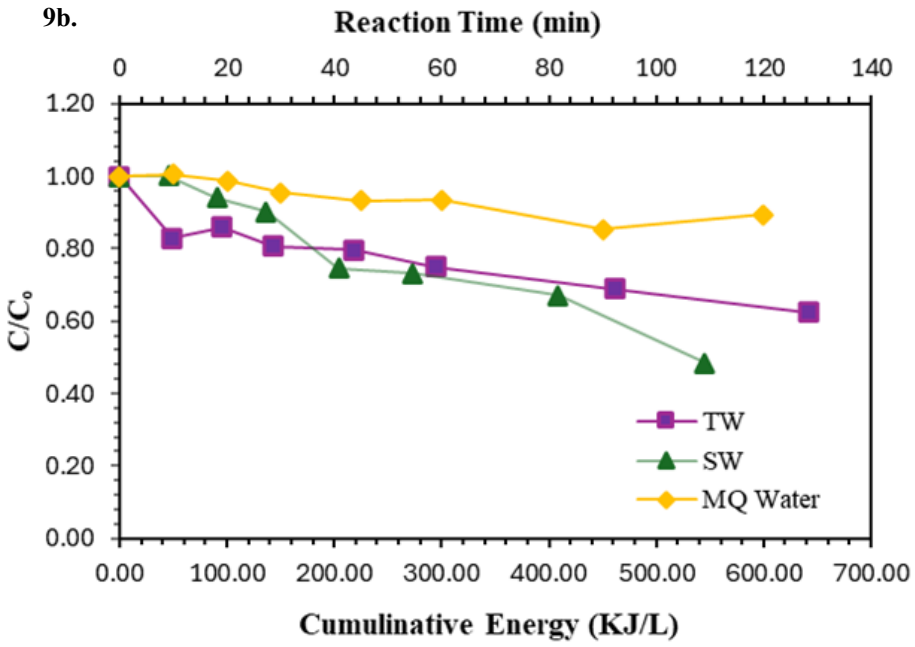

Figure. 9b. Photo-degradation of anti- COVID drug RTR in aquatic matrices

In addition, the same experiment was carried out with the third selected drug, REM at a concentration of 1.0 mg/L, across three different water types under solar light irradiance of 500 W/m^2 as represented in figure 9c. The results revealed that, after a reaction time of 120 minutes, REM was degraded by 15% in Milli water (MQW), 27% in tap water (TW), and 23% in surface water (SW). These findings indicate that the drug may not undergo substantial further degradation when exposed to solar light. The pseudo first order kinetics of degradation of selected drugs is represented in Table 7.

Table. 7. Kinetic parameters−first-order pseudo constants of photolysis of selected drugs

Drugs	Water matrices	[a]*Kt*, min^{-1}	[b]½ t , min^{-1}	[c]R^2
Isoprinosine	MQW	0.0007	990.2	0.6092
	TW	0.0003	2310.5	0.8154
	SW	0.0001	6931.5	0.8726
Ritonavir	MQW	0.0012	577.6	0.8201
	TW	0.0005	1386.3	0.8488
	SW	0.001	693.1	0.9583
Remdesivir	MQW	0.0016	433.2	0.8563
	TW	0.0005	1386.3	0.9488
	SW	0.0004	1732.9	0.9124

a). Pseudo first order kinetic rate constant, b). Half-life of the reaction, c). Coefficient of determination.

In a published study, researchers investigated the degradation kinetics of REM in both alkaline and acidic environments, employing High-Performance Thin-Layer Chromatography (HPTLC) as their analytical method. The findings revealed that under photolytic conditions, REM exhibited significant stability, with only a minimal degradation rate of 3% observed (Abo-Gharam & El-Kafrawy, 2022). This suggests that REM can maintain its integrity in the presence of light, highlighting its potential resilience in various chemical settings.

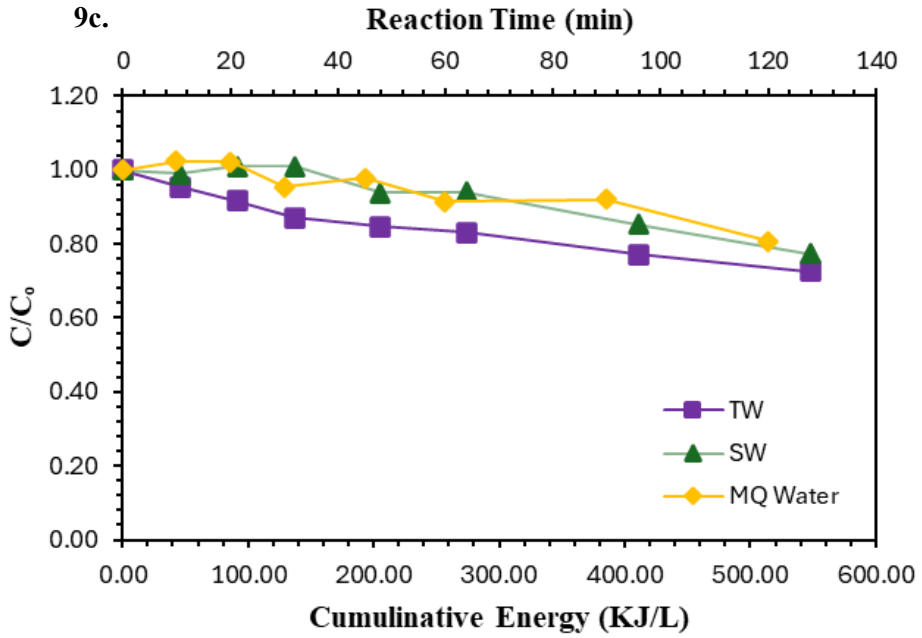

Figure. 9c. Photo-degradation of anti- COVID drug REM in aquatic matrices

The susceptibility of antiviral drugs to direct solar photolysis varies widely by compound. Some antivirals with chromophores that absorb sunlight undergo appreciable direct photolysis in pure water, while many others are relatively photostable and degrade very slowly under natural or simulated sunlight (Guo et al., 2023). For example, laboratory work on several classical antivirals (e.g., acyclovir, zidovudine, lamivudine) documented measurable photolytic rate constants in pure and natural waters, but the rates changed markedly with matrix composition (DOM, ions, salinity) (Zhou et al., 2015b).

However, direct photolysis is often insufficient as a standalone remediation strategy for many COVID-19 related and other modern antiviral compounds (Baena-Nogueras et al., 2017). Previously published studies emphasize that while sunlight can partially transform some drugs such as sulfamethoxazole, carbamazepine, and trimethoprim, residual parent compounds and toxic transformation products frequently persist at the end of photolytic experiments, and removal under environmentally realistic conditions is frequently incomplete (Alharbi et al., 2017). Consequently, authors commonly recommend coupling photolysis with additional oxidation pathways when the goal is effective removal or mineralization (Morales-Paredes et al., 2022).

In conclusion, simple solar photolysis is often insufficient for degrading antiviral drugs due to two main reasons. First, most antivirals have molecular structures with low light

absorptivity, meaning they do not effectively utilize the solar spectrum for direct degradation (De la Cruz et al., 2013). Second, the composition of natural waters including organic matter, inorganic ions (e.g., Cl^-, HCO_3^-, NO_3^-), and suspended particles can reduce photolytic efficiency by quenching reactive species or scavenging hydroxyl radicals (Eitzen et al., 2024).

These factors significantly limit the effectiveness of direct photolysis in real environmental conditions. Therefore, the next part of this study focused on enhanced photochemical methods, such as advanced oxidation processes (AOPs), to achieve efficient degradation such as photocatalysis using seven different photocatalysts (both synthesized and commercially available) as well as photolysis assisted with H_2O_2.

It has been noted that there are some studies on the photolysis or photochemical treatment of antiviral drugs, none appear to have focused specifically on the compounds REM, RTR and IPN under solar or simulated-solar conditions in aquatic environments. This absence of data underscores the novelty and relevance of the present work, which systematically investigates the degradation behavior of IPN, RTR, and REM under simulated solar irradiation, both in pure and realistic water matrices, and compares the performance of different photocatalytic systems.

4.1.3. Photocatalysis Experiments

4.1.3.1. Photocatalytic removal of isoprinosine

The photocatalytic degradation of IPN (2.0 mg/L) was initially studied in MQ water using seven different semiconductors: TiO_2 P25, ZnO, ZrO_2, $BaWO_4$, Ag-TiO_2, $BaTiO_3$, and SnO_2. Among the photocatalysts used, Ag-TiO_2 and $BaTiO_3$ were synthesized by fellow researchers as part of separate projects; therefore, their capabilities to degrade the selected drugs were evaluated in this study. Each photocatalyst was tested at different dosages, 5.0 mg/L (TiO_2 P25 and ZnO only), 10.0 mg/L and 20.0 mg/L, under solar light irradiance of 500 W/m^2. Following this, the degradation efficiency was evaluated in real environmental matrices, such as TW and SW, utilizing the most effective photocatalysts identified in the initial experiments.

The findings indicated that in Figure 10a, at a dose of 5.0 mg/L of TiO_2 P25 and ZnO, IPN was degraded significantly: TiO_2 P25 achieved a complete degradation of 100%, while ZnO reached 88% after reaction times of 30 minutes and 120 minutes, respectively. In the case of

a photocatalytic dose of 10.0 mg/L, the degradation rates of IPN by the various photocatalysts were as follows: ZnO (98%), ZrO_2 (46%), $BaWO_2$ (11%), Ag-TiO_2 (20%), and $BaTiO_3$ (12%) (laboratory synthesized) after a reaction time of 120 minutes. Furthermore, TiO_2 P25 and SnO_2, at a dose of 10.0 mg/L, achieved degradation rates of IPN 100% and 10% after 30 minutes and 90 minutes, respectively, as illustrated in Figure 10b. All the experiment followed the pseudo first order kinetics (Table 8).

10a.

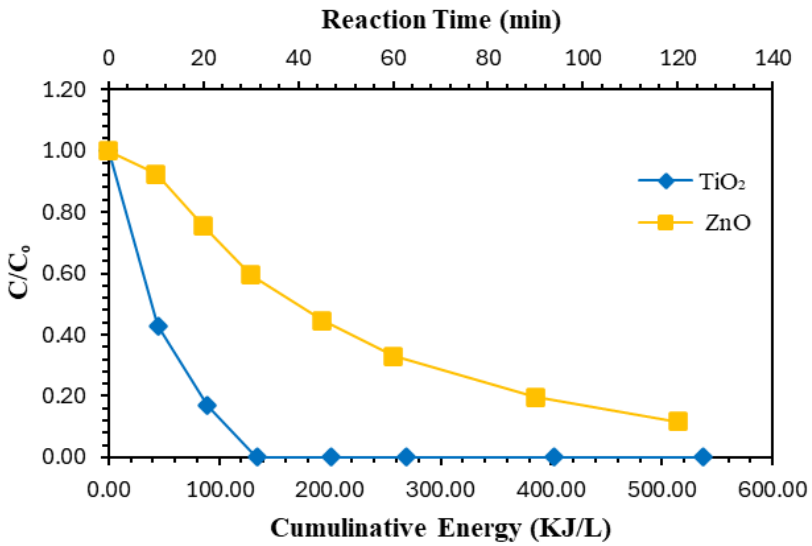

Figure. 10a. Degradation of anti- COVID drug IPN in MQ-water by selected photocatalysts at dose 5.0 mg/L

10b.

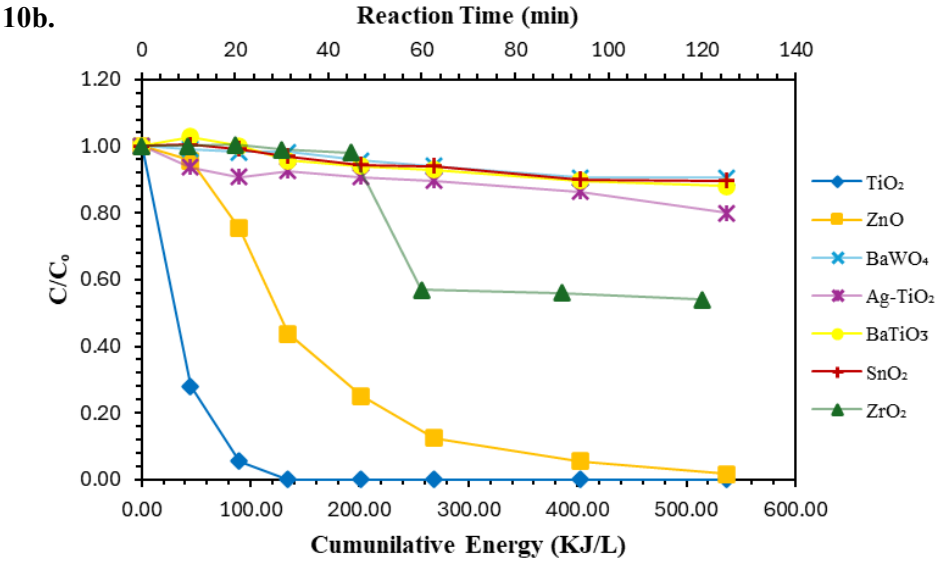

Figure. 10b. Degradation of anti- COVID drug IPN in MQ-water by selected photocatalysts at dose 10.0 mg/L

In addition, similar experiments were performed with the higher dose of photocatalysts (20.0 mg/L) except ZnO and TiO_2 P25, and the findings showed in Figure 10c, that $BaWO_2$ showed the similar efficiency to removing IPN, 11% at 120 minutes. It might be because higher concentrations of $BaWO_2$ could lead to light scattering and reduced penetration of photons into the reaction medium. This self-shielding effect can limit the generation of reactive species due to the low redox potential (Nabeel et al., 2023).

Table.8. Kinetic parameters−first-order pseudo constants of isoprinosine degradation in MQ-water

Process	Conc., mg/L	*Kt*, min^{-1}	½ t , min^{-1}	R^2
UV-TiO_2 P25	5.0	0.0093	74.53	0.956
	10.0	0.0105	66.0	0.9159
UV- ZnO	5.0	0.0076	91.2	0.9101
	10.0	0.0036	192.5	0.9569
UV- ZrO_2	10.0	0.0049	141.5	0.7847
	20.0	0.0009	770.2	0.8664
UV- $BaWO_2$	10.0	0.0002	3465.7	0.9494
	20.0	0.0002	3465.7	0.8263
UV- Ag-TiO_2	10.0	0.0003	2310.5	0.876
	20.0	0.0005	1386.3	0.8972
UV- $BaTiO_3$	10.0	0.0003	2310.5	0.8945
	20.0	0.0005	1386.3	0.9659
UV- SnO_2	10.0	0.0002	3465.7	0.9494
	20.0	0.0005	1386.3	0.9924

a). Pseudo first order kinetic rate constant, b). Half-life of the reaction, c). Coefficient of determination.

Furthermore, it has been noted that the removal efficiency of ZrO_2 and $BaTiO_3$ decreased to 9% and 1%, respectively, with the increases of catalytic dose of 20.0 mg/L. The decrease in removal efficiency of ZrO_2 (from 46% to 9%) and $BaTiO_3$ (from 12% to 1%) when the catalytic dose increased to 20.0 mg/L can be explained by several key factors: light scattering and blocking effect, agglomeration of catalyst particles, recombination of charge carrier, change in solution turbidity, and photocatalyst loading (Zhang et al., 2020). In case

of Ag-TiO_2 and SnO_2, the degrading efficiency at higher dose were 21% and 28% respectively.

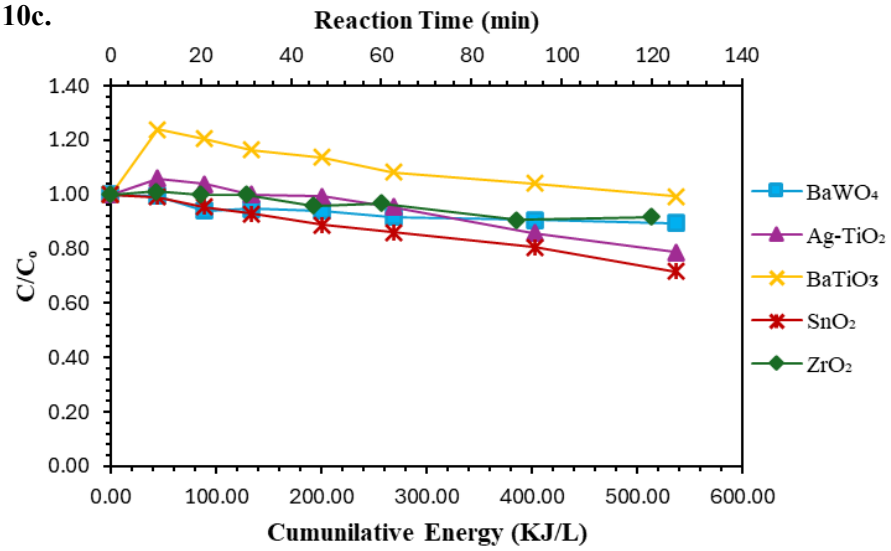

Figure. 10c. Degradation of anti- COVID drug IPN in MQ-water by selected photocatalysts at dose 20.0 mg/L

Based on the experiments conducted with MQ water, TiO_2 P25, ZnO, and SnO_2 were selected for further investigation within real environmental matrices: TW. The findings revealed that in TW, applying a lower photocatalyst dose of 10.0 mg/L resulted in a degradation of IPN by 36% with ZnO, and by 15% with both TiO_2 P25 and SnO_2 (Figure 11a). When the photocatalyst dose was increased to 20.0 mg/L, the removal efficiencies improved significantly, reaching 93% for ZnO, 88% for TiO_2 P25, and 38% for SnO_2 after a period of 120 minutes (Figure 11b).The first order kinetic calculations for degradation of drug in TW is listed in Table 9.

Table.9. Kinetic parameters–first-order pseudo constants of isoprinosine degradation in TW

Process	Water matrices	Conc., mg/L	*Kt*, min^{-1}	½ t , min^{-1}	R^2
UV-TiO_2 P25	TW	10.0	0.0018	385.1	0.7832
		20.0	0.0079	87.7	0.9497
UV- ZnO	TW	10.0	0.0032	216.6	0.8419
		20.0	0.0101	68.6	0.9178
UV- SnO_2	TW	10.0	0.001	693.1	0.7377
		20.0	0.0025	277.3	0.9588

a). Pseudo first order kinetic rate constant, b). Half-life of the reaction, c). Coefficient of determination.

11a

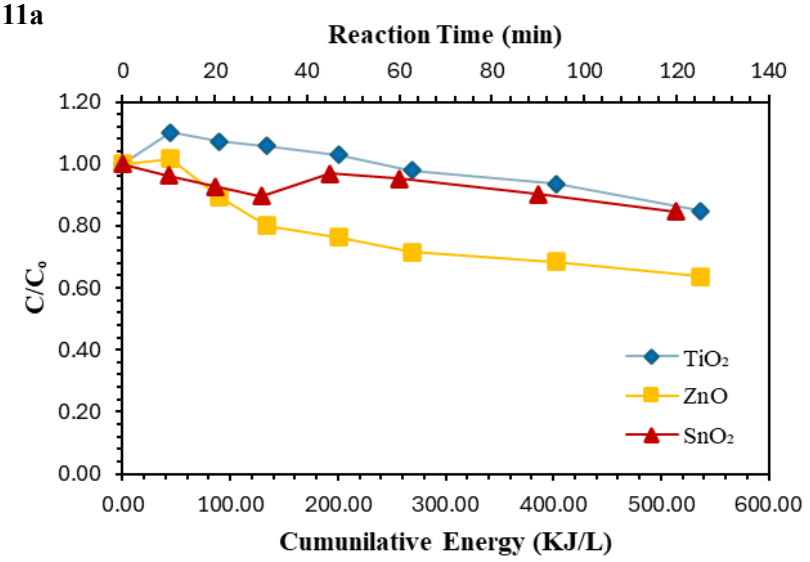

Figure. 11a. Degradation of anti- COVID drug IPN in TW by selected photocatalysts at dose 10.0 mg/L

11b.

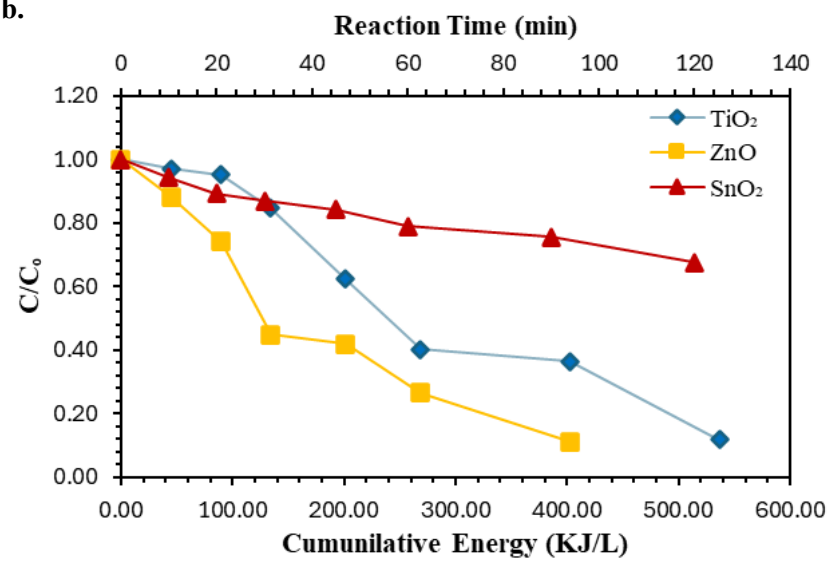

Figure. 11b. Degradation of anti- COVID drug IPN in TW by selected photocatalysts at dose 20.0 mg/L

In the case of SW, experiments were conducted using a single photocatalyst dose of 20.0 mg/L, focusing on TiO_2 P25 and ZnO due to their superior removal efficiencies observed in TW. The results indicated that TiO_2 P25 was able to degrade IPN by 23%, while ZnO achieved a degradation rate of 22% (Figure 11c). The pseudo-kinetic calculations for all selected photocatalyst in SW are shown in Table 10. All experiments followed pseudo-first order kinetics.

Table.10. Kinetic parameters−first-order pseudo constants of isoprinosine degradation in SW

Process	Water matrices	Conc., mg/L	*Kt*, min^{-1}	½ t , min^{-1}	R^2
UV-TiO_2 P25	SW	20.0	0.0008	866.4	0.9123
UV- ZnO	SW	20.0	0.0053	130.8	0.9272

a). Pseudo first order kinetic rate constant, b). Half-life of the reaction, c). Coefficient of determination.

11c.

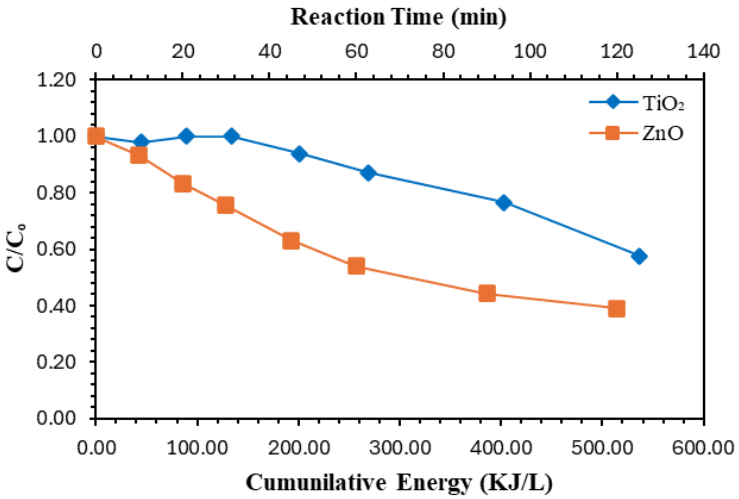

Figure. 11c. Degradation of anti- COVID drug IPN in SW by selected photocatalysts at dose 20.0 mg/L

4.1.3.2. Photocatalytic removal of ritonavir

The photocatalytic activity of selected photocatalysts at a fixed dose of 10.0 mg/L was evaluated using the anti-COVID drug RTR, a class of protease inhibitor, in three different water matrices (MQW, TW, and SW) under UV light (500 W/m^2). The results indicated that RTR was completely adsorbed (100%) on the surfaces of ZnO and SnO_2:ZnO (2:1) within just 30 seconds of the reaction in all three water matrices. Among the selected photocatalysts, TiO_2 P25 showed 72% adsorption on its surface after 120 minutes of the experiment. It was also observed that the initial concentration of RTR (2.0 mg/L) remained stable for the first 45 minutes; however, it decreased rapidly afterward, with the equilibrium point reached 60 minutes into the reaction. Notably, ZnO and SnO_2:ZnO (1:2) achieved complete (100%) adsorption within 1 minute of the reaction, as illustrated in Figure 12. The kinetic parameters of the Langmuir adsorption isotherm are presented in (Table 11), with high KL values

indicating a highly favourable adsorption process (Araújo et al., 2018) demonstrating that the adsorbent has a strong affinity for the adsorbate.

12.

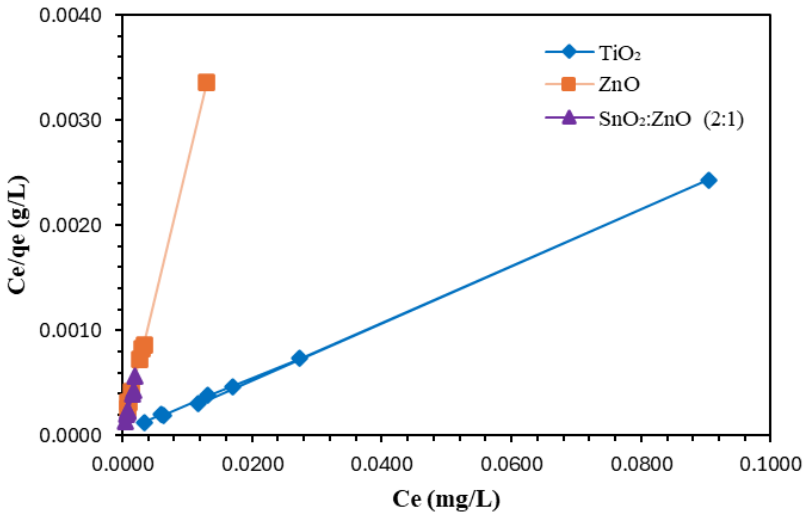

Figure. 12. Adsorption of RTR on the surface of selected photocatalysts at dose 10.0 mg/L with solar light in MQ water.

To evaluate the performance of an adsorbent in removing a selected pollutant, RTR, from TW and SW at an initial concentration of 2.0 mg/L, experiments were formed. For this purpose, two of the best-performing photocatalysts, TiO_2 P25 and ZnO, were chosen based on experiments conducted using MQW to assess the degradation behaviour of RTR in real environmental matrices. The RTR exhibited similar behaviour in both TW and SW as it did in MQW, showing rapid adsorption within 30 seconds of the reaction. This validation was necessary because the TW and SW sources contain additional ions and organic matter that are not present in MQW (Eitzen et al., 2024).

Figures 13a & 13b present plots of the data, showing the relationship between (Ce/qe) and (Ce), which fit the Langmuir adsorption isotherm model. The experimental results indicated that the Langmuir isotherm model was a good fit for the data. Table 12 reveals that ZnO had the highest maximum adsorption capacity (q_{max}) of 37.74 mg/g in TW, followed by TiO_2 P25 at 34.97 mg/g. The Langmuir constant (KL) for ZnO was the highest at 8833.3 L/mg, suggesting a stronger interaction with the adsorbate.

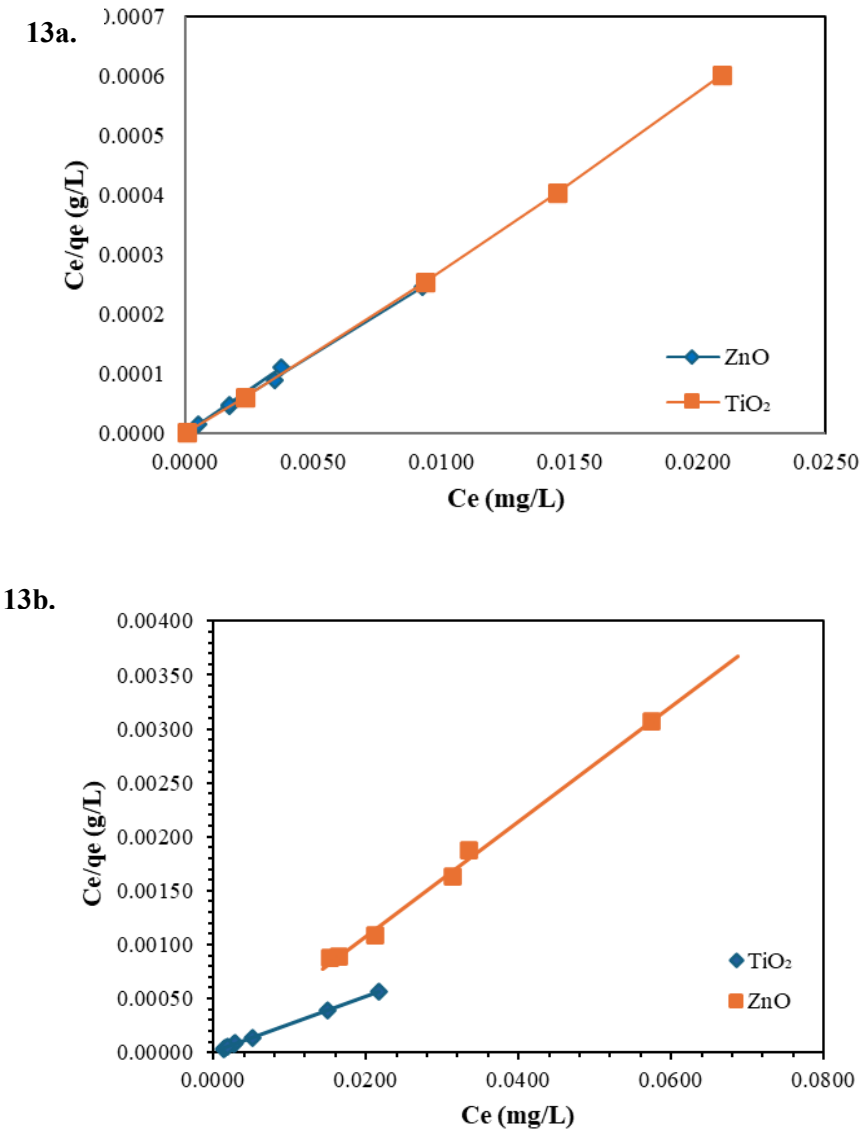

Figure. 13. Rapid adsorption of RTR on the surface of selected photocatalysts in a.)TW, and b). SW

In contrast, the maximum adsorption capacity in SW was 39.06 mg/g for TiO_2 P25, with a KL value of 5120 L/mg. These findings suggest that while ZnO offers greater adsorption capacity in TW, TiO_2 P25 may be more effective in SW. The results provide insights into the monolayer adsorption behaviour of the materials studied, indicating a significant decrease in the concentration of RTR. These results suggest that the interaction between the adsorbent and the solute is strong enough to facilitate efficient pollutant removal, which is a crucial consideration for environmental engineers in the design of treatment plants. For transparency and reproducibility, supporting HPLC data has been documented. Please refer to supporting information section (Chapter 8).

Table.11. Kinetic parameters−Langmuir Isotherm model for ritonavir adsorption under solar light

Process	Water matrices	Conc., mg/L	[a]*Kt*, min^{-1}	[b]R^2	[c]KL L/mg	[d]q_{max} (mg/g)
UV-TiO_2 P25	MQW	10.0	0.2661	0.9995	1330.5	3.76
	TW		0.0286	0.9927	5720	34.97
	SW		0.0256	0.9995	5120	39.06
UV- ZnO	MQW	10.0	0.2532	0.9992	5064.0	3.95
	TW		0.0265	0.9954	8833.3	37.74
	SW		0.0532	0.9958	2660.0	18.80
UV-SnO_2:ZnO	MQW	10.0	0.2605	0.9657	13025.0	3.84

a). Pseudo first order kinetic rate constant, b). Coefficient of determination, c). Langmuir constant, d). Maximum adsorption capacity.

The antiretroviral drugs efavirenz and nevirapine could be removed from water was investigated by (Adeola et al., 2021) effectively. Their results showed that efavirenz had a notably high adsorption capacity of 899 mg/g, while nevirapine's capacity was significantly lower at 5.547 mg/g. The strong adsorption of efavirenz suggests a complex and highly variable interaction between the drug and the graphene wool (GW) adsorbent, likely due to the heterogeneous nature of the surface.

In the case of RTR, there is potential for it to form coordination complexes with TiO_2 P25. This is because RTR contains several functional groups, such as a nitrogen-containing thiazole ring, hydroxyl (-OH) groups, amide (-CONH-) linkages, and ether (-O-) bonds; that can interact with TiO_2 P25. However, the strength and nature of this interaction are influenced by both the surface characteristics of TiO_2 P25 and external factors like pH and the solvent used, as noted by (Natarajan et al., 2022).

To confirm whether such a coordination complex forms, further analytical studies are necessary. For instance, Fourier-transform infrared (FTIR) spectroscopy could help identify shifts in key vibrational bands (like C=O, N-H, and O-H), indicating possible binding. Similarly, X-ray photoelectron spectroscopy (XPS) could detect changes in the binding

energies of elements such as titanium, nitrogen, and oxygen further supporting evidence of coordination between RTR and TiO_2 P25.

A separate study explored how the concentrations of tetracycline (TC) and ibuprofen (IBP) affect their adsorption onto two types of nano-sized zinc oxide (ZnO) particles, using concentrations of 10 mg/L and 0.5 mg/L. Overall, TC and IBP showed greater adsorption on the ZnO sample referred to as 'ZnO-top' compared to 'ZnO-bottom,' which can be attributed to differences in their specific surface areas (Choina et al., 2015). Interestingly, the specific adsorption of TC (expressed as mg of TC per mg of catalyst) was significantly higher at low concentrations (around 200 ppb) than at higher concentrations (above 5 ppm). This enhanced adsorption at lower concentrations, even when the catalyst-to-substrate ratio remains constant, appears to begin below the 10-ppm range. Changes in TC loading over time (both increases and decreases) may be linked to modifications on the ZnO surface, such as hydration or hydroxylation.

4.1.3.3. Photocatalytic removal of remdesivir

The adsorption behavior of the REM (1.0 mg/L) on two widely used photocatalysts; TiO_2 P25 and ZnO (20.0 mg/L) was investigated through both experimental measurements and theoretical modeling in selected aquatic matrices (MQW, TW, and SW). This dual approach not only provides insight into the real-time adsorption efficiency of each photocatalyst but also assesses the predictive capacity of the proposed adsorption - desorption kinetic model.

Both TiO_2 P25 and ZnO exhibited strong adsorption tendencies, with the experimental data showing high surface coverage values over time. In the case of TiO_2 P25, adsorption reached approximately 98.92% by 120 minutes, while ZnO achieved a comparable value of 81% within the same duration. This suggests that, despite having different physicochemical properties, both materials are effective in retaining the target compound on their surfaces under the given experimental conditions. However, some distinct differences emerged when evaluating their adsorption-desorption profiles. The TiO_2 P25 system demonstrated a slightly higher overall adsorption percentage (99.21%) compared to ZnO (100%), but ZnO displayed no measurable desorption, suggesting a possibly stronger or more irreversible interaction between the adsorbate and ZnO surface. This is further supported by the desorption percentages modelled (0% for ZnO vs. 0.79% for TiO_2 P25), reinforcing ZnO has superior binding affinity in this specific system.

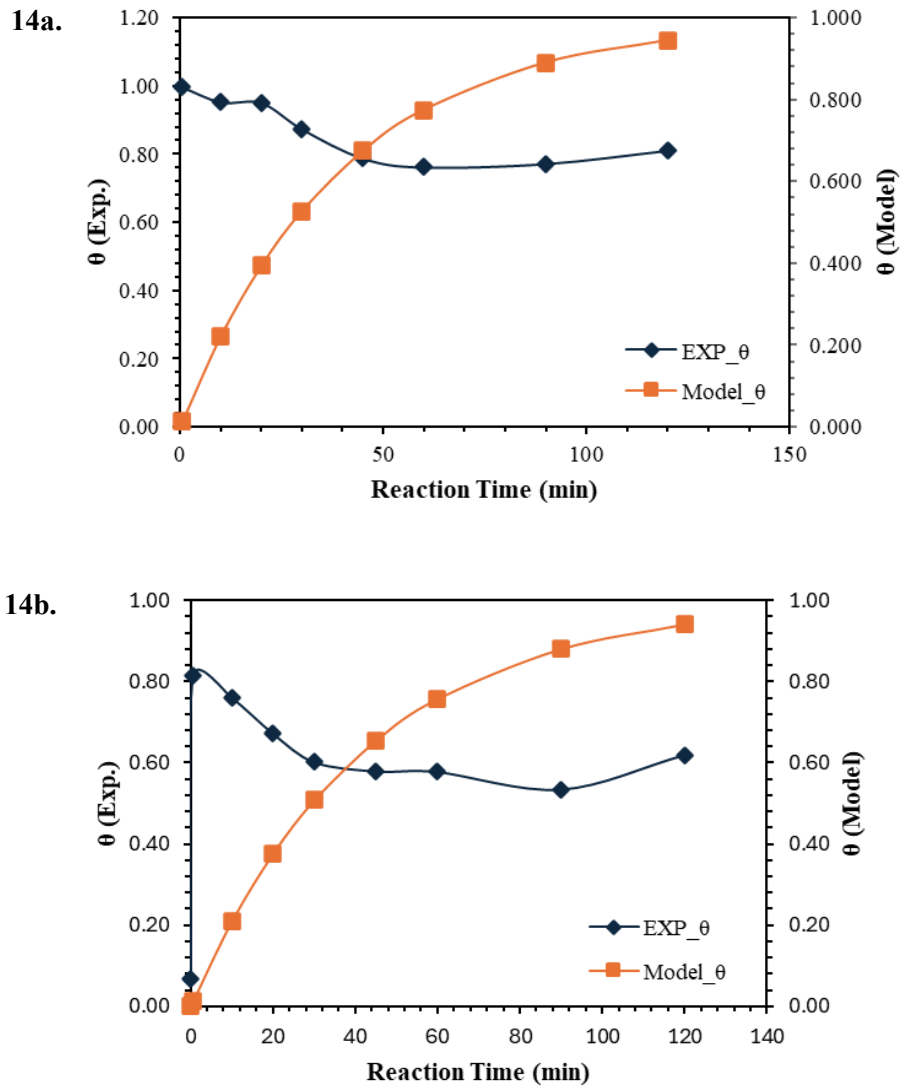

Figure. 14. Comparison of experimental and modeled surface coverage (θ) of REM over time using a). TiO_2, b). ZnO in MQ water

From a modeling standpoint, the theoretical adsorption curves closely followed the general trends observed in both systems. For TiO_2 P25 (Figure 14a), the correlation coefficient (R^2 = 0.8610) reflects a reasonably good fit, though the model slightly overestimates adsorption during the early reaction phase. This suggests potential kinetic delays or surface activation phenomena not fully captured by the model, which assumes immediate site availability and homogeneous surface behavior.

For ZnO (Figure 14b), the model fit was somewhat less consistent, with an R^2 of 0.8747, though still acceptable. Interestingly, while ZnO showed excellent real-world adsorption

efficiency, the model consistently underestimated experimental θ values at intermediate times (20–90 minutes), implying that the kinetic parameters (e.g., Kads = 0.0236) may not fully account for complex interactions such as surface heterogeneity or diffusion effects. Notably, ZnO model also incorporated a desorption rate constant of effectively zero, reinforcing the strong retention behaviour experimentally observed.

Another point of interest is the sum of squared errors (SSE), which remains very low for both systems (SSE = 0.000 for TiO_2 and 0.0044 for ZnO at t = 0), indicating high agreement between modeled and experimental starting points. However, for ZnO, error accumulation becomes more pronounced at longer times, likely due to oversimplified assumptions in the model (e.g., no desorption, constant adsorption rate).

The kinetic constants derived suggest that TiO_2 P25 and ZnO operate under similar total rate constants (0.0253 and 0.0236 min^{-1} respectively), yet the absence of measurable desorption in ZnO implies a more strongly adsorbing surface or possibly a stronger chemical interaction (e.g., through surface complexation). TiO_2 P25, while slightly more accurate in terms of model fit, appears to allow minor reversibility in surface interaction, which may influence long-term stability and regeneration behaviour. These findings have practical implications. ZnO is more irreversible adsorption behaviour may be beneficial in applications requiring maximum removal efficiency, though it could pose challenges for photocatalyst regeneration. TiO_2 P25, on the other hand, offers a slightly more reversible system, potentially enhancing its reusability despite a marginally lower adsorption capacity.

The performance of TiO_2 P25 and ZnO photocatalysts was further evaluated in TW and SW to simulate more realistic environmental conditions. The results reveal a clear divergence between theoretical predictions and actual experimental outcomes, particularly regarding adsorption and desorption efficiency.

15a.

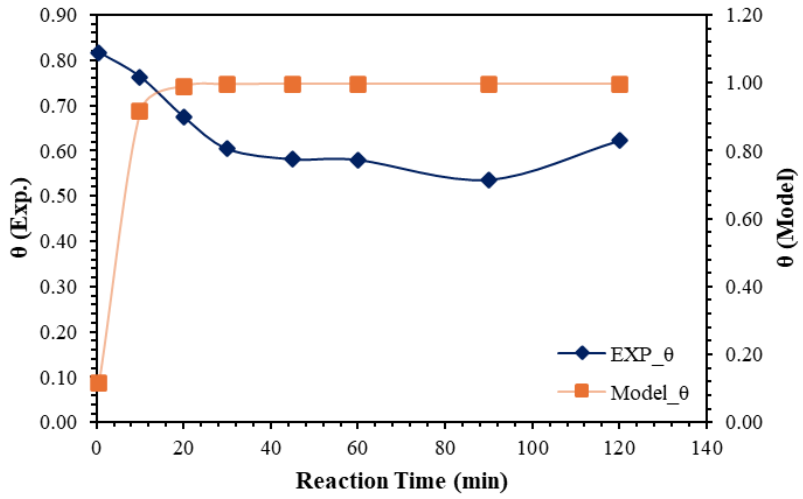

15b.

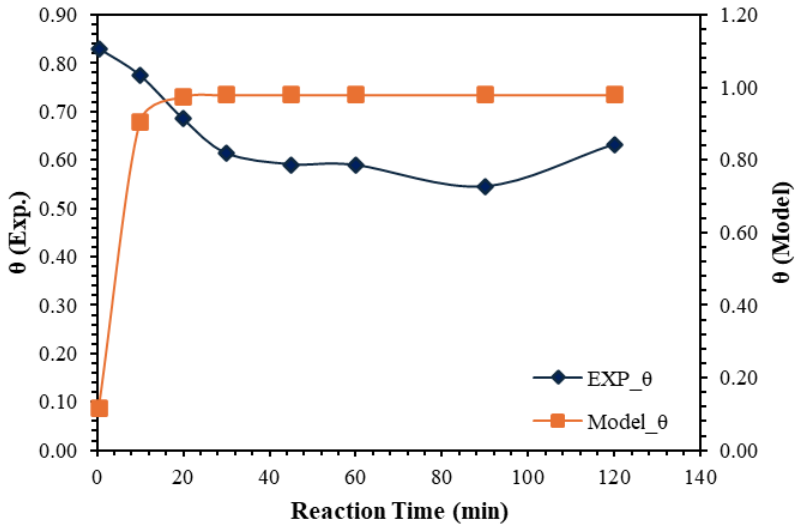

Figure. 15. Comparison of experimental and modeled surface coverage (θ) of REM over time using a). TiO_2, b). ZnO in TW

In TW, TiO_2 P25 theoretically achieved 99.60% adsorption with minimal 40% desorption, suggesting near-complete surface coverage under ideal conditions. However, in real water samples, experimental adsorption dropped to 81%, while desorption increased significantly to 18%. This discrepancy indicates the influence of water matrix components such as natural organic matter, competing ions, or pH variability, which may interfere with the active sites or displace adsorbed species (Figure 15a). For ZnO, the trend was similar. The theoretical adsorption and desorption were 98% and 1.96%, respectively, yet experimental values showed only 81% adsorption and a significantly elevated 18% desorption (Figure 15b). These results highlight the more pronounced impact of matrix interference on ZnO, likely due to its surface charge sensitivity or lower resistance to ionic competition compared to

TiO_2 P25. Overall, the comparison suggests that while both photocatalysts show high efficiency in controlled environments, their real-world performance can be substantially compromised by matrix complexity. TiO_2 P25 generally maintains better stability, with slightly lower desorption than ZnO, making it more robust for practical applications in natural or wastewater systems. Detailed kinetic parameters are reported in Table 12.

Table.12. Kinetic parameters−Two-phase adsorption desorption model for remdesivir under light conditions

Process	Water matrices	*Kads.*	*Kdes*, min^{-1}	*Kt*, min^{-1}	θ_{max} Model	θ_{max} Exp.	$^a\theta_{eq}$	R^2
UV-TiO_2 P25	MQW	0.0251	0.0002	0.0253	0.94	1.00	0.99	0.8610
	TW	0.0250	0.001	0.0251	1.00	0.82	1.00	0.8553
	SW	0.0118	0.0000	0.0118	0.74	0.99	1.00	0.9655
UV- ZnO	MQW	0.0236	0.0000	0.0236	0.94	0.81	1.00	0.8747
	TW	0.2500	0.0050	0.2550	0.98	0.83	0.98	0.8226
	SW	0.0100	0.0001	0.0010	0.67	0,99	0.91	0.9655

a). Surface coverage at equilibrium

The performance of TiO_2 P25 and ZnO in SW reveals significant deviations from theoretical expectations, highlighting the challenges of translating controlled laboratory models into real-world applications. Under ideal conditions, TiO_2 P25 was predicted to achieve 100% adsorption with 0% desorption, implying complete and stable uptake of the target compound. However, experimental results in SW demonstrated a substantial drop in performance, with only 5% adsorption and an unexpectedly high 56% desorption (Figure 16a). This sharp contrast strongly suggests that the matrix composition; potentially rich in natural organic matter, inorganic ions, or competing contaminants, significantly interferes with both adsorption kinetics and surface stability.

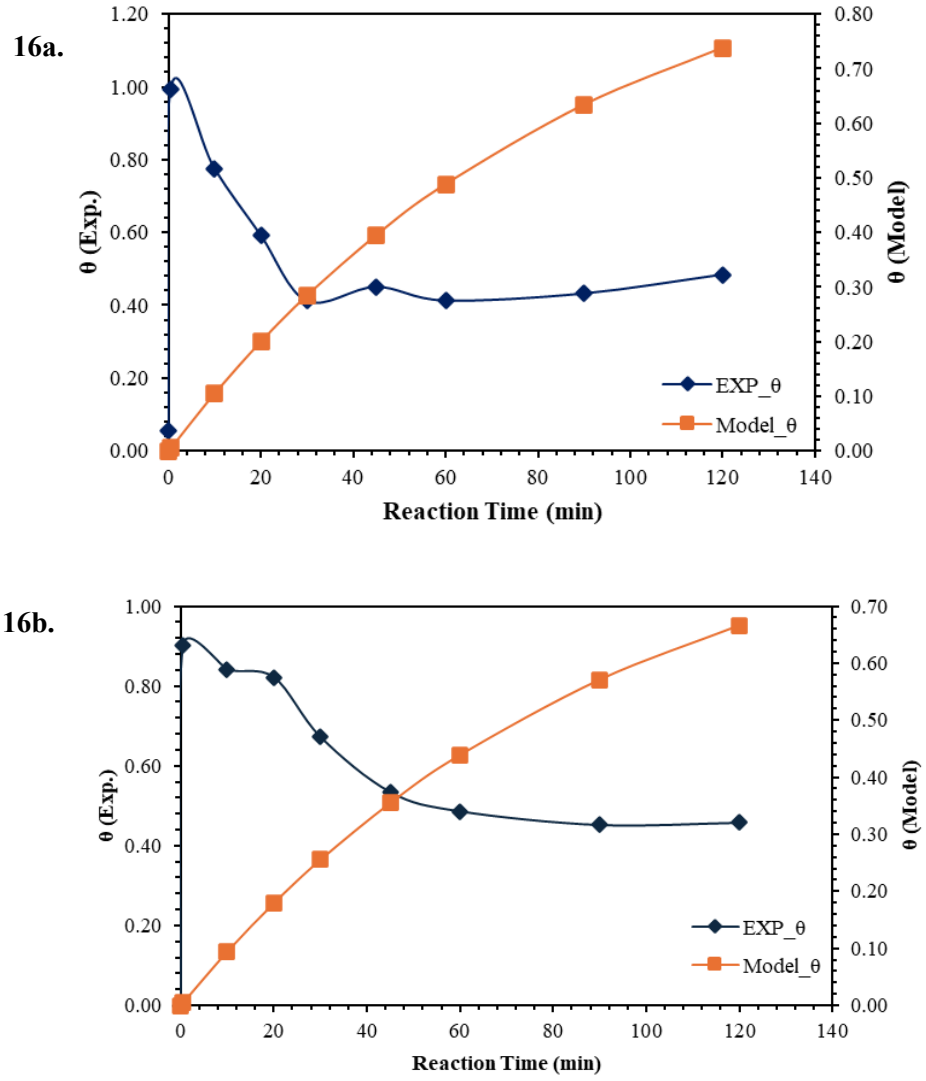

Figure. 16. Comparison of experimental and modeled surface coverage (θ) of REM over time using a). TiO_2 P25, b). ZnO in SW

ZnO (Figure 16b) followed a similarly concerning trend. Although theoretical estimations (based on TiO_2 parameters) suggested 91% adsorption and 9% desorption, the actual recorded values were 1% adsorption and 37% desorption. These results point to ZnO being even more susceptible to interference in complex aqueous environments, likely due to differences in surface chemistry, point of zero charge, and lower resistance to competitive adsorption or surface passivation.

The low performance of both photocatalysts in SW underscores an important practical consideration: adsorption efficiency in real water systems cannot be reliably inferred from idealized kinetic models alone. The presence of background solutes, fluctuating pH, or

suspended solids may block active sites, destabilize adsorbed species, or alter catalyst surface properties; ultimately leading to reduced uptake and increased desorption.

Overall, these findings emphasize the necessity for site-specific evaluations and robust photocatalyst designs that can withstand the physicochemical complexity of real water matrices. While TiO_2 P25 retains a marginally higher stability compared to ZnO, both materials require further surface modifications or operational strategies to ensure consistent performance in non-ideal conditions.

4.1.4. Sorption tests (Dark experiments)

To ensure the chemical stability and degradation efficiencies of the selected drug pollutants in aquatic environment, dark experiments performed. These experiments are important to perform to validate and to make sure either it is degradation or adsorption.

For IPN, dark tests were performed using seven different semiconductors:TiO_2 P25, ZnO, ZrO_2, $BaWO_4$, Ag-TiO_2, $BaTiO_3$, and SnO_2. Each photocatalyst was tested at highest dosages, 10.0 mg/L in MQ water due to its high purity. Results revealed that TiO_2 P25 and ZnO achieved the highest removal efficiencies, with 33% and 26% drug degradation observed after 90 minutes, respectively. $BaTiO_3$, $BaWO_4$, Ag–TiO_2, ZrO_2, and SnO_2 exhibited lower removal rates ranging from 4% to 22% after 2 hours (Figure 17). IPN followed pseudo degradation first order kinetics as shown in Table 13. In contrast, similar experiments were conducted with other pollutant used in this study i.e., RTR, with selected photocatalysts (TiO_2 P25, ZnO, and SnO_2:ZnO (2:1) and with REM (TiO_2 P25, and ZnO), under similar conditions.

Table.13. Kinetic parameters−first-order pseudo constants of isoprinosine degradation in MQ-water

Process	*Conc., mg/L*	[a]*Kt*, min^{-1}	[b]½ t , min^{-1}	[c]R^2
Dark-TiO_2 P25	10.0	0.0034	203.9	0.7815
Dark- ZnO	10.0	0.0009	770.2	0.9549
Dark - ZrO_2	10.0	0.0001	6931.5	0.9557
Dark - $BaWO_2$	10.0	0.0002	3465.7	0.9275
Dark - Ag-TiO_2	10.0	0.0001	6931.5	0.9407
Dark - $BaTiO_3$	10.0	0.0001	6931.5	0.8441
Dark - SnO_2	10.0	0.00008	8664.3	0.9454

a). Pseudo first order kinetic rate constant, b). Half-life of the reaction, c). Coefficient of determination.

17.

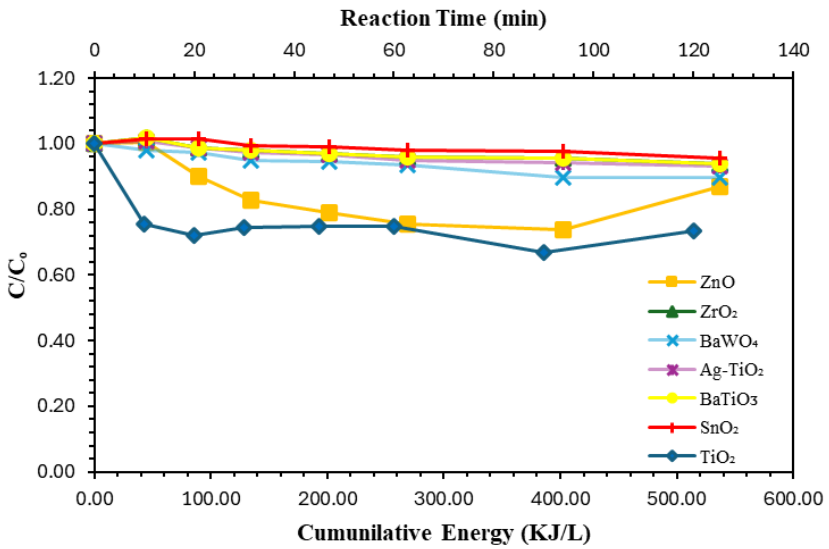

Figure. 17. Sorption test (dark experiments) of degradation of IPN in MQ water

According to Figure 18, RTR showed strong adsorption within the 30 seconds of the reaction with the highest KL values of 12515 mg/L (TiO_2 P25), 823.33 mg/L (ZnO), and 555432.1 mg/L (SnO_2:ZnO). The highest KL values as well as q_{max} values indicated the strong adsorption of RTR on to the selected photocatalysts. All the experiments with RTR followed Langmuir isotherm adsorption model (Table 14).

Table.14. Kinetic parameters−first-order pseudo constants of RTR adsorption.

Process	**Conc., mg/L**	**[a]*Kt*, min^{-1}**	**[b]KL, L/mg**	**[c]q_{max}, mg/g**	**[d]R^2**
Dark-TiO_2 P25	10.0	0.0325	1625	30.77	0.9996
Dark- ZnO	10.0	0.2276	11380	4.39	0.9998
Dark- SnO_2: ZnO	10.0	0.2572	36743	3.89	0.9990

a). Pseudo first order kinetic rate constant, b). Langmuir constant, c). Maximum adsorption capacity, d). Coefficient of determination.

Since these experiments were conducted in the absence of light, where photocatalytic activity is inactive, the observed reductions are attributed to adsorption of drug molecules onto the surface of the semiconductor particles rather than chemical degradation. The relatively high adsorption capacities of TiO_2 P25 and ZnO are likely due to their high surface area, hydroxyl-rich surfaces, and favorable surface charges that enhance interactions with the drug. The dark condition results serve as a baseline for understanding physical removal mechanisms and highlight the importance of distinguishing between adsorption and true photodegradation when evaluating the efficacy of semiconductor-based water treatment systems. This emphasizes that adsorption plays a role in initial removal, effective and sustained degradation requires photoactivation of the catalysts. For transparency and reproducibility, supporting HPLC data has been documented. Please refer to the supporting information section (Chapter 8).

18.

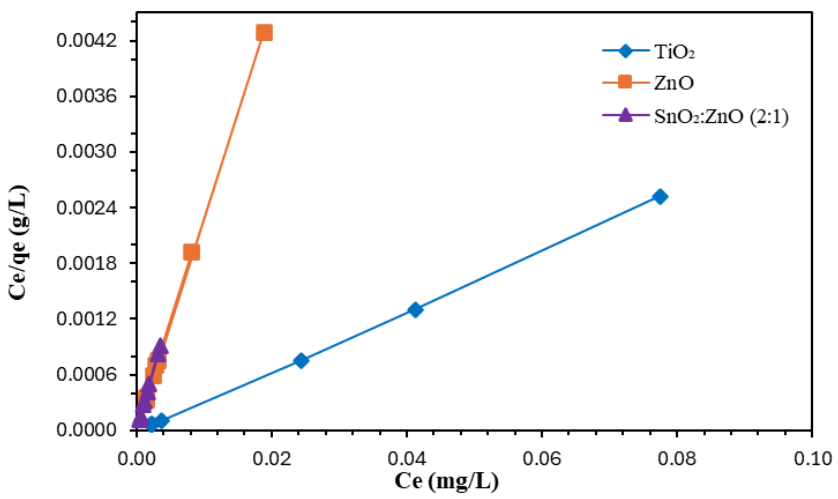

Figure. 18. Sorption test (dark experiments) of degradation of RTR in MQ water

In case of REM, adsorption–desorption kinetics on the selected photocatalyst (TiO_2 P25 and ZnO) under dark conditions were successfully modeled using a two-parameter equilibrium approach. A strong agreement between the experimental and modeled surface coverage (θ) was observed, with a R^2 value 0.9624 and 0.9197, TiO_2 P25 and ZnO, respectively, indicating excellent predictive capability of the model (Table 15).

Table.15. Kinetic parameters−Two-phase adsorption desorption model for remdesivir under dark conditions

Process	*K*ads min^{-1}	*K*des min^{-1}	*K*t min^{-1}	θ_{max} Model	θ_{max} Exp.	$^{a}\theta_{eq}$	R^2
Dark- TiO_2 P25	0.0102	0.0015	0.0117	1.00	0.91	0.87	0.9624
Dark- ZnO	0.0151	0.0029	0.0179	1.00	0.96	0.84	0.9197

a). Surface coverage at equilibrium.

The experimental data represented in (Figure 19a), desorption dominates after 10 min, likely due to reversible or weak adsorption. This predicts a steady-state adsorption consistent with equilibrium kinetics, but experimental data reveal a sharp decrease in adsorbed fraction after initial uptake, indicating significant desorption likely driven by weak interactions or environmental effects. This deviation supports a diffusion-limited and reversible adsorption mechanism. In addition, a high coefficient of determination (R^2 = 0.9624) between the

experimental and modeled surface coverage (θ) validates the reliability of the adsorption–desorption kinetic model for REM removal using the TiO_2 P25.

19a.

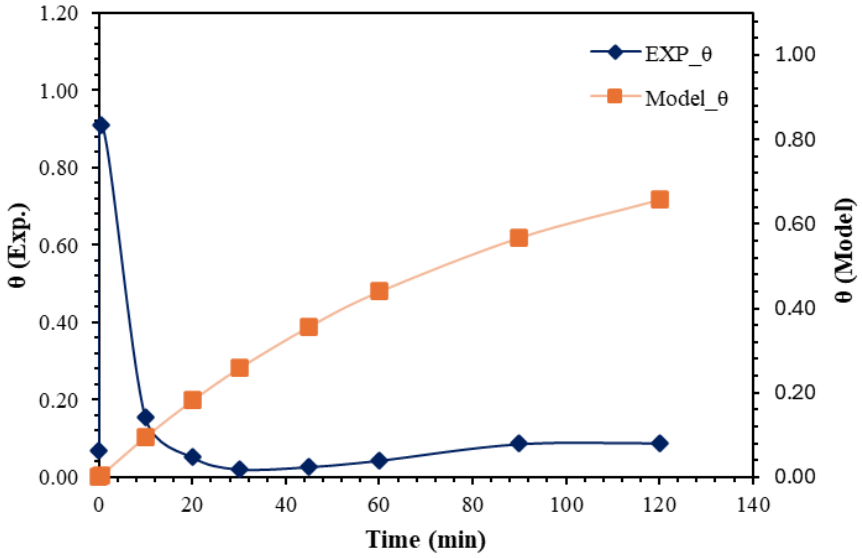

19b.

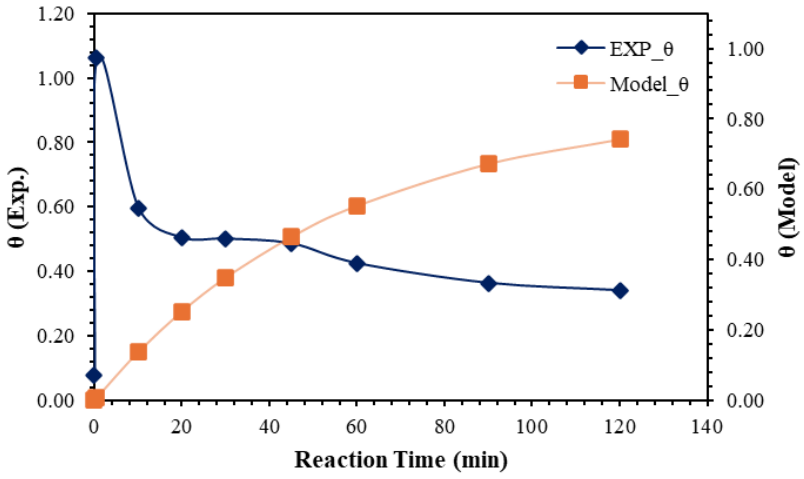

Figure. 19. Comparison of experimental and modeled surface coverage (θ) of REM over time under dark condition using a). TiO_2 P25, b). ZnO

In the case of ZnO, (Figure 19b), a flat model θ curve over time indicates that the system rapidly reaches equilibrium between the free drug molecules and those bound to the ZnO surface. This supports the conclusion that the adsorption–desorption dynamics are fast and that changes in surface loading are minimal after equilibrium is established. Furthermore, the adsorption and desorption rates are both high, also indicating a rapid dynamic equilibrium between bound and unbound REM molecules. Since kdes > kads, desorption is

slightly more dominant, which may suggest that concentration rebounds over time (after initial drop).

The kinetic constants kads and kdes, optimized using Excel Solver, captured the rapid initial adsorption followed by desorption over time. This model accurately reflects the dynamic interaction between REM molecules and the photocatalyst surface under the dark experimental conditions. The use of a two-parameter adsorption–desorption kinetic model, incorporating the adsorption rate constant (kads) and desorption rate constant (kdes), provides a mechanistic understanding of the interaction between REM and the photocatalyst surface. This approach captures both the initial binding of drug molecules to active sites and their potential release back into the solution, which aligns with the experimental observation of concentration rebound over time. Unlike simplified pseudo-first or pseudo-second-order models that assume irreversible uptake or equilibrium, this dual-parameter framework accounts for the dynamic nature of surface interactions, especially under photocatalytic conditions. The model's strong predictive performance, based on the R^2 values, confirms that considering both adsorption and desorption pathways is a more appropriate and realistic strategy for systems where physical or reversible adsorption plays a significant role.

4.1.5. Photolysis assisted with H_2O_2

In AOPs, one of the primary sources of hydroxyl radicals (•OH) is hydrogen peroxide (H_2O_2). To assess the degradation susceptibility of the drugs used in this study, varying concentrations of H_2O_2, i.e., 125 µL (108.8 mg/L), 250 µL (217.5 mg/L), and 500 µL (435 mg/L) were utilized in the presence of solar light (500 W/m^2) in Milli-Q water (MQW), chosen for its high purity. Since in real aquatic environment, water components like organic anions, cations, and natural organic matter influence the degradation of pollutants by scavenging radicals during AOP processes (D. Li et al., 2022). Figure 20a presents the results of the degradation of the antiviral drug IPN under UV-assisted conditions with H_2O_2 at the concentrations mentioned above. The findings indicate that IPN is completely degraded (100%) with 125 µL and 250 µL of H_2O_2 after 30 minutes of reaction time. In contrast, with 500 µL of H_2O_2, IPN achieved complete degradation within 120 minutes. For the second drug, RTR, complete degradation (100%) was achieved within 45 minutes across all tested concentrations of H_2O_2 (Figure 20b).

Table.16. Kinetic parameters−first-order pseudo drug degradation constants of selected drugs in MQ water at irradiance 500 W/m²

Process	Volume of H_2O_2 (µL)	Drugs	Conc., mg/L	^1Kt, min^{-1}	½ t , min^{-1}	R^2
UV – H_2O_2	125.0	IPN	10.0	0.0050	138.6	0.9373
	250.0			0.0064	108.3	0.9844
	500.0			0.0302	22.95	0.9473
UV - H_2O_2	125.0	RTR	10.0	0.0069	100.5	0.9009
	250.0			0.0068	101.93	0.9180
	500.0			0.0475	14.59	0.8938
UV - H_2O_2	125.0	REM	10.0	0.0010	693.1	0.9906
	250.0			0.0009	770.2	0.9628
	500.0			0.0076	91.2	0.9784
Dark - H_2O_2	500.0	IPN	10.0	0.0018	385.1	0.7710
		RTR		0.0005	1386.3	0.9851
		REM		0.0013	533.2	0.7931

In the case of REM, the first FDA-approved drug used to treat COVID-19, degradation rates were 55% for 125 µL, 53% for 250 µL, and 83% for 500 µL of H_2O_2 after 120 minutes of the process (Figure 20c). Among these processes, the highest pseudo-drug degradation was observed in RTR (kt = 0.0475) with an R^2 value of 0.8938 with a dose of 500 µL H_2O_2. The pseudo-drug degradation kinetics of each experiment are presented in Table 16. It has been observed that after adding H_2O_2, the degradation efficiency is improved as compared to photolysis experiment. According to previously published work, the degradation of the antiviral drug favipiravir (FAV) was investigated using a UV/H_2O_2 system with various concentrations of H_2O_2. After 15 minutes, the degradation rates of FAV were recorded as follows: 46.2%, 66.6%, 77.6%, 98.8%, and over 99% for H_2O_2 concentrations of 0, 1, 2, 5, and 10 µM, respectively. Initially, FAV exhibited rapid degradation at a fixed dose of H_2O_2, but its concentration gradually declined over time ($p < 0.05$) (Eryildiz-Yesir et al., 2025). This phenomenon is attributed to the substantial generation of unselective hydroxyl radicals

(•OH) within the UV/H_2O_2 system, which effectively decompose micropollutants in wastewater (Rosario-Ortiz et al., 2010).

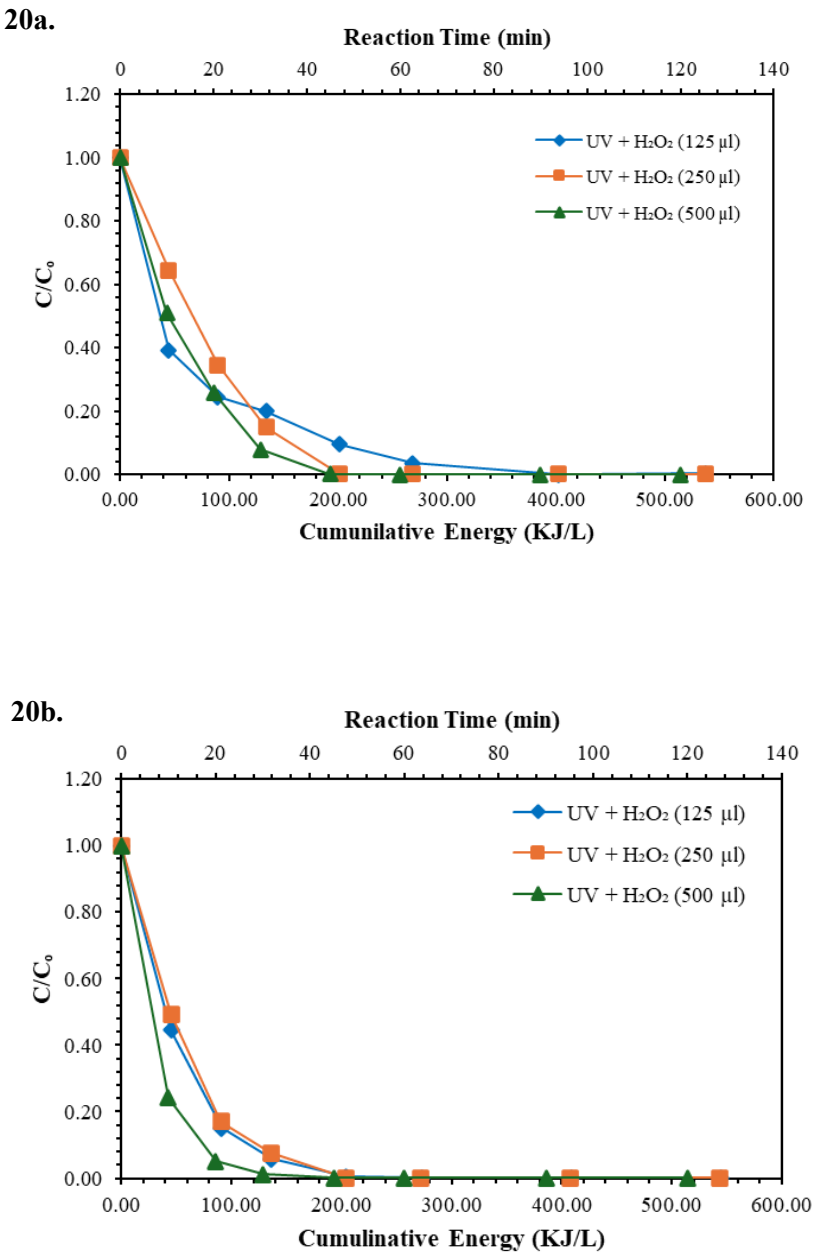

Figure. 20. UV - assisted H_2O_2 degradation of a). IPN, and b). RTR at different concentration of H_2O_2 in MQ water

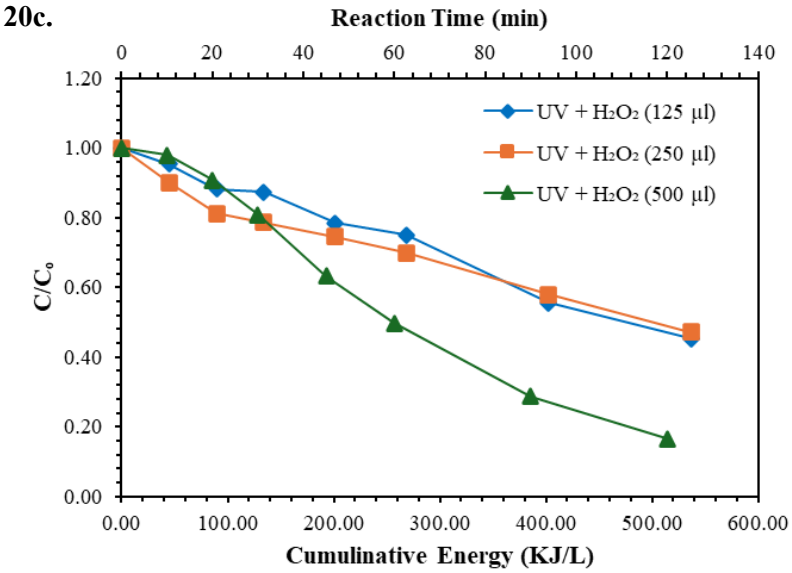

Figure. 20c. UV - assisted H_2O_2 degradation of REM at different concentration of H_2O_2 in MQ water

In addition, dark experiments were performed to confirm the efficiency of H_2O_2 (500 µL) in removal of selected pharmaceuticals and results are given in Figure 21. Under dark condition, the removal efficiencies of selected pharmaceuticals IPN, RTR, and REM are 46%, 25%, and 18% , respectively, after 120 minutes of the process. The highest pseudo drug degradation kinetic constant was observed in IPN (0.0018 min^{-1}) with R^2 value of 0.7710 (Table 16). To avoid photo-induced degradation, pharmaceutical degradation tests are conducted in a dark environment. Numerous drugs are light-sensitive and break down in the presence of light, which might change the chemical structure and effectiveness of the drugs (Mansouri et al., 2021b). In addition, degradation without irradiance suggests clearer picture of drug's stability to ensure that any degradation observed is caused by something other than light exposure.

21.

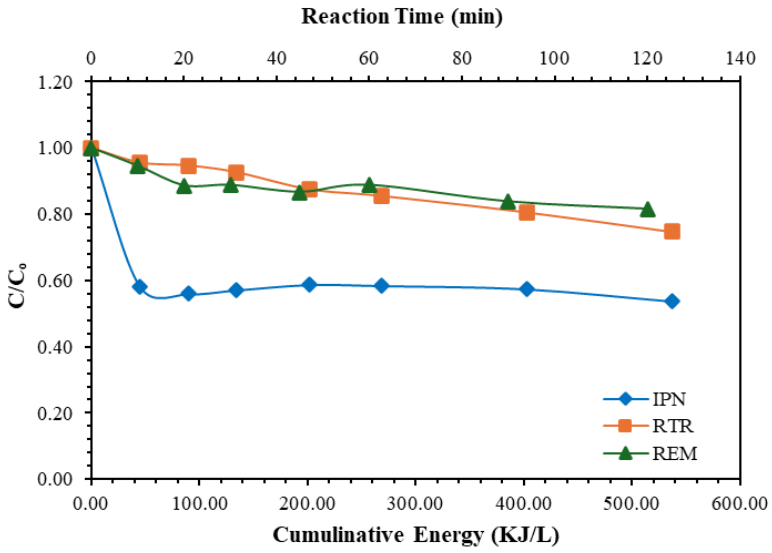

Figure. 21. Degradation of selected drugs using H_2O_2 (500 µL) under dark conditions in MQ water

4.1.6. Photocatalytic degradation of IPN in the presence of selected anions

4.1.6.1 Effect of SO_4^{-2} ions in degradation of IPN

Figure 22a presents the rate of concentration decreases of IPN in MQ water in the presence of SO_4^{-2} ions using selected heterogeneous photocatalysts, i.e., TiO_2 P25, ZnO, and SnO_2, with an amount of 20.0 mg/L each. The investigation revealed that with the exposure of solar light irradiance at 500 W/m^2 for about 120 minutes, the rate of degradation of IPN was <LOQ: 86%, <LOQ: 84%, and <LOQ: 25% of TiO_2 P25, ZnO, and SnO_2, respectively, in the presence of 2.0 mg/200 ml of IPN and 250 mg/L of SO_4^{-2} ions. In contrast, the rate of degradation of IPN in TW Figure 22b, with 20.0 mg/L of TiO_2 P25, ZnO, and SnO_2, the <LOQ: 69%, <LOQ: 72%, and <LOQ: 19% observed after 120 minutes of the process, respectively. The degradation kinetics of the above-mentioned results follow a pseudo-first-order reaction. Table 17 lists the kinetic parameters of the results. The experimental data of this study matches the regression model, according to the coefficient of determination (R^2). The findings imply that the IPN in water matrices can be removed by raising the dosage of the chosen photocatalyst.

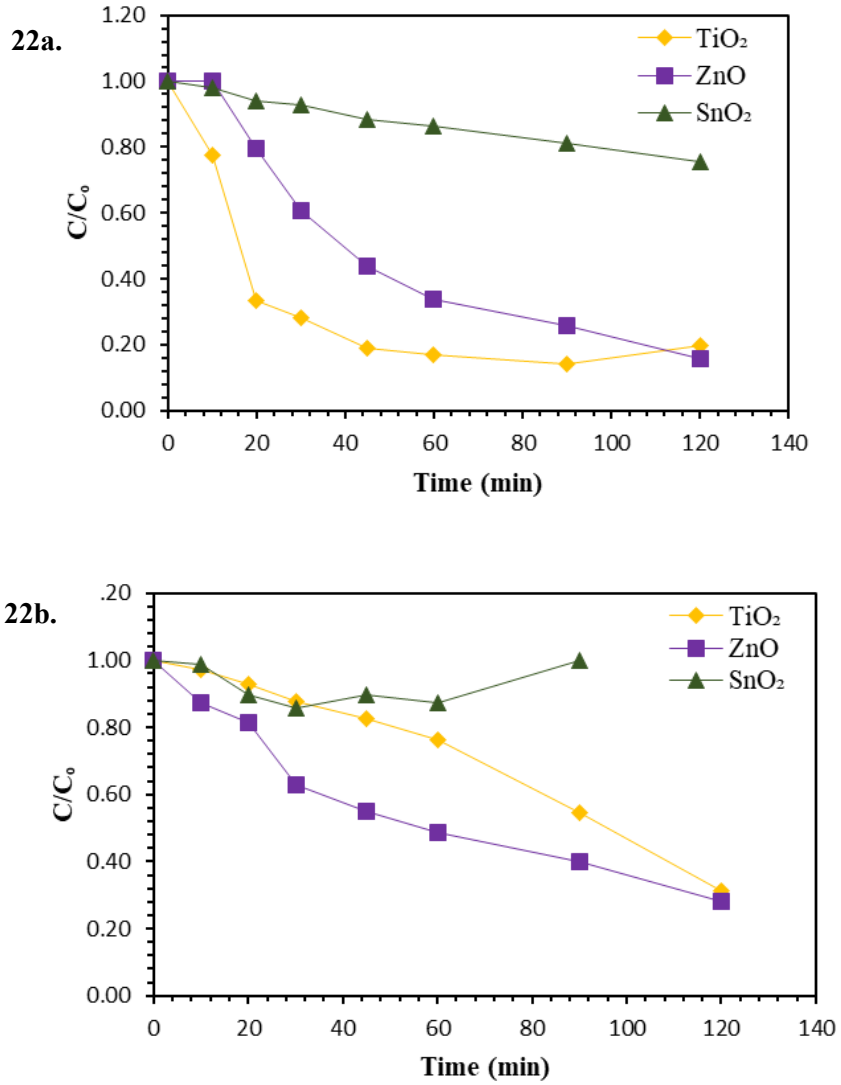

Figure. 22. Degradation of IPN in the presence of SO_4^{-2} ions in (a) MQW (b) TW

The mechanism underlying the heterogeneous photo-catalysis pathway, compounds undergo decomposition only when they are either adsorbed on the surface of the photocatalyst or near it, thereby initiating a reaction with $OH^{\bullet}$ radicals. Reactive sulfate anion radicals $SO_4^{\bullet -}$ were produced because of organic pollutants being broken down by sulfate ion radiation because SO_4^{-2} ions lose an electron to valance band holes or to a $OH^{\bullet}$ radical of photocatalysts surface and became $SO^{\bullet -}$ radical (equation 10 and 11).

$$SO_4^{-2} + h^{+} \longrightarrow SO_4^{\bullet -} \qquad (10)$$

$$SO_4^{-2} + OH^{\bullet} \longrightarrow SO_4^{\bullet -} + OH^{-} \qquad (11)$$

The research findings reveal the edge of the method used to adsorb on SO_4^{-2} ions on the outer layer of selected photocatalysts (TiO_2 P25, ZnO, and SnO_2). It also suppresses the breakdown of IPN against its oxidation by $SO^{\bullet-}$ radicals. Also sulfate radicals facilitate the degradation process of IPN by enhancing the formation of radicals. Moreover, the reaction conditions and the intermediates created during the process determine the precise type of degradation products.

4.1.6.2 Effect of Cl^- ions in degradation of IPN

The findings from the experiment on the photocatalytic removal of a 2.0 mg/200 ml IPN solution containing 20.0 mg/L of each selected photocatalyst (TiO_2 P25, ZnO, and SnO_2) individually, in the presence of 250 mg/L chloride ions, are presented in figures (23a & 23b) for two different water matrices (MQW and TW). In MQ water, <LOQ: 91% w.r.t. TiO_2 P25 with the passage of 90 minutes of the process, <LOQ: 86% (ZnO), and <LOQ: 21% (SnO_2), with reaction time of 120 minutes had been observed. However, in TW, the degradation of IPN was 53% (TiO_2 P25), 67% (ZnO), and 13% (SnO_2) after 120 minutes for TiO_2 P25 and ZnO and 30 minutes for SnO_2. The highest pseudo-drug degradation rate observed was Kt = 0.015 min^{-1} with a correlation (R^2) value of 0.7239 in MQ water concerning TiO_2 P25. Table 18 shows the kinetic parameters of pseudo first order drug degradation.

23a.

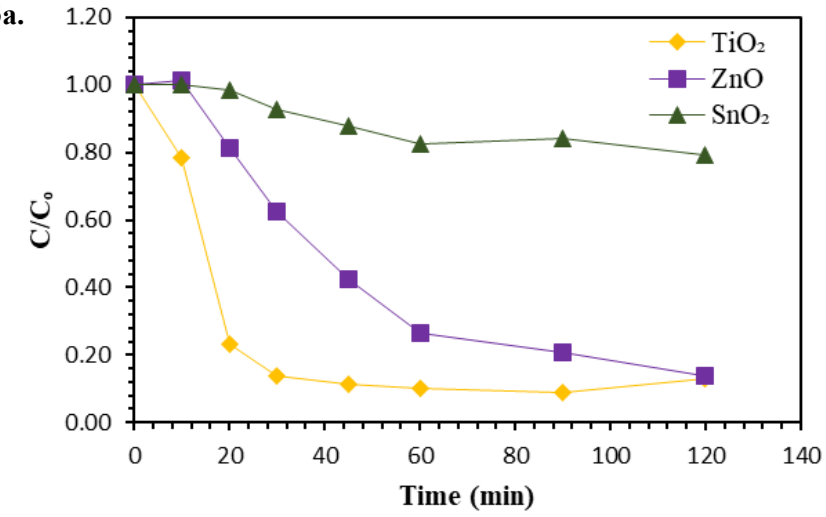

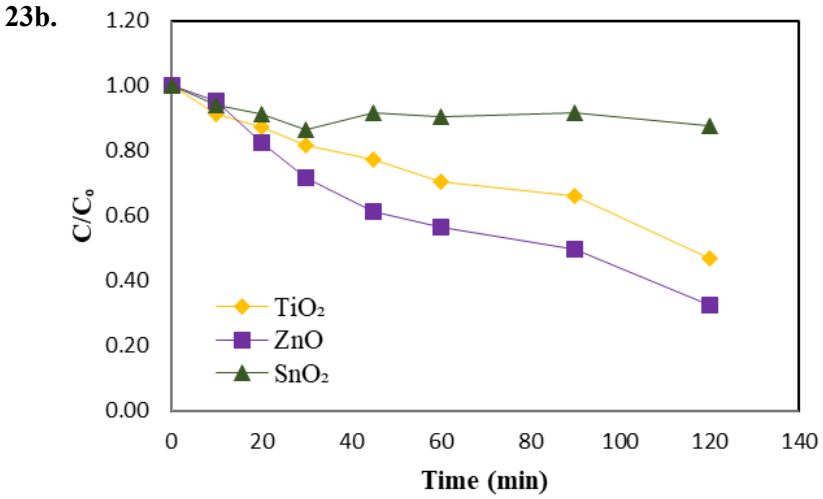

Figure. 23. Degradation of IPN in the presence of Cl^- ions in (a) MQ water (b) TW

During the photocatalytic process, the interaction between Cl^- and positive e^- holes (h^+) / $OH^\bullet$ radical (Chi et al., 2020) reported that chloride ion could quench h^+ and hydroxyl radical to produce chloride radical ($Cl^\bullet$) and chloro-hydroxide anion radical ($ClOH^{\bullet-}$) respectively. Chloride ions inhibit photocatalysis through $OH^\bullet$ scavenging radicals and it can scavenge positive electron holes. However, among these reactions, equations (12-15), no superoxide anions ($O^{\bullet-2}$) radical was involved, indicating that superoxide anions ($O^{\bullet-2}$) radical quenching involving h^+ and $OH^\bullet$ is not a direct process themselves.

$$Cl^- + h^+ \longrightarrow Cl^\bullet \qquad (12)$$

$$Cl^- + OH^\bullet \longrightarrow ClOH^{\bullet-} \qquad (13)$$

$$ClOH^{\bullet-} \longrightarrow OH^- + Cl^\bullet \qquad (14)$$

$$Cl^\bullet + Cl^- \longrightarrow Cl^{\bullet-} \qquad (15)$$

The above-mentioned radicals and compounds are considered as well-known oxidants. Their chemical structure and functional groups (alkyl, alcohol, amide, acid, etc.) are related to their capacity to break down organic molecules. (Soufan et al., 2012) reported that, in the presence of Cl^-, the degradation of diclofenac sodium salt, an anti-inflammatory drug (NSAID) with analgesic, antipyretic and anti-inflammatory activity was not satisfactory at pH 7 because of the deprotonation of HOCl to produced ClO^- at a pH level over 6. Generally, ClO^- has an insignificant reactivity, especially with ionized organic molecules.

Table. 17. Kinetic calculation of pseudo first order rate of degradation of IPN

Photocatalysts	Water matrices	Anions	K_t[a], min^{-1}	R^2	$t_{½}$[b], min^{-1}
TiO_2 P–25	MQW	SO_4^{-2}	0.0088	0.6554	78.76
		Cl^-	0.0150	0.7239	46.20
		NO_3^-	0.0334	0.8875	20.75
		CO_3^{-2}	0.0331	0.9910	87.17
	TW	SO_4^{-2}	0.0481	0.9862	14.41
		Cl^-	0.0040	0.9688	173.28
		NO_3^-	0.0073	0.9727	94.95
		CO_3^{-2}	0.0087	0.9671	79.69
ZnO	MQW	SO_4^{-2}	0.0075	0.8570	0.81
		Cl^-	0.0102	0.9067	0.76
		NO_3^-	0.0080	0.7916	8.66
		CO_3^{-2}	0.0231	0.9473	30.01
	TW	SO_4^{-2}	0.0057	0.9082	121.60
		Cl^-	0.0054	0.9348	128.36
		NO_3^-	0.0066	0.9132	105.02
		CO_3^{-2}	0.0080	0.9321	86.64
SnO_2	MQW	SO_4^{-2}	0.0020	0.9892	0.70
		Cl^-	0.0019	0.8616	364.81
		NO_3^-	0.0046	0.9854	150.68
		CO_3^{-2}	0.0028	0.9731	247.55
	TW	SO_4^{-2}	0.0052	0.9358	133.29
		Cl^-	0.0043	0.9800	161.19
		NO_3^-	0.0018	0.9877	385.08
		CO_3^{-2}	0.0020	0.9873	346.57

4.1.6.3. Effect of NO_3^- ions in degradation of IPN

The degradation of IPN in the presence of NO_3^- ions in the presence of three different photocatalysts (TiO_2 P25, ZnO, and SnO_2) has been investigated in two different water matrices (MQW and TW). According to EU water guidelines, the recommended concentration limit for NO_3^- ions in water is 50 mg/L. Figure 24a depicts the degradation kinetics of the selected drug in MQ water with the solar light irradiance (500 W/m^2). It has been noted that the concentration of IPN was below its <LOD: 100% after 30 minutes with TiO_2 P25 and after 90 minutes with SnO_2. While in ZnO, the <LOD: 96% was observed, with a reaction time of 120 minutes in Milli-Q water. However, in the case of TW, the <LOQs of 80%, 82%, and 21% were observed in the presence of TiO_2 P25, ZnO, and SnO_2, respectively (Figure 24b). According to a reported study, in IPN photodegradation, using selected photocatalysts in selected water matrices obtained in direct photolysis increased the drug degradation rate of reaction, confirmed by the estimation of the kinetic parameters of these reactions (H. Ahmed & Felis, 2024). Based on the obtained results by UV-TiO_2 P25, the rate constant of IPN is higher in MQ water at 0.0334 min^{-1} with a coefficient of determination (R^2) value of 0.8875. The experimental data of this study (Table 17) followed a pseudo-first-order model. It may imply that raising the dose of the chosen photocatalyst can remove IPN in natural water systems.

Furthermore, in the presence of TiO_2 P25 and SnO_2 in MQ water, nitrate ions play a role in the complete mineralization of target pollutant. The mechanism of participation of NO_3^- ions, in the degradation of targeted pollutants (IPN) is shown in equations 15 to 18:

$$NO_3^- + 2H^+ + 2e^- \longrightarrow NO_2^- + H_2O \qquad (15)$$

$$NO_2^- + OH^- \longrightarrow NO_2 + OH^- \qquad (16)$$

$$NO_3^- + h^+ \longrightarrow {}^{\bullet}NO_3 \qquad (17)$$

$$^{\bullet}NO_3 + H_2O \longrightarrow NO_3^- + OH^{\bullet} + H^+ \qquad (18)$$

According to the reported study by (Gligorovski et al., 2015), NO_3^- ion plays a significant role as a precursor of OH^- under solar light exposure as a powerful oxidizing agent. The reaction of NO_3^- with OH^- radicals is a significant pathway for the degradation of Acyclovir, zidovudine, and lamivudine due to their resistance to direct photolysis (Zhou et al., 2015c).

The impact of nitrate ions on the degradation of pharmaceuticals through the photocatalysis process has become increasingly important in environmental research. However, there have been only a few studies that have investigated the influence of nitrate ions on the degradation of antivirals. Further research is needed to fully understand the role of nitrate ions in the degradation of pharmaceuticals.

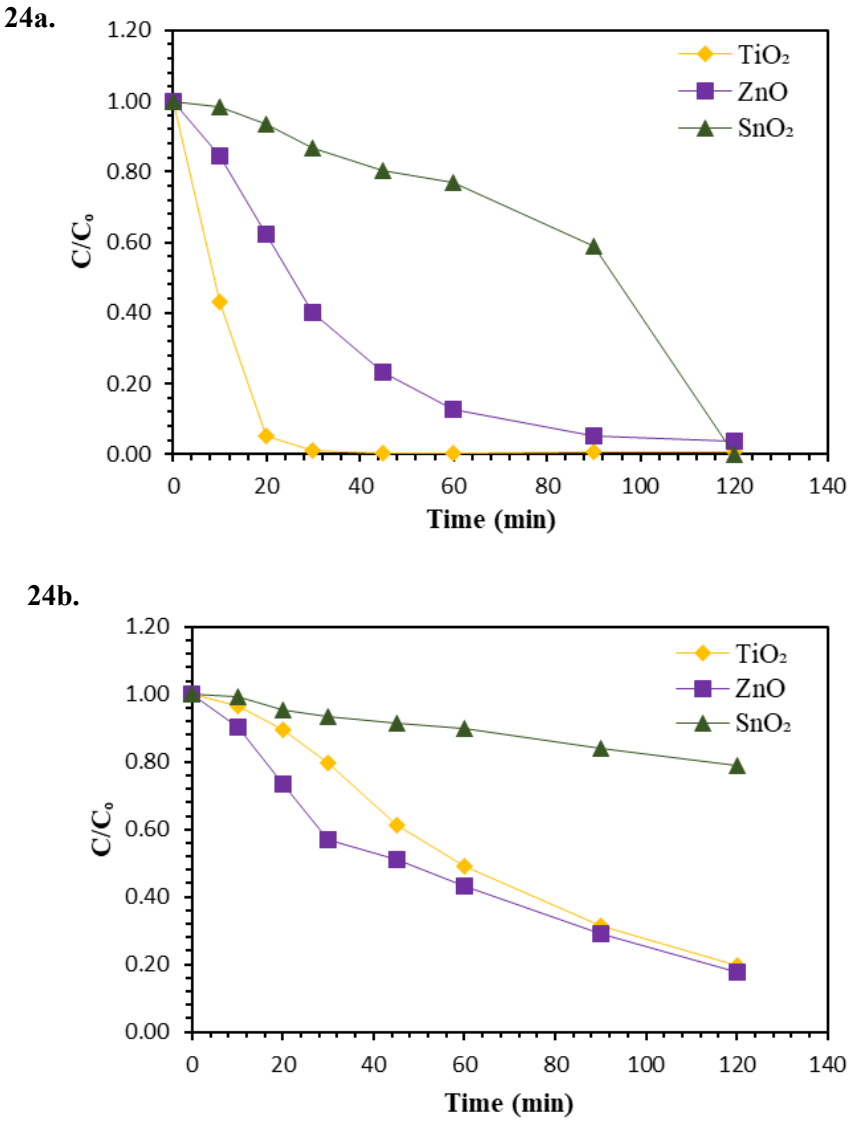

Figure. 24. Degradation of IPN in the presence of NO_3^- ions in (a) MQ water (b) TW

4.1.6.4. Effect of CO_3^{-2} ions in degradation of IPN

Figure 25a & 25b shows the effects of CO_3^{-2} ions in the degradation of selected antiviral drug IPN in two different water matrices in the presence of three different photocatalysts (TiO_2 P25, ZnO, and SnO_2), separately with the recommended concentration of carbonate ions i.e., 250 mg/L in aquatic environment. Our results showed that the concentration of IPN

in MQ water was below its <LOD: 100% after 30 minutes with TiO_2 P25 and after 45 minutes with ZnO, respectively. While in SnO_2, the <LOQ: 29% was observed, with a reaction time of 120 minutes in Milli-Q water. However, in the case of TW, the <LOQs 93%, and 23% were observed in the presence of ZnO, and SnO_2, respectively. In case of TiO_2 P25, the <LOD: 100% after 90 minutes of the reaction was observed.

The principal reactive compound in AOPs is the $OH^{\bullet}$ radical, and the rate of degradation is determined by the bimolecular rate constant of the reactive species and the target molecule. The mechanism of participation of CO_3^{-2} ions, in the degradation of targeted pollutants (IPN) is show in equations 19 and 20:

$$CO_3^{-2} + h^+ \longrightarrow CO_3^{\bullet -} \qquad (19)$$

$$HCO_3^- + OH^{\bullet} \longrightarrow CO_3^{\bullet -} + H_2O \qquad (20)$$

According to (Sánchez-Polo et al., 2013), $CO_3^{\bullet -}$ radicals exhibit higher selectivity and a lower redox potential (1.59 V) when compared to $OH^{\bullet}$ radicals. Organic pollutants can be degraded by $CO_3^{\bullet -}$ radicals. Another reported study, in case of $CO_3^{\bullet -}$ radicals, the rate of reaction for organic pollutants rich in electrons ranges from 10^3 to 10^9 $M^{-1}s^{-1}$ (J. Wang & Wang, 2021). Therefore, the influence of CO_3^{-2} ions on the decomposition of organic pollutants induced by $OH^{\bullet}$ radical depends on the organic pollutants that are being addressed. Furthermore, in CO_3^{-2} ions, the amount of $CO_3^{\bullet -}$ radical was greater than $OH^{\bullet}$ radicals in certain techniques, such as ozone and UV/H_2O_2.

25a.

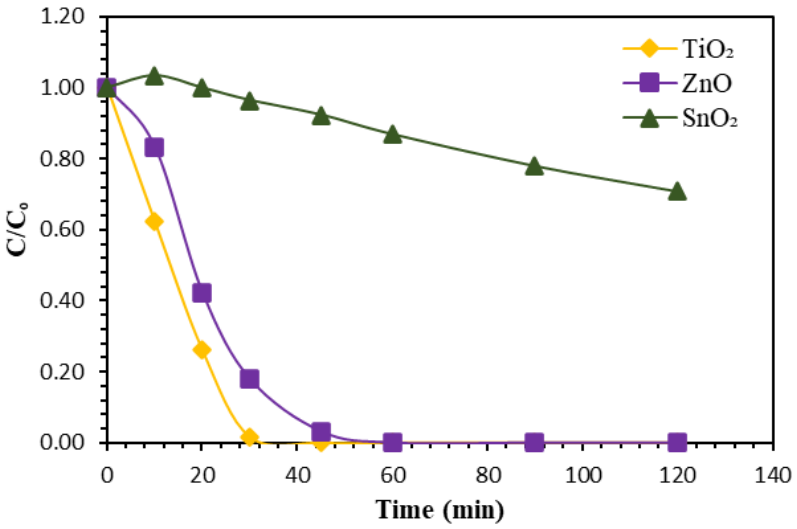

25b.

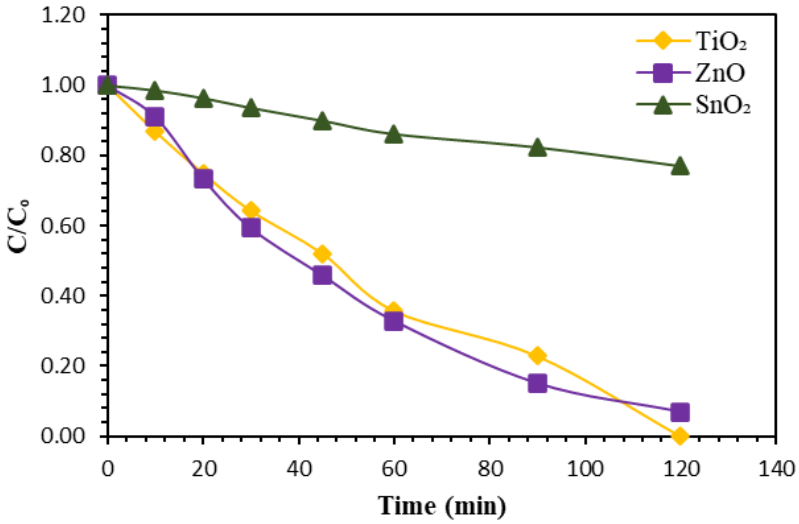

Figure. 25. Degradation of IPN in the presence of CO_3^- ions in (a) MQ water (b) TW

4.1.7. Adsorption of RTR in the presence of selected anions

To conserve time and reagents, analogous experiments were conducted with RTR in the presence of selected inorganic anions. Measurements were taken at only two points: 0 and 0.5 minutes. Preliminary results indicated significant adsorption behavior, consistent with earlier observations of RTR in the absence of inorganic ions. Due to the limited number of data points, graphical representation was not feasible. Nonetheless, the findings support the conclusion that RTR primarily undergoes adsorption rather than degradation. For transparency of the results, screenshots of the HPLC displays are provided in the supporting information section (Chapter 8).

4.1.8. Solar-induced mineralization of organic matter in selected water samples

The photodegradation behavior of selected drugs (IPN, RTR, and REM) under solar irradiation was assessed in three different water matrices: MQW, TW, and SW, over a 120-minute exposure period. In case of IPN, results revealed that in MQW, a significant reduction in Total Carbon (TC), Non-Purgeable Organic Carbon (NPOC), and Total Nitrogen (TN) was observed, indicating effective photodegradation of the drug in a simplified, contaminant-free matrix. Specifically, TC decreased from 18.91 mg/L to 3.02 mg/L, and TN dropped from 4.520 mg/L to 0.242 mg/L. Interestingly, Total Inorganic Carbon (TIC) slightly increased (from 5.774 to 5.851 mg/L), suggesting that some of the organic matter was mineralized into inorganic forms such as carbon dioxide. While in TW, minimal changes were observed with TC slightly increasing from 1.571 to 2.045 mg/L and NPOC from 1.503 to 1.855 mg/L after

120 minutes. These variations may be attributed to background organic content or interference from constituents commonly found in TW, which can affect the degradation kinetics or measurement accuracy. SW showed unexpected trends TOC increased markedly from 16.73 mg/L to 55.32 mg/L post-irradiation, while IC decreased from 51.91 to 9.533 mg/L (Table 18). This increase in TOC and decrease in IC could indicate the release of natural organic matter or other interfering substances from the complex surface water matrix during irradiation. Such behavior highlights the challenges associated with applying photodegradation processes in real-world aquatic environments, where matrix effects can obscure degradation outcomes.

In the case of RTR, TC showed an increase from 3.940 mg/L to 4.694 mg/L, while IC remained almost constant (4.859 to 4.856 mg/L). NPOC increased from 1.595 to 2.141 mg/L, and TN increased from 0.167 to 0.238 mg/L. These changes suggest minimal photodegradation and possibly minor contamination or measurement variability, given the slight rise in organic and nitrogen content over the irradiation period. The near-constant IC further supports the lack of significant mineralization during the process. In SW, TOC increased from 6.640 mg/L to 16.05 mg/L after 120 minutes, while TC rose from 24.21 mg/L to 28.89 mg/L. Although IC decreased from 17.57 mg/L to 12.83 mg/L, both NPOC and TN exhibited slight increases from 2.802 to 3.880 mg/L and 0.486 to 0.585 mg/L, respectively. The increase in TOC and NPOC may be attributed to interactions with naturally occurring organic matter or the release of organic constituents from the water matrix during irradiation. The decline in IC suggests a partial transformation of inorganic carbon or a shift in carbon speciation due to photoreactions in a complex matrix.

In the case of REM, initial TOC concentrations were notably high in all samples, with values reaching 373.1 mg/L in MQW, 402.6 mg/L in TW, and 318.6 mg/L in SW, reflecting substantial organic contamination. Following solar exposure (till 120 mins), TOC levels decreased sharply by 65.5% in MQW, 55.4% in TW, and 50.5% in SW indicating effective photodegradation or mineralization processes. This trend was mirrored in the Non-Purgeable Organic Carbon (NPOC) values, which also exhibited marked reductions, suggesting substantial removal of stable organic constituents. In contrast, Inorganic Carbon (IC) levels remained relatively low and stable across treatments, with only minor fluctuations, likely due to the conversion of organic matter into inorganic forms during exposure. Interestingly,

Total Nitrogen (TN) remained undetectable (0.000 mg/L) in all samples, which may suggest either the absence of nitrogen-containing compounds or limitations in analytical sensitivity.

Overall, the photodegradation efficiency of anti-COVID-19 drugs varied significantly across water matrices. In MQW, compounds like IPN showed effective degradation, while RTR remained largely persistent. TW and SW demonstrated reduced degradation efficiency, likely due to the presence of natural organic matter and matrix interferences. Across all drugs studied, TOC and TN often increased or remained stable, indicating incomplete mineralization and the formation or release of additional organic by-products during solar exposure. These results suggest that natural sunlight alone is insufficient for the complete removal of these pharmaceuticals from complex aquatic environments.

Table. 18. Carbon and nitrogen parameter changes during solar photodegradation of anti-COVID-19 drugs in different water matrices

Drugs	Process	Time, min	TOC, mg/L	TC, mg/L	IC, mg/L	NPOC, mg/L	TN, mg/L
Isoprinosine	Solar, MQ	0	13.13	18.91	5.774	14.48	4.520
		120	–	3.020	5.851	2.515	0.242
	Solar, TW	0	–	1.571	5.667	1.503	0.157
		120	–	2.045	5.608	1.855	0.197
	Solar, SW	0	16.73	68.64	51.91	56.91	1.140
		120	55.32	64.85	9.533	54.20	1.402
Ritonavir	Solar, MQ	0	–	3.940	4.859	1.595	0.167
		120	–	4.694	4.856	2.141	0.238
	Solar, TW	0	–	–	–	–	–
		120	–	–	–	–	–
	Solar, SW	0	6.640	24.21	17.57	2.802	0.486
		120	16.05	28.89	12.83	3.880	0.585
Remdesivir	Solar, MQ	0	373.1	377.1	3.973	318.5	–
		120	128.7	133.5	4.813	112.5	–
	Solar, TW	0	402.6	420.5	17.84	306.3	–
		120	179.5	188.7	9.170	116.7	–
	Solar, SW	0	318.6	331.8	13.20	204.1	–
		120	157.7	172.0	14.35	70.47	–

Chapter 5 – Summary and Conclusion

5.1 Summary

This study provides a comprehensive evaluation of the degradation behavior of three antiviral drugs used in COVID-19 therapy i.e., isoprinosine (IPN), ritonavir (RTR), and remdesivir (REM) using various Advanced Oxidation Processes (AOPs), including direct photolysis, photolysis assisted with hydrogen peroxide (H_2O_2), and using selected heterogeneous photocatalysis (TiO_2 P25, ZnO, ZrO_2, $BaWO_4$, Ag-TiO_2, $BaTiO_3$, and SnO_2.) with concentration 5.0 mg/L, 10.0 mg/L, and 20.0 mg/L in three different water matrices i.e., MQ water, TW, and SW. The work not only underscores the potential of AOPs for the treatment of pharmaceutical contaminants but also highlights the interactions between drug molecules, reactive species, and environmental matrices, such as inorganic ions. Also, this study was based on hybrid approach; using real environmental matrices with controlled pollutant spiking, allows to model real-world behavior while keeping the system scientifically robust. It was a step between pure lab tests and full-scale environmental application.

5.1.1. Research contribution

This research makes several original contributions to the field of environmental engineering and water/ wastewater treatment technologies, particularly in understanding the degradation behaviour of antiviral drugs used during and after the COVID-19 pandemic. Through a systematic investigation of photolysis, photolysis assisted with H_2O_2, and photocatalytic processes under simulated solar irradiation, this work bridges key knowledge gaps in the current literature and offers practical insights for real-world applications.

5.1.2. Key Contributions

i. *First comparative study on the solar degradation of remdesivir, ritonavir, and isoprinosine*

   To the best of current knowledge, this is the first study to systematically evaluate the direct photolysis and solar-light-driven photocatalytic degradation of these three antiviral drugs, providing new environmental data on their stability and transformation behaviour.

ii. *Comprehensive evaluation of direct photolysis efficiency*

The study demonstrated that simple solar photolysis results in only limited degradation of these drugs, confirming their high photostability and the inadequacy of photolysis as a standalone treatment approach.

iii. *Photocatalytic enhancement and performance comparison*

By introducing various photocatalysts (TiO_2, ZnO, SnO_2, Ag–TiO, and SnO_2:ZnO composites), the research revealed significant improvements in degradation efficiency, highlighting the superior performance of composite and doped catalysts under solar irradiation.

iv. *Influence of water matrix composition*

Experiments conducted in Milli-Q water, tap water, and surface water from the Ostropka River (Gliwice, Poland) provided a realistic assessment of matrix effects. The presence of salts, ions, and organic matter was shown to influence both the rate and mechanism of degradation, underlining the importance of testing in environmental conditions.

v. *Influence of inorganic anions on degradation of selected drugs*

Experiments conducted in Milli-Q water by adding selected inorganic anions provided realistic matrix effects. Their presence influences the degradation efficiency of selected photocatalysts.

vi. *Kinetic modeling and mechanistic insights*

The degradation kinetics were modeled using first-order, pseudo-second-order, and Langmuir–Hinshelwood equations, enabling a quantitative understanding of rate constants and adsorption–reaction dynamics across different catalysts and matrices.

vii. *Novel adsorption–desorption kinetic approach for remdesivir*

A unique two-phase kinetic model was developed and applied for the first time to describe the adsorption–desorption dynamics and percent removal of remdesivir, providing a deeper understanding of its surface interaction behaviour.

viii. *Contribution to sustainable remediation strategies*

The findings collectively demonstrate the potential of solar-driven photocatalysis as a green, energy-efficient, and scalable approach for mitigating antiviral contamination in aquatic environments.

In summary, this thesis provides pioneering insights into the photochemical fate of key antiviral drugs, establishing a foundation for future studies on the environmental persistence, degradation pathways, and treatment technologies of emerging pharmaceutical pollutants.

5.2 Conclusion

This research successfully achieved its primary objective of investigating the photodegradation behavior of selected COVID-19 pharmaceutical compounds in aquatic environments under simulated solar irradiation. The results demonstrated that direct photolysis alone was not fully satisfactory for effective degradation due to the inherent photostability of the studied drugs i.e., IPN, RTR, and REM and the influence of water matrix composition. However, the incorporation of selected photocatalysts, and in particular, such as TiO_2 P25, and SnO_2 and their composites particularly the TiO_2 and ZnO significantly enhanced degradation efficiency at the catalytic dose 20 mg/L, confirming the potential of solar-driven photocatalysis as a viable treatment approach.

The effects of key operational parameters, including catalyst dosage, pollutant concentration, and reaction time, were systematically evaluated, providing insights into the optimal conditions for maximum degradation performance. Kinetic modeling further revealed that the degradation followed pseudo-first-order behavior, supporting the reproducibility and predictability of the process. ***Overall, the findings confirm the research hypothesis and contribute valuable knowledge toward developing sustainable, solar-assisted advanced oxidation processes for the removal of antiviral and other pharmaceutical pollutants from aquatic environments***.

1. The results confirm that simple solar photolysis is not an effective degradation pathway for selected antiviral drugs due to their low light absorptivity and matrix interferences.

   However, solar-driven photocatalysis proved to be a promising, sustainable method for their removal, particularly using composite catalysts such as SnO_2:ZnO. These

findings contribute valuable data to the limited body of knowledge on antiviral degradation and support the development of solar-based advanced oxidation processes for water treatment. In case of IPN, the highest pseudo drug degradation rate during photolysis was observed in MQW (kt = 0.0007 min^{-1}) with R^2 value of 0.6092. Similarly, in RTR and REM the highest pseudo drug degradation rate was also noted in MQW i.e., kt = 0.0012 min^{-1} (R^2 = 0.8201) and kt = 0.0016 min^{-1} (R^2 = 0.8563) , respectively.

2. Isoprinosine (IPN) underwent significant degradation under AOP conditions, with kinetic analysis best described by a pseudo-first-order model. This indicates a dominant reaction pathway governed by hydroxyl radicals or other short-lived reactive intermediates, especially under photocatalytic conditions. The addition of H_2O_2 enhanced the photolytic degradation rate, suggesting synergistic effects in reactive oxygen species generation. It has been observed that under UV-H_2O_2 experiments, the highest drug degradation rate was achieved with the 500 µL (435 mg/L) i.e., kt = 0.0302 min^{-1} (R^2 = 0.9473). IPN also show the degradation w.r.t time using different selected photocatalysts in all three aquatic matrices. Among selected photocatalysts, IPN showed strong degradation in the presence of UV-TiO_2 P25 (10.0 mg/L) with kt = 0.0105 min^{-1}, correlation coefficient value of R^2 = 0.9159 in MQW. While in TW and SW, the highest drug degradation rate was observed with 20 mg/L ZnO i.e., kt = 0.0101 min^{-1} and kt = 0.0053 min^{-1} respectively.

3. In contrast, ritonavir (RTR) exhibited strong adsorption onto the surface of selected photocatalysts for example, TiO_2 P25 (kt = 0.0286 min^{-1} ; KL= 5720 L/mg), ZnO (kt = 0.2532 min^{-1}; KL= 5064 L/mg), and SnO_2:ZnO (1:2) (kt = 0.2605 min^{-1}; KL= 13025 L/mg) in MQW, which limited its photocatalytic degradation. The equilibrium data aligned well with the Langmuir isotherm, indicating monolayer adsorption on a homogenous surface. This suggests that while photocatalysis may not be effective for degrading RTR, its removal through adsorption could still be harnessed, particularly in systems designed for recovery or reuse of the adsorbent.

4. Remdesivir (REM) displayed a unique adsorption–desorption dynamic. It rapidly adsorbed onto the photocatalyst surface, followed by a gradual desorption phase. This reversible behavior was best described by a two-phase model, reflecting both rapid

surface interaction and subsequent release back into solution. This phenomenon highlights the complexity of photocatalyst-drug interactions, which can be influenced by physicochemical properties of both the compound and the photocatalyst, in three different matrices.

Furthermore, the study explored the influence of inorganic ions i.e., (SO_4^-, Cl^-, NO_3^-, and CO_3^-) commonly found in natural waters were selected for the study with IPN and RTR only. These ions showed varied effects on degradation efficiency, either scavenging reactive species or altering surface charge interactions, further reinforcing the importance of matrix composition in environmental applications of AOPs.

Overall, the findings emphasize the need for tailored AOP strategies depending on the physicochemical nature of the target contaminant. A thorough understanding of reaction kinetics, adsorption behaviour, and environmental influences is essential for optimizing degradation pathways and improving the sustainability of water treatment technologies. Despite these valuable insights, the record to further research directions is addressed in chapter 6.

5.3 Novelty Statement

This work determined the efficiency of photochemical decomposition of drugs, kinetic constants, and main products of photodegradation depending on matrix composition, radiation intensity, dose, and photocatalyst type and contributed to better understanding of abiotic degradation in the aquatic environment. Furthermore, this was the first study to explored photocatalytic degradation of anti-viral drug isoprinosine with a focus on degradation kinetics, and real-world applicability. In addition, the study on ritonavir and the evaluation of the percentage removal of remdesivir using a two-phase kinetic model based on a unique adsorption–desorption dynamic represented a novel contribution to this field. To the best of our knowledge, no previous studies have reported such an approach in the available literature. This study also developed an eco-friendly and energy-efficient approach to tackle pharmaceutical pollution.

Chapter 6 – Future Research Directions

6.1 Future Work and Recommendations

Although this research provides new insights into the solar photolysis and photocatalytic degradation of antiviral drugs in aquatic environments, several aspects warrant further exploration to expand understanding and optimize treatment strategies.

1. Future studies should focus on identifying and characterizing the transformation products formed during both photolytic and photocatalytic processes. Advanced analytical tools such as LC–MS/MS and high-resolution mass spectrometry should be employed to evaluate the environmental safety and potential ecotoxicity of intermediate compounds.
2. To better understand the degradation pathways, experiments incorporating radical scavengers and reactive species quantification ($^{\bullet}OH$, $O_2^{\bullet-}$) are recommended. This would clarify the roles of direct and indirect photochemical mechanisms and support the optimization of catalyst design.
3. Reusability and recyclability of the photocatalyst used in this study.
4. Performing the FTIR and XRD analyses, which are essential for a comprehensive understanding of the adsorption mechanism. Fourier-transform infrared spectroscopy (FTIR) could have provided insight into the specific functional groups involved in the interaction between RTR and the photocatalyst or the influence of inorganic anions. Similarly, X-ray diffraction (XRD) analysis would have allowed for the evaluation of any structural changes in the crystalline phases of the photocatalyst before and after adsorption, which could suggest surface modifications or phase transformations.

In conclusion, while this study establishes a foundational understanding of the solar-light-driven degradation behaviour of key antiviral drugs, future research should move toward mechanistic elucidation, catalyst innovation, and large-scale validation to develop sustainable, real-world applications for pharmaceutical pollution control.

Chapter 7 – References

Abo-Gharam, A. H., & El-Kafrawy, D. S. (2022). Eco-friendly stability-indicating HPTLC micro-determination of the first FDA approved SARS-CoV-2 antiviral prodrug Remdesivir: Study of degradation kinetics and structural elucidation of the degradants using HPTLC-MS. *Sustainable Chemistry and Pharmacy*, *29*, 100744. https://doi.org/10.1016/J.SCP.2022.100744

Adeola, A. O., de Lange, J., & Forbes, P. B. C. (2021). Adsorption of antiretroviral drugs, efavirenz and nevirapine from aqueous solution by graphene wool: Kinetic, equilibrium, thermodynamic and computational studies. *Applied Surface Science Advances*, *6*, 100157. https://doi.org/10.1016/J.APSADV.2021.100157

Ahmed, A. B., Gamal, M., Naguib, I. A., Ali, H. M., & Abdallah, F. F. (2022). Environmental impact of the reported chromatographic methods for the determination of the first FDA-Approved therapy for COVID-19 Patients, Remdesivir: A comparative study. *Microchemical Journal*, *176*, 107242. https://doi.org/10.1016/J.MICROC.2022.107242

Ahmed, H., & Felis, E. (2023a). Drugs used in COVID-19 therapy and their effects on the environment. *DESALINATION AND WATER TREATMENT*, *301*, 52–62. https://doi.org/10.5004/dwt.2023.29574

Ahmed, H., & Felis, E. (2023b). Drugs used in COVID-19 therapy and their effects on the environment. *DESALINATION AND WATER TREATMENT*, *301*, 52–62. https://doi.org/10.5004/dwt.2023.29574

Ahmed, H., & Felis, E. (2024). Solar Light-Driven Degradation of Isoprinosine - Efficiency of the Processes and Kinetic Calculations. *Journal of Ecological Engineering*, *25*(3). https://doi.org/10.12911/22998993/178190

Ahmed, H., Siddiqui, B., & Felis, E. (2025a). Adsorption and photodegradation as processes enabling the removal of antiviral drug ritonavir from the aquatic environment. *Journal of Ecological Engineering*, *26*(5), 195–202. https://doi.org/10.12911/22998993/200281

Ahmed, H., Siddiqui, B., & Felis, E. (2025b). Adsorption and photodegradation as processes enabling the removal of antiviral drug ritonavir from the aquatic environment. *Journal of Ecological Engineering*, *26*(5), 195–202. https://doi.org/10.12911/22998993/200281

Albiter, E., Valenzuela, M. A., Alfaro, S., Valverde-Aguilar, G., & Martínez-Pallares, F. M. (2015). Photocatalytic deposition of Ag nanoparticles on TiO_2: Metal precursor effect on the structural and photoactivity properties. *Journal of Saudi Chemical Society*, *19*(5), 563–573. https://doi.org/10.1016/J.JSCS.2015.05.009

Alexandra Chera, & Antoanela Tanca. (2022). Remdesivir: the first FDA-approved anti-COVID-19 Treatment for Young Children. *Discoveries (Craiova)*, *10*(2:e151).

Alharbi, S. K., Kang, J., Nghiem, L. D., van de Merwe, J. P., Leusch, F. D. L., & Price, W. E. (2017). Photolysis and UV/H_2O_2 of diclofenac, sulfamethoxazole, carbamazepine, and trimethoprim: Identification of their major degradation products by ESI–LC–MS and assessment of the toxicity of reaction mixtures. *Process Safety and Environmental Protection*, *112*, 222–234. https://doi.org/10.1016/J.PSEP.2017.07.015

Aljundi, I. H. (2011). Bromate formation during ozonation of drinking water: A response surface methodology study. *Desalination*, *277*(1–3), 24–28. https://doi.org/10.1016/J.DESAL.2011.03.090

Anderson, E. P., Jackson, S., Tharme, R. E., Douglas, M., Flotemersch, J. E., Zwarteveen, M., Lokgariwar, C., Montoya, M., Wali, A., Tipa, G. T., Jardine, T. D., Olden, J. D., Cheng, L., Conallin, J., Cosens, B., Dickens, C., Garrick, D., Groenfeldt, D., Kabogo, J., … Arthington, A. H. (2019). Understanding rivers and their social relations: A critical step to advance environmental water management. In *Wiley Interdisciplinary Reviews: Water* (Vol. 6, Issue 6). John Wiley and Sons Inc. https://doi.org/10.1002/WAT2.1381

Babu Ponnusami, A., Sinha, S., Ashokan, H., V Paul, M., Hariharan, S. P., Arun, J., Gopinath, K. P., Hoang Le, Q., & Pugazhendhi, A. (2023). Advanced oxidation process (AOP) combined biological process for wastewater treatment: A review on advancements, feasibility and practicability of combined techniques. *Environmental Research*, *237*, 116944. https://doi.org/10.1016/J.ENVRES.2023.116944

Baena-Nogueras, R. M., González-Mazo, E., & Lara-Martín, P. A. (2017). Degradation kinetics of pharmaceuticals and personal care products in surface waters: photolysis vs biodegradation. *Science of The Total Environment*, *590–591*, 643–654. https://doi.org/10.1016/J.SCITOTENV.2017.03.015

Bera, S. P., Godhaniya, M., & Kothari, C. (2022). Emerging and advanced membrane technology for wastewater treatment: A review. In *Journal of Basic Microbiology* (Vol. 62, Issues 3–4, pp. 245–259). John Wiley and Sons Inc. https://doi.org/10.1002/jobm.202100259

Beran, J., Špajdel, M., & Slíva, J. (2021). Inosine pranobex deserves attention as a potential immunomodulator to achieve early alteration of the covid-19 disease course. *Viruses*, *13*(11). https://doi.org/10.3390/v13112246

Biswas, P. , Hasan, M. M. , & Dey, D. et al. (2021). Candidate antiviral drugs for COVID-19 and their environmental implications: a comprehensive analysis. *Environmental Science and Pollution Research*, *28*, 59570–59593.

Chai, W. S., Cheun, J. Y., Kumar, P. S., Mubashir, M., Majeed, Z., Banat, F., Ho, S. H., & Show, P. L. (2021). A review on conventional and novel materials towards heavy metal adsorption in wastewater treatment application. *Journal of Cleaner Production*, *296*, 126589. https://doi.org/10.1016/J.JCLEPRO.2021.126589

Chen, Y. di, Duan, X., Zhou, X., Wang, R., Wang, S., Ren, N. qi, & Ho, S. H. (2021). Advanced oxidation processes for water disinfection: Features, mechanisms and

prospects. *Chemical Engineering Journal*, *409*, 128207. https://doi.org/10.1016/J.CEJ.2020.128207

Chen, X., Wang, N., Li, X., Wen, M., Song, S., Hou, X., Wang, X., & Gao, J. (2019). The Impact of Urban Wastewater Treatment on Carbon Emissions: Current Status, Challenges, and Future Perspectives. *SCIREA Journal of Environment*. https://doi.org/10.54647/environmental610411

Chi, Y., Xu, S., Li, M., He, M., Yu, H., Li, L., Yue, Q., & Gao, B. (2020). Effective blockage of chloride ion quenching and chlorinated by-product generation in photocatalytic wastewater treatment. *Journal of Hazardous Materials*, *396*, 122670. https://doi.org/10.1016/J.JHAZMAT.2020.122670

Choina, J., Bagabas, A., Fischer, C., Flechsig, G. U., Kosslick, H., Alshammari, A., & Schulz, A. (2015). The influence of the textural properties of ZnO nanoparticles on adsorption and photocatalytic remediation of water from pharmaceuticals. *Catalysis Today*, *241*(PA), 47–54. https://doi.org/10.1016/J.CATTOD.2014.05.014

Choudhury, A., Ojha, P. K., & Ray, S. (2024). Hazards of antiviral contamination in water: Dissemination, fate, risk and their impact on fish. *Journal of Hazardous Materials*, *476*, 135087. https://doi.org/10.1016/J.JHAZMAT.2024.135087

Coha, M., Farinelli, G., Tiraferri, A., Minella, M., & Vione, D. (2021). Advanced oxidation processes in the removal of organic substances from produced water: Potential, configurations, and research needs. *Chemical Engineering Journal*, *414*, 128668. https://doi.org/10.1016/J.CEJ.2021.128668

Dawood, T., Elwakil, E., Novoa, H. M., & Gárate Delgado, J. F. (2021). Toward urban sustainability and clean potable water: Prediction of water quality via artificial neural networks. *Journal of Cleaner Production*, *291*, 125266. https://doi.org/10.1016/J.JCLEPRO.2020.125266

De la Cruz, N., Dantas, R. F., Giménez, J., & Esplugas, S. (2013). Photolysis and TiO_2 photocatalysis of the pharmaceutical propranolol: Solar and artificial light. *Applied Catalysis B: Environmental*, *130–131*, 249–256. https://doi.org/10.1016/J.APCATB.2012.10.003

de Sousa Filho, I. A., Lobo, T. M., Grisolia, C. K., Weber, I. T., & Osugi, M. E. (2019). Toxicological study of the degradation products of antineoplastic agent etoposide in commercial formulation treated by heterogeneous photocatalysis using $SrSnO_3$. *Environmental Science and Pollution Research*, *26*(5), 4224–4233. https://doi.org/10.1007/S11356-018-1524-2

Dhamorikar, R. S., Lade, V. G., Kewalramani, P. V., & Bindwal, A. B. (2024). Review on integrated advanced oxidation processes for water and wastewater treatment. *Journal of Industrial and Engineering Chemistry*, *138*, 104–122. https://doi.org/10.1016/J.JIEC.2024.04.037

Domingo-Echaburu, S., Irazola, M., Prieto, A., Rocano, B., Lopez de Torre-Querejazu, A., Quintana, A., Orive, G., & Lertxundi, U. (2022a). Drugs used during the

COVID-19 first wave in Vitoria-Gasteiz (Spain) and their presence in the environment. *Science of The Total Environment*, *820*, 153122. https://doi.org/10.1016/J.SCITOTENV.2022.153122

Domingo-Echaburu, S., Irazola, M., Prieto, A., Rocano, B., Lopez de Torre-Querejazu, A., Quintana, A., Orive, G., & Lertxundi, U. (2022b). Drugs used during the COVID-19 first wave in Vitoria-Gasteiz (Spain) and their presence in the environment. *Science of The Total Environment*, *820*, 153122. https://doi.org/10.1016/J.SCITOTENV.2022.153122

Domínguez-García, P., Rodríguez, R. R., Barata, C., & Gómez-Canela, C. (2023). Presence and toxicity of drugs used to treat SARS-CoV-2 in Llobregat River, Catalonia, Spain. *Environmental Science and Pollution Research*, *30*(17), 49487–49497. https://doi.org/10.1007/s11356-023-25512-9

Dong, G., Chen, B., Liu, B., Hounjet, L. J., Cao, Y., Stoyanov, S. R., Yang, M., & Zhang, B. (2022). Advanced oxidation processes in microreactors for water and wastewater treatment: Development, challenges, and opportunities. *Water Research*, *211*, 118047. https://doi.org/10.1016/J.WATRES.2022.118047

Eitzen, L., Ruhl, A. S., & Jekel, M. (2024). Impact of natural organic matter and inorganic ions on the stabilization of polystyrene micro-particles. *Science of The Total Environment*, *927*, 172043. https://doi.org/10.1016/J.SCITOTENV.2024.172043

Emile, R., Clammer, J. R., Jayaswal, P., & Sharma, P. (2022). Addressing water scarcity in developing country contexts: a socio-cultural approach. *Humanities and Social Sciences Communications*, *9*(1). https://doi.org/10.1057/s41599-022-01140-5

Eryildiz, B., Ozgun, H., Ersahin, M. E., & Koyuncu, I. (2022). Antiviral drugs against influenza: Treatment methods, environmental risk assessment and analytical determination. *Journal of Environmental Management*, *318*, 115523. https://doi.org/10.1016/J.JENVMAN.2022.115523

Eryildiz, B., Yavuzturk Gul, B., & Koyuncu, I. (2022). A sustainable approach for the removal methods and analytical determination methods of antiviral drugs from water/wastewater: A review. *Journal of Water Process Engineering*, *49*, 103036. https://doi.org/10.1016/J.JWPE.2022.103036

Eryildiz-Yesir, B., Ozgun, H., Ersahin, M. E., Rajabi, H. R., Vatanpour, V., & Koyuncu, I. (2025). Degradation of Antiviral Drug Favipiravir Using UV, UV/H_2O_2, and Photocatalysis with Co-Doped ZnS Quantum Dots: Operational Parameters, Kinetic Studies, and Toxicity Assessment. *Langmuir*. https://doi.org/10.1021/acs.langmuir.4c03639

Eryildiz-Yesir, B., Polat, E., Altınbaş, M., Gul, B. Y., & Koyuncu, I. (2024). Long term study on the fate and environmental risks of favipiravir in wastewater treatment plants and comparison with COVID-19 cases. *Science of The Total Environment*, *949*, 175014. https://doi.org/10.1016/J.SCITOTENV.2024.175014

Frediansyah, A., Tiwari, R., Sharun, K., Dhama, K., & Harapan, H. (2021). Antivirals for COVID-19: A critical review. *Clinical Epidemiology and Global Health*, *9*, 90–98. https://doi.org/10.1016/J.CEGH.2020.07.006

Ganzenko, O., Huguenot, D., van Hullebusch, E. D., Esposito, G., & Oturan, M. A. (2014). Electrochemical advanced oxidation and biological processes for wastewater treatment: A review of the combined approaches. In *Environmental Science and Pollution Research* (Vol. 21, Issue 14, pp. 8493–8524). Springer Verlag. https://doi.org/10.1007/s11356-014-2770-6

Garrido, J. A., Brillas, E., Cabot, P. L., Centellas, F., Arias, C., & Rodríguez, R. M. (2007). Mineralization of Drugs in Aqueous Medium by Advanced Oxidation Processes. *Portugaliae Electrochimica Acta*, *25*(1), 19–41. https://doi.org/10.4152/pea.200701019

Ghosh, G. C., Nakada, N., Yamashita, N., & Tanaka, H. (2010). Oseltamivir carboxylate, the active metabolite of oseltamivir phosphate (tamiflu), detected in sewage discharge and river water in Japan. *Environmental Health Perspectives*, *118*(1), 103–107. https://doi.org/10.1289/ehp.0900930

Giwa, A., Yusuf, A., Balogun, H. A., Sambudi, N. S., Bilad, M. R., Adeyemi, I., Chakraborty, S., & Curcio, S. (2021). Recent advances in advanced oxidation processes for removal of contaminants from water: A comprehensive review. *Process Safety and Environmental Protection*, *146*, 220–256. https://doi.org/10.1016/J.PSEP.2020.08.015

Gligorovski, S., Strekowski, R., Barbati, S., & Vione, D. (2015). Environmental Implications of Hydroxyl Radicals (•OH). *Chemical Reviews*, *115*(24), 13051–13092. https://doi.org/10.1021/cr500310b

Grassi, P., Drumm, F. C., Georgin, J., Franco, D. S. P., Foletto, E. L., Dotto, G. L., & Jahn, S. L. (2020). Water treatment plant sludge as iron source to catalyze a heterogeneous photo-Fenton reaction. *Environmental Technology & Innovation*, *17*, 100544. https://doi.org/10.1016/J.ETI.2019.100544

Guo, Z., He, H., Liu, K., Li, Z., Yang, S., Liao, Z., Lai, C., Ren, X., Huang, B., & Pan, X. (2023). The photolytic behavior of COVID-19 antivirals ribavirin in natural waters and the increased environmental risk. *Journal of Hazardous Materials*, *452*, 131320. https://doi.org/10.1016/J.JHAZMAT.2023.131320

Gupta, P., & Rani, V. (2024). A Comprehensive Assessment of Environmental Implications, Ecotoxicity and Bioaccumulation Potential of Repurposed Drug Hydroxychloroquine: From Challenges to Sustainability. In *Reviews of Environmental Contamination and Toxicology* (Vol. 262, Issue 1). Springer. https://doi.org/10.1007/s44169-024-00061-5

Gupta, S., Singh, A., Sharma, T., Kaur, R., Khandelwal, V., Rawat, K. D., Pathak, S., Sharma, M. K., Singh, J., Shah, M. P., Chauhan, S. C., Parashar, D., Shankar, P., & Kashyap, V. K. (2024). Applications of ultrafiltration, nanofiltration, and reverse osmosis in pharmaceutical wastewater treatment. *Development in Wastewater Treatment Research and Processes: Innovative Trends in Removal*

of Refractory Pollutants from Pharmaceutical Wastewater, 33–49. https://doi.org/10.1016/B978-0-323-99278-7.00017-1

Gwenzi, W. , Selvasembian, R. , Offiong, N. A. O. , & El Din, A. (2022). COVID-19 drugs in aquatic systems: a review. *Environmental Chemistry Letters*, *20*(2), 1275–1294.

Gwenzi, W. , Selvasembian, R. , & Offiong, NA. O. et al. (2022). COVID-19 drugs in aquatic systems: a review. *Environmental Chemistry Letters*, *20*, 1275–1294.

Heberer, T. (2002). Occurrence, fate, and removal of pharmaceutical residues in the aquatic environment: a review of recent research data. *Toxicology Letters*, *131*(1–2), 5–17. https://doi.org/10.1016/S0378-4274(02)00041-3

Hong, B. A. P. (r B. A. Y., & Editors, S. (n.d.). *Recent Advances on Coagulation-Based Treatment of Wastewater: Transition from Chemical to Natural Coagulant*. https://doi.org/10.1007/s40726-021-00191-7/Published

Huda R. Taha, Nour Keewan, Farah Slati, & Nour A. Al-Sawalha. (2021). Remdesivir: A Closer Look at Its Effect in COVID-19 Pandemic. *Pharmacology* , *106*(09–10), 462–468.

Igor A. Shiklomanov. (2000). Appraisal and Assessment of World Water Resources. *Water International*, *20*(1), 11–32.

Issakhov, A., Alimbek, A., & Zhandaulet, Y. (2021). The assessment of water pollution by chemical reaction products from the activities of industrial facilities: Numerical study. *Journal of Cleaner Production*, *282*, 125239. https://doi.org/10.1016/J.JCLEPRO.2020.125239

J. M. Poyatos, M. C. Almecija, M. M. Muñio, J. C. Torres, E. Hontoria, & F. Osorio. (2009). Advanced Oxidation Processes for Wastewater Treatment: State of the Art. *Water, Air, and Soil Pollution*, *205*(2010), 187–204. https://doi.org/https://doi.org/10.1007/s11270-009-0065-1

Jaya P. Ambhore, Vaibhav S. Adhao, Rameshwar S. Cheke, Rameshwar S. Cheke, Ritesh R. Popat, & Shital J. Gandhi. (2021). Futuristic review on progress in force degradation studies and stability indicating assay method for some antiviral drugs. *GSC Biological and Pharmaceutical Sciences*, *16*(1), 133–149. https://doi.org/10.30574/gscbps.2021.16.1.0172

Jayanthi, C. R., Swain, A. K., Ganga, R. T., Halnor, D., Avhad, A., Khan, M. S., Ghosh, A., Choudhary, S. S., Yannawar, A. N., Despande, S., Patel, M., Anne, K. P., & Bangar, Y. (2022). Efficacy and Safety of Inosine Pranobex in COVID-19 Patients: A Multicenter Phase 3 Randomized Double-Blind, Placebo-Controlled Trial. *Advanced Therapeutics*, *5*(12). https://doi.org/10.1002/adtp.202200159

Jha, P., & Schmidt, S. (2021). State of biofuel development in sub-Saharan Africa: How far sustainable? *Renewable and Sustainable Energy Reviews*, *150*, 111432. https://doi.org/10.1016/J.RSER.2021.111432

Jin, J., El-Din, M. G., & Bolton, J. R. (2011). Assessment of the UV/Chlorine process as an advanced oxidation process. *Water Research*, *45*(4), 1890–1896. https://doi.org/10.1016/J.WATRES.2010.12.008

Kalugendo, E., Singh, P., & Agarwal, R. (2025). Azithromycin in the Sabarmati River as an indicator of aquatic environment contamination. *Sustainable Chemistry One World*, *7*, 100106. https://doi.org/10.1016/J.SCOWO.2025.100106

Kang, Y. M., Kim, T. K., Kim, M. K., & Zoh, K. D. (2020a). Greenhouse gas emissions from advanced oxidation processes in the degradation of bisphenol A: a comparative study of the H_2O_2/UV, TiO_2 /UV, and ozonation processes. *Environmental Science and Pollution Research*, *27*(11), 12227–12236. https://doi.org/10.1007/s11356-020-07807-3

Kang, Y. M., Kim, T. K., Kim, M. K., & Zoh, K. D. (2020b). Greenhouse gas emissions from advanced oxidation processes in the degradation of bisphenol A: a comparative study of the H_2O_2/UV, TiO_2 /UV, and ozonation processes. *Environmental Science and Pollution Research*, *27*(11), 12227–12236. https://doi.org/10.1007/s11356-020-07807-3

Kavitha, V., & Palanivelu, K. (2004). The role of ferrous ion in Fenton and photo-Fenton processes for the degradation of phenol. *Chemosphere*, *55*(9), 1235–1243. https://doi.org/10.1016/J.CHEMOSPHERE.2003.12.022

Khan, Z. U. H., Gul, N. S., Sabahat, S., Sun, J., Tahir, K., Shah, N. S., Muhammad, N., Rahim, A., Imran, M., Iqbal, J., Khan, T. M., Khasim, S., Farooq, U., & Wu, J. (2023). Removal of organic pollutants through hydroxyl radical-based advanced oxidation processes. *Ecotoxicology and Environmental Safety*, *267*, 115564. https://doi.org/10.1016/J.ECOENV.2023.115564

Li, D., Feng, Z., Zhou, B., Chen, H., & Yuan, R. (2022). Impact of water matrices on oxidation effects and mechanisms of pharmaceuticals by ultraviolet-based advanced oxidation technologies: A review. *Science of The Total Environment*, *844*, 157162. https://doi.org/10.1016/J.SCITOTENV.2022.157162

Li, J., Ma, L. Y., Li, L. S., & Xu, L. (2017). Photodegradation kinetics, transformation, and toxicity prediction of ketoprofen, carprofen, and diclofenac acid in aqueous solutions. *Environmental Toxicology and Chemistry*, *36*(12), 3232–3239. https://doi.org/10.1002/ETC.3915

Liu, Q., Feng, X., Chen, N., Shen, F., Zhang, H., Wang, S., Sheng, Z., & Li, J. (2022). Occurrence and risk assessment of typical PPCPs and biodegradation pathway of ribavirin in wastewater treatment plants. *Environmental Science and Ecotechnology*, *11*, 100184. https://doi.org/10.1016/J.ESE.2022.100184

Liu, Y., Wang, P., Gojenko, B., Yu, J., Wei, L., Luo, D., & Xiao, T. (2021). A review of water pollution arising from agriculture and mining activities in Central Asia: Facts, causes and effects. *Environmental Pollution*, *291*, 118209. https://doi.org/10.1016/J.ENVPOL.2021.118209

Mansouri, F., Chouchene, K., Roche, N., & Ksibi, M. (2021a). Removal of pharmaceuticals from water by adsorption and advanced oxidation processes: State of the art and trends. *Applied Sciences (Switzerland)*, *11*(14). https://doi.org/10.3390/app11146659

Mansouri, F., Chouchene, K., Roche, N., & Ksibi, M. (2021b). Removal of pharmaceuticals from water by adsorption and advanced oxidation processes: State of the art and trends. *Applied Sciences (Switzerland)*, *11*(14). https://doi.org/10.3390/app11146659

M'Arimi, M. M., Mecha, C. A., Kiprop, A. K., & Ramkat, R. (2020). Recent trends in applications of advanced oxidation processes (AOPs) in bioenergy production: Review. *Renewable and Sustainable Energy Reviews*, *121*, 109669. https://doi.org/10.1016/J.RSER.2019.109669

Matbiangthew Shadap, & Sakunthala Ayyasamy. (2025). Cultivating Power: A Conceptual Review on Harnessing Bio-derived Activated Carbon for Advanced Electrical Energy Storage in the Environmentally Conscious Era. In Senthilkumar Kandasamy, Maulin P Shah, Kavitha Subbiah, & Naveenkumar Manickam (Eds.), *Microbial Niche Nexus Sustaining Environmental Biological Wastewater and Water-Energy-Environment Nexus. Environmental Science and Engineering* (73–119). Springer, Cham.

Miklos, D. B., Remy, C., Jekel, M., Linden, K. G., Drewes, J. E., & Hübner, U. (2018a). Evaluation of advanced oxidation processes for water and wastewater treatment – A critical review. *Water Research*, *139*, 118–131. https://doi.org/10.1016/j.watres.2018.03.042

Miklos, D. B., Remy, C., Jekel, M., Linden, K. G., Drewes, J. E., & Hübner, U. (2018b). Evaluation of advanced oxidation processes for water and wastewater treatment – A critical review. *Water Research*, *139*, 118–131. https://doi.org/10.1016/j.watres.2018.03.042

Mohan, H., Vadivel, S., & Rajendran, S. (2022). Removal of harmful algae in natural water by semiconductor photocatalysis- A critical review. *Chemosphere*, *302*, 134827. https://doi.org/10.1016/J.CHEMOSPHERE.2022.134827

Morales-Paredes, C. A., Rodríguez-Díaz, J. M., & Boluda-Botella, N. (2022). Pharmaceutical compounds used in the COVID-19 pandemic: A review of their presence in water and treatment techniques for their elimination. *Science of The Total Environment*, *814*, 152691. https://doi.org/10.1016/J.SCITOTENV.2021.152691

Nabeel, M. I., Hussain, D., Ahmad, N., Xiao, H.-M., & Musharraf, S. G. (2023). Improved visible light-driven photocatalytic degradation of an industrial dye Acid Orange 7 using metal-free sulfur-doped graphitic carbon nitride. *Environmental Science: Nano*, *10*(10), 2810–2830. https://doi.org/10.1039/D3EN00289F

Nannou, C., Ofrydopoulou, A., Evgenidou, E., Heath, D., Heath, E., & Lambropoulou, D. (2020). Antiviral drugs in aquatic environment and wastewater treatment

plants: A review on occurrence, fate, removal and ecotoxicity. *Science of the Total Environment*, *699*. https://doi.org/10.1016/J.SCITOTENV.2019.134322

Natarajan, R., Saikia, K., Ponnusamy, S. K., Rathankumar, A. K., Rajendran, D. S., Venkataraman, S., Tannani, D. B., Arvind, V., Somanna, T., Banerjee, K., Mohideen, N., & Vaidyanathan, V. K. (2022). Understanding the factors affecting adsorption of pharmaceuticals on different adsorbents – A critical literature update. *Chemosphere*, *287*, 131958. https://doi.org/10.1016/J.CHEMOSPHERE.2021.131958

Ncube, S., Madikizela, L. M., Chimuka, L., & Nindi, M. M. (2018). Environmental fate and ecotoxicological effects of antiretrovirals: A current global status and future perspectives. *Water Research*, *145*, 231–247. https://doi.org/10.1016/J.WATRES.2018.08.017

Nidheesh, P. V., Couras, C., Karim, A. V., & Nadais, H. (2022). A review of integrated advanced oxidation processes and biological processes for organic pollutant removal. In *Chemical Engineering Communications* (Vol. 209, Issue 3, pp. 390–432). Taylor and Francis Ltd. https://doi.org/10.1080/00986445.2020.1864626

Nugnes, R., Orlo, E., Russo, C., Lavorgna, M., & Isidori, M. (2024a). Comprehensive eco-geno-toxicity and environmental risk of common antiviral drugs in aquatic environments post-pandemic. *Journal of Hazardous Materials*, *480*, 135947. https://doi.org/10.1016/J.JHAZMAT.2024.135947

Nugnes, R., Orlo, E., Russo, C., Lavorgna, M., & Isidori, M. (2024b). Comprehensive eco-geno-toxicity and environmental risk of common antiviral drugs in aquatic environments post-pandemic. *Journal of Hazardous Materials*, *480*, 135947. https://doi.org/10.1016/J.JHAZMAT.2024.135947

Obaideen, K., Shehata, N., Sayed, E. T., Abdelkareem, M. A., Mahmoud, M. S., & Olabi, A. G. (2022). The role of wastewater treatment in achieving sustainable development goals (SDGs) and sustainability guideline. *Energy Nexus*, *7*, 100112. https://doi.org/10.1016/J.NEXUS.2022.100112

Omotola, E. O., Genthe, B., Ndlela, L., & Olatunji, O. S. (2021). Environmental risk characterization of an antiretroviral (Arv) lamivudine in ecosystems. *International Journal of Environmental Research and Public Health*, *18*(16). https://doi.org/10.3390/ijerph18168358

Pal, S., Ahamed, Z., & Pal, P. (2022). Removal of antibiotics and pharmaceutically active compounds from water Environment: Experiments towards industrial scale up. *Separation and Purification Technology*, *295*, 121249. https://doi.org/10.1016/J.SEPPUR.2022.121249

Pandian, A. M. K., Rajamehala, M., Singh, M. V. P., Sarojini, G., & Rajamohan, N. (2022). Potential risks and approaches to reduce the toxicity of disinfection by-product – A review. *Science of The Total Environment*, *822*, 153323. https://doi.org/10.1016/J.SCITOTENV.2022.153323

Papagiannaki, D., Belay, M. H., Gonçalves, N. P. F., Robotti, E., Bianco-Prevot, A., Binetti, R., & Calza, P. (2022). From monitoring to treatment, how to improve water quality: The pharmaceuticals case. *Chemical Engineering Journal Advances*, *10*, 100245. https://doi.org/10.1016/J.CEJA.2022.100245

Priyadarshini, M., Das, I., Ghangrekar, M. M., & Blaney, L. (2022). Advanced oxidation processes: Performance, advantages, and scale-up of emerging technologies. *Journal of Environmental Management*, *316*, 115295. https://doi.org/10.1016/J.JENVMAN.2022.115295

Qiu, Y., Ren, L. F., Shao, J., Xia, L., & Zhao, Y. (2022). An integrated separation technology for high fluoride-containing wastewater treatment: Fluoride removal, membrane fouling behavior and control. *Journal of Cleaner Production*, *349*, 131225. https://doi.org/10.1016/J.JCLEPRO.2022.131225

Rosario-Ortiz, F. L., Wert, E. C., & Snyder, S. A. (2010). Evaluation of UV/H2O2 treatment for the oxidation of pharmaceuticals in wastewater. *Water Research*, *44*(5), 1440–1448. https://doi.org/10.1016/J.WATRES.2009.10.031

Sánchez-Polo, M., Abdel daiem, M. M., Ocampo-Pérez, R., Rivera-Utrilla, J., & Mota, A. J. (2013). Comparative study of the photodegradation of bisphenol A by HO, SO4− and CO3−/HCO3 radicals in aqueous phase. *Science of The Total Environment*, *463–464*, 423–431. https://doi.org/10.1016/J.SCITOTENV.2013.06.012

Saravanan, A., Deivayanai, V. C., Kumar, P. S., Rangasamy, G., Hemavathy, R. V., Harshana, T., Gayathri, N., & Alagumalai, K. (2022). A detailed review on advanced oxidation process in treatment of wastewater: Mechanism, challenges and future outlook. *Chemosphere*, *308*, 136524. https://doi.org/10.1016/J.CHEMOSPHERE.2022.136524

Sawicka, B., Aslan, I., Della Corte, V., Del Gaudio, G., Nevola, G., Periasamy, A., Krishnamurthy, S. K., Mohammed, A., Tolba Said, M. M., Saravanan, P., Adom, D., Sawicki, B., Hanchate, D. B., & Umachandran, K. (2022). The coronavirus global pandemic and its impacts on society. *Coronavirus Drug Discovery: Volume 1: SARS-CoV-2 (COVID-19) Prevention, Diagnosis, and Treatment*, 267–311. https://doi.org/10.1016/B978-0-323-85156-5.00037-7

Shi, J., Jiang, J., Chen, Q., Wang, L., Nian, K., & Long, T. (2023). Production of higher toxic intermediates of organic pollutants during chemical oxidation processes: A review. *Arabian Journal of Chemistry*, *16*(7), 104856. https://doi.org/10.1016/J.ARABJC.2023.104856

Silva, T. L. da, Costa, C. S. D., Silva, M. G. C. da, & Vieira, M. G. A. (2022). Overview of non-steroidal anti-inflammatory drugs degradation by advanced oxidation processes. *Journal of Cleaner Production*, *346*, 131226. https://doi.org/10.1016/J.JCLEPRO.2022.131226

Singh, N., & Narayan, M. (2023). Pollution in Freshwater: Impact and Prevention. In *Current Status of Fresh Water Microbiology* (347–358). Springer.

Soufan, M., Deborde, M., & Legube, B. (2012). Aqueous chlorination of diclofenac: Kinetic study and transformation products identification. *Water Research*, *46*(10), 3377–3386. https://doi.org/10.1016/J.WATRES.2012.03.056

Srivastava, B., & Reddy, P. B. (2022). Environmental Impacts of COVID-19 Pharmaceuticals and Disinfectants. *Asian Pacific Journal of Health Sciences*, *9*(4), 263–268. https://doi.org/10.21276/apjhs.2022.9.4s.50

Steve Chaplin. (2022). Paxlovid: antiviral combination for the treatment of COVID-19. *Wiley Online Library*, *33*(3–4), 31–33.

Swati, J., Vyas, R. K., Prabhat, P., & Sangeeta, V. (2011). A review on fate of antiviral drugs in environment and detection techniques. In *INTERNATIONAL JOURNAL OF ENVIRONMENTAL SCIENCES* (Vol. 1, Issue 7). www.IndianJournals.com

Tang, Z., Tao, Z., Cao, Y., Zhang, Q., Liu, W., & Cao, C. (2024). Capacitively coupled contactless conductivity detection-based sensor for liquid level measurement and application to clinical infusion monitoring. *Sensors and Actuators A: Physical*, *367*, 115073. https://doi.org/10.1016/J.SNA.2024.115073

Thi, L. A. P., Panchangam, S. C., Do, H. T., & Nguyen, V. H. (2021). Prospects and challenges of photocatalysis for degradation and mineralization of antiviral drugs. *Nanostructured Photocatalysts: From Fundamental to Practical Applications*, 489–517. https://doi.org/10.1016/B978-0-12-823007-7.00012-2

Tobólska, S., Terpiłowska, S., Jaroszewski, J., & Siwicki, A. K. (2018). Influence of inosine pranobex on cell viability in normal fibroblasts and liver cancer cells. *Journal of Veterinary Research (Poland)*, *62*(2), 215–220. https://doi.org/10.2478/jvetres-2018-0031

Tompa, D. R., Immanuel, A., Srikanth, S., & Kadhirvel, S. (2021). Trends and strategies to combat viral infections: A review on FDA approved antiviral drugs. *International Journal of Biological Macromolecules*, *172*, 524–541. https://doi.org/10.1016/J.IJBIOMAC.2021.01.076

United Nations. (2025). *Sustainable Development Goals*.

Vardanyan, R., & Hruby, V. (2016). Antiviral Drugs. *Synthesis of Best-Seller Drugs*, 687–736. https://doi.org/10.1016/B978-0-12-411492-0.00034-1

Vitiello, A., & Ferrara, F. (2022). Remdesivir versus ritonavir/lopinavir in COVID-19 patients. *Irish Journal of Medical Science*, *2021*(190), 1249–1250. https://doi.org/10.1016/j.ejphar.2020.173373

Voigt, M., & Jaeger, M. (2025). 5 Years of Covid19—do antiviral drugs and their metabolites pose a danger to the aquatic environment?—a short review. In *Toxicological and Environmental Chemistry* (Vol. 107, Issue 7, pp. 1267–1290). Taylor and Francis Ltd. https://doi.org/10.1080/02772248.2025.2521748

Wallace, V. J., Sakowski, E. G., Preheim, S. P., & Prasse, C. (2023). Bacteria exposed to antiviral drugs develop antibiotic cross-resistance and unique resistance

profiles. *Communications Biology*, *6*(1). https://doi.org/10.1038/s42003-023-05177-3

Wang, J., & Wang, S. (2021). Effect of inorganic anions on the performance of advanced oxidation processes for degradation of organic contaminants. *Chemical Engineering Journal*, *411*, 128392. https://doi.org/10.1016/J.CEJ.2020.128392

Wang, K., Zhuang, T., Su, Z., Chi, M., & Wang, H. (2021). Antibiotic residues in wastewaters from sewage treatment plants and pharmaceutical industries: Occurrence, removal and environmental impacts. *Science of The Total Environment*, *788*, 147811. https://doi.org/10.1016/J.SCITOTENV.2021.147811

Wang, R., Luo, J., Li, C., Chen, J., & Zhu, N. (2023). Antiviral drugs in wastewater are on the rise as emerging contaminants: A comprehensive review of spatiotemporal characteristics, removal technologies and environmental risks. *Journal of Hazardous Materials*, *457*, 131694. https://doi.org/10.1016/J.JHAZMAT.2023.131694

Wang, R., Wang, Z., Yuan, H., Li, C., & Zhu, N. (2024). Mechanistic exploration of COVlD-19 antiviral drug ritonavir on anaerobic digestion through experimental validation coupled with metagenomics analysis. *Journal of Hazardous Materials*, *479*, 135603. https://doi.org/10.1016/J.JHAZMAT.2024.135603

Yang, Y., Xie, Z. H., Wang, H., Yang, S. R., Wang, T., He, C. S., & Lai, B. (2024). Ecological risk assessment methods for oxidative by–products in the oxidation degradation process of emerging pollutants: A review. *Science of the Total Environment*, *950*. https://doi.org/10.1016/J.SCITOTENV.2024.175401

Yao, L., Chen, Z. Y., Dou, W. Y., Yao, Z. K., Duan, X. C., Chen, Z. F., Zhang, L. J., Nong, Y. J., Zhao, J. L., & Ying, G. G. (2021). Occurrence, removal and mass loads of antiviral drugs in seven wastewater treatment plants with various treatment processes. *Water Research*, *207*, 117803. https://doi.org/10.1016/J.WATRES.2021.117803

Zhang, D., Lv, S., & Luo, Z. (2020). A study on the photocatalytic degradation performance of a [KNbO3]0.9-[BaNi0.5Nb0.5O3-: δ]0.1 perovskite. *RSC Advances*, *10*(3), 1275–1280. https://doi.org/10.1039/c9ra07310h

Zhou, C., Chen, J., Xie, Q., Wei, X., Zhang, Y. nan, & Fu, Z. (2015a). Photolysis of three antiviral drugs acyclovir, zidovudine and lamivudine in surface freshwater and seawater. *Chemosphere*, *138*, 792–797. https://doi.org/10.1016/j.chemosphere.2015.08.033

Zhou, C., Chen, J., Xie, Q., Wei, X., Zhang, Y. nan, & Fu, Z. (2015b). Photolysis of three antiviral drugs acyclovir, zidovudine and lamivudine in surface freshwater and seawater. *Chemosphere*, *138*, 792–797. https://doi.org/10.1016/J.CHEMOSPHERE.2015.08.033

Zhou, C., Chen, J., Xie, Q., Wei, X., Zhang, Y. nan, & Fu, Z. (2015c). Photolysis of three antiviral drugs acyclovir, zidovudine and lamivudine in surface freshwater

and seawater. *Chemosphere*, *138*, 792–797. https://doi.org/10.1016/J.CHEMOSPHERE.2015.08.033

Zhu, G., Sun, Q., Wang, C., Yang, Z., & Xue, Q. (2019). Removal of sulfamethoxazole, sulfathiazole and sulfamethazine in their mixed solution by UV/H_2O_2 process. *International Journal of Environmental Research and Public Health*, *16*(10). https://doi.org/10.3390/IJERPH16101797

Zinicovscaia, I. (2016). Conventional methods of wastewater treatment. *Cyanobacteria for Bioremediation of Wastewaters*, 17–25. https://doi.org/10.1007/978-3-319-26751-7_3/COVER

Chapter 8 – Supporting information

To enhance the transparency and reproducibility of the experimental results presented in this thesis, supplementary documentation has been included. Specifically, screenshots of the High-Performance Liquid Chromatography (HPLC) display, captured both prior to and following the addition of the selected photocatalysts, are provided. These images serve as visual evidence supporting the observed changes in chromatographic profiles and further substantiate the conclusions drawn from the analysis. This supplementary material is appended after the conclusion section of the thesis and is intended to assist readers in validating the methodology and data interpretation. The chromatograms represent the baseline profile of the reaction mixture in the absence of any photocatalytic influence, serving as a reference for subsequent analysis. In addition, with the modified chromatographic profiles following photocatalyst introduction, highlighting the changes in peak intensities and retention times that support the conclusions drawn in the results section.

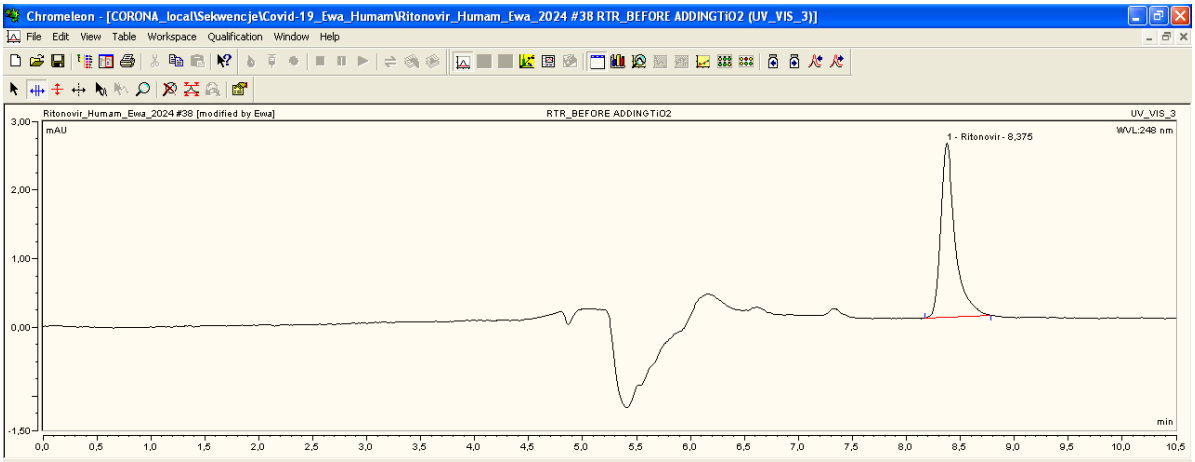

No.	Peakname	Ret.Time min	Area mAU*min	Amount	Type	Height mAU	Rel.Area %	Resolution
1	Ritonovir	8,375	0,3962	2,5598	BMB	2,533	100,00	n.a.
Total:			0,3962	2,5598		2,533	100,00	

Figure S.1a. HPLC chromatogram of antiviral drug RTR before the addition of TiO_2

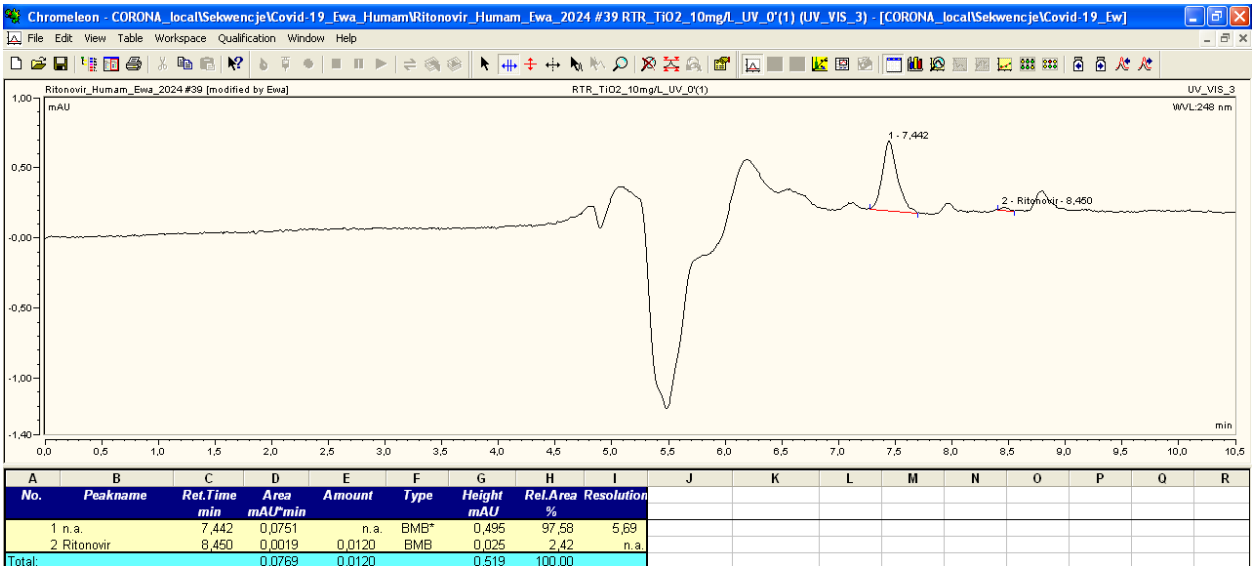

No.	Peakname	Ret.Time min	Area mAU*min	Amount	Type	Height mAU	Rel.Area %	Resolution
1	n.a.	7,442	0,0751	n.a.	BMB*	0,495	97,58	5,69
2	Ritonovir	8,450	0,0019	0,0120	BMB	0,025	2,42	n.a.
Total:			0.0769	0.0120		0.519	100.00	

Figure S.1b. HPLC chromatogram of antiviral drug RTR after the addition of TiO_2

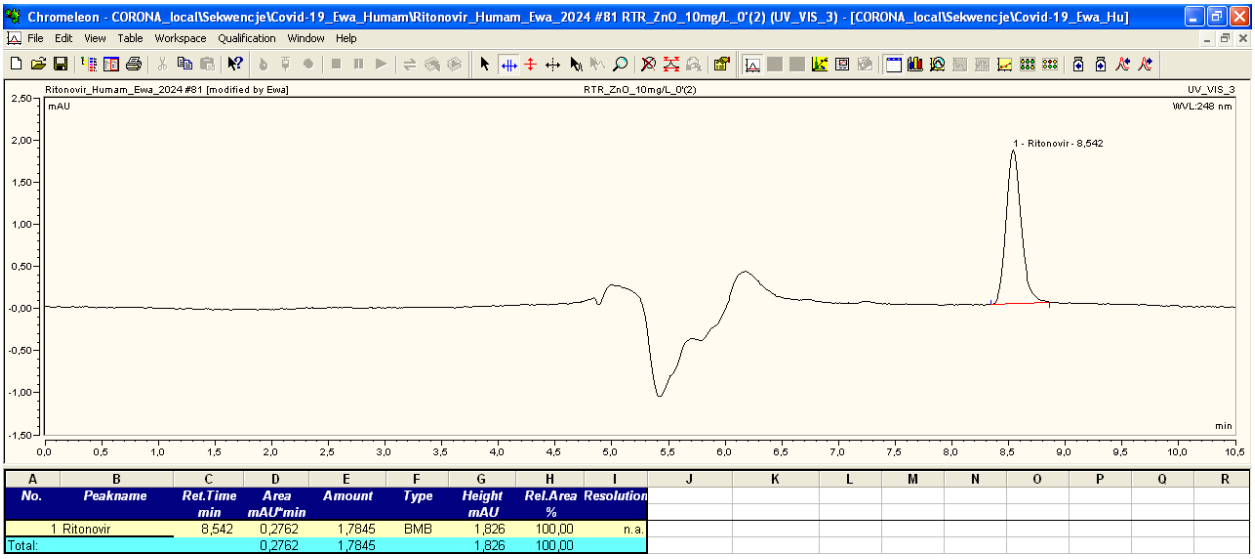

No.	Peakname	Ret.Time min	Area mAU*min	Amount	Type	Height mAU	Rel.Area %	Resolution
1	Ritonovir	8,542	0,2762	1,7845	BMB	1,826	100,00	n.a.
Total:			0,2762	1,7845		1,826	100,00	

Figure S.2a. HPLC chromatogram of antiviral drug RTR before the addition of ZnO

No.	Peakname	Ret.Time min	Area mAU*min	Amount	Type	Height mAU	Rel.Area %	Resolution
1	n.a.	7,542	0,0673	n.a.	BMB*	0,507	70,26	2,85
2	n.a.	8,067	0,0080	n.a.	BMB	0,078	8,40	4,03
3	Ritonovir	8,533	0,0002	0,0015	BMB	0,007	0,25	2,72
4	n.a.	8,908	0,0202	n.a.	BMB	0,145	21,09	n.a.
Total:			0,0958	0,0015		0,737	100,00	

Figure S.2b. HPLC chromatogram of antiviral drug RTR after the addition of ZnO

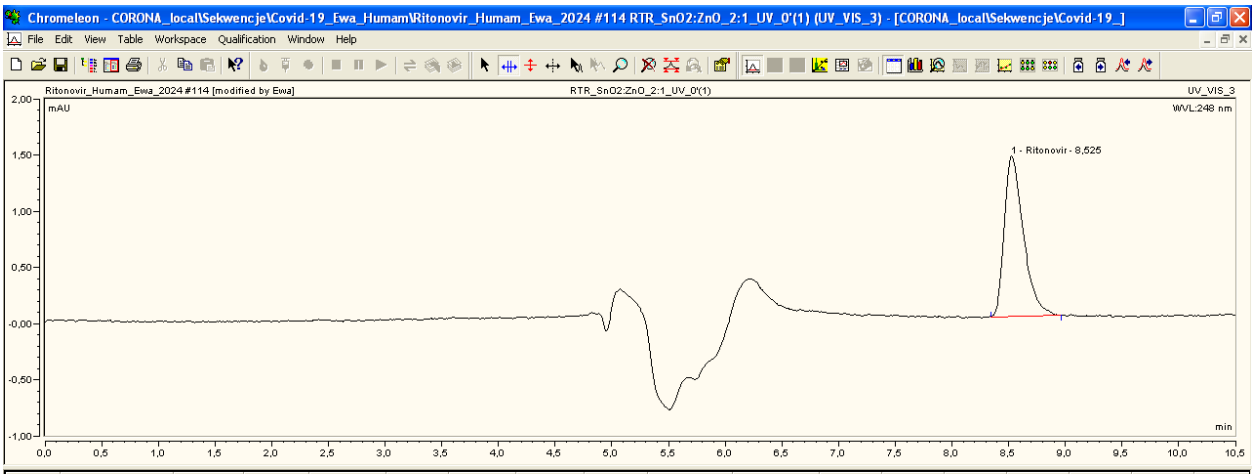

No.	Peakname	Ret.Time min	Area mAU*min	Amount	Type	Height mAU	Rel.Area %	Resolution
1	Ritonovir	8,525	0,2759	1,7829	BMB*	1,427	100,00	n.a.
Total:			0,2759	1,7829		1,427	100,00	

Figure S.3a. HPLC chromatogram of antiviral drug RTR before the addition of SnO_2:ZnO (2:1)

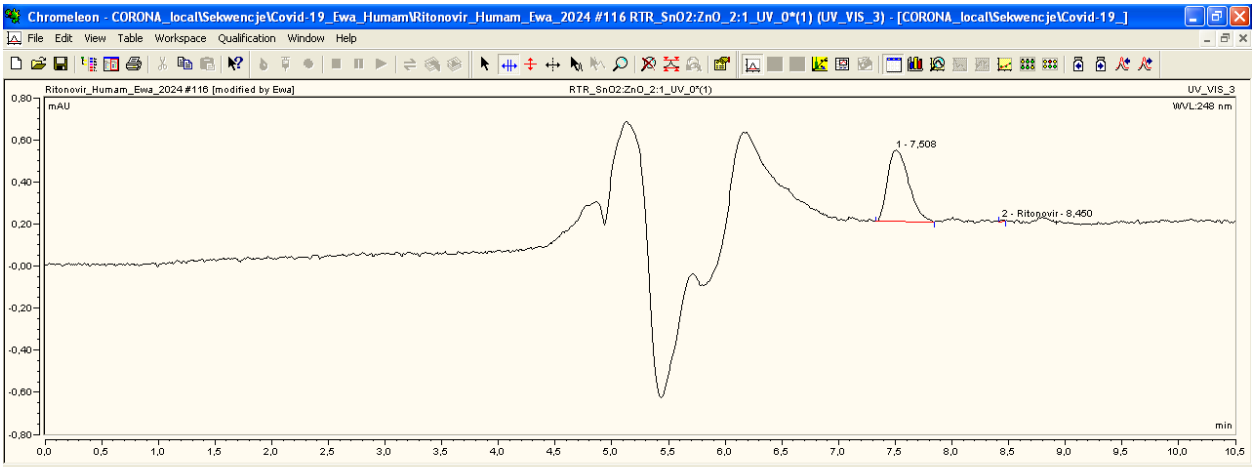

No.	Peakname	Ret.Time min	Area mAU*min	Amount	Type	Height mAU	Rel.Area %	Resolution
1	n.a.	7,508	0,0739	n.a.	BMB	0,340	99,55	4,42
2	Ritonovir	8,460	0,0003	0,0021	BMB	0,009	0,45	n.a.
Total:			0,0743	0,0021		0,349	100,00	

Figure S.3b. HPLC chromatogram of antiviral drug RTR after the addition of SnO_2:ZnO (2:1)

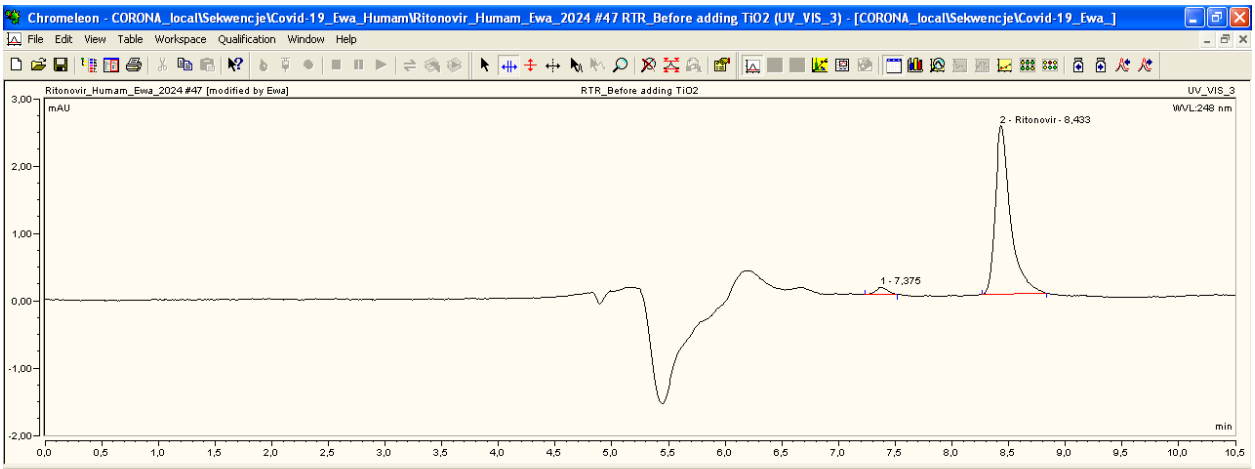

No.	Peakname	Ret.Time min	Area mAU*min	Amount	Type	Height mAU	Rel.Area %	Resolution
1	n.a.	7,375	0,0142	n.a.	BMB*	0,113	3,48	5,09
2	Ritonovir	8,433	0,3933	2,5411	BMB	2,503	96,52	n.a.
Total:			0,4075	2,5411		2,617	100,00	

Figure S.4a. HPLC chromatogram of antiviral drug RTR before the addition of TiO_2 under dark conditions

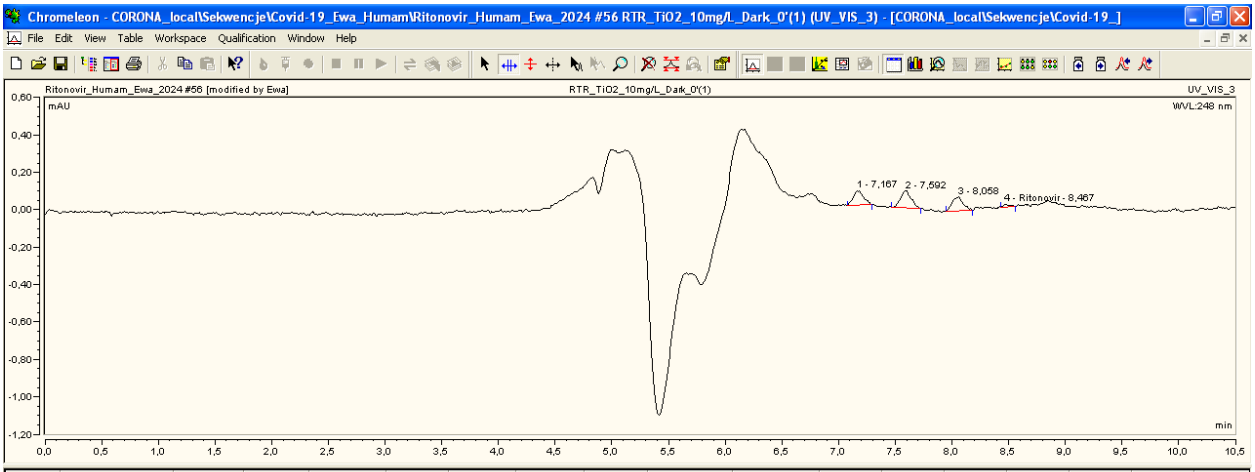

No.	Peakname	Ret.Time min	Area mAU*min	Amount	Type	Height mAU	Rel.Area %	Resolution
1	n.a.	7,167	0,0081	n.a.	BMB	0,078	29,57	2,48
2	n.a.	7,592	0,0103	n.a.	BMB	0,090	37,45	2,61
3	n.a.	8,058	0,0081	n.a.	BMB*	0,075	29,48	2,71
4	Ritonovir	8,467	0,0010	0,0062	BMB	0,016	3,51	n.a.
Total:			0,0274	0,0062		0,259	100,00	

Figure S.4b. HPLC chromatogram of antiviral drug RTR after the addition of TiO_2 under dark conditions

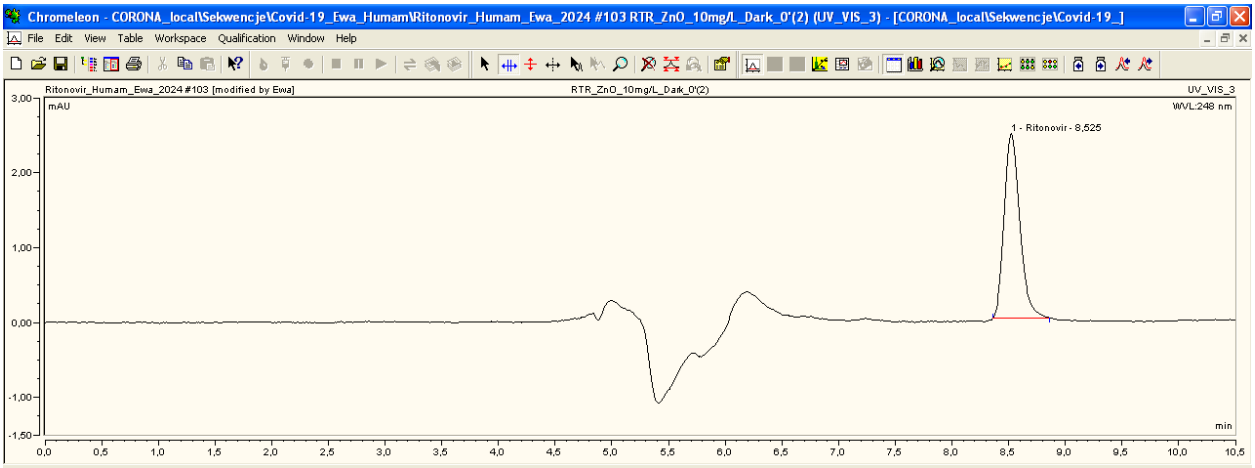

No.	Peakname	Ret.Time min	Area mAU*min	Amount	Type	Height mAU	Rel.Area %	Resolution
1	Ritonovir	8,525	0,3882	2,5081	BMB*	2,462	100,00	n.a.
Total:			0,3882	2,5081		2,462	100,00	

Figure S.5a. HPLC chromatogram of antiviral drug RTR before the addition of ZnO under dark conditions

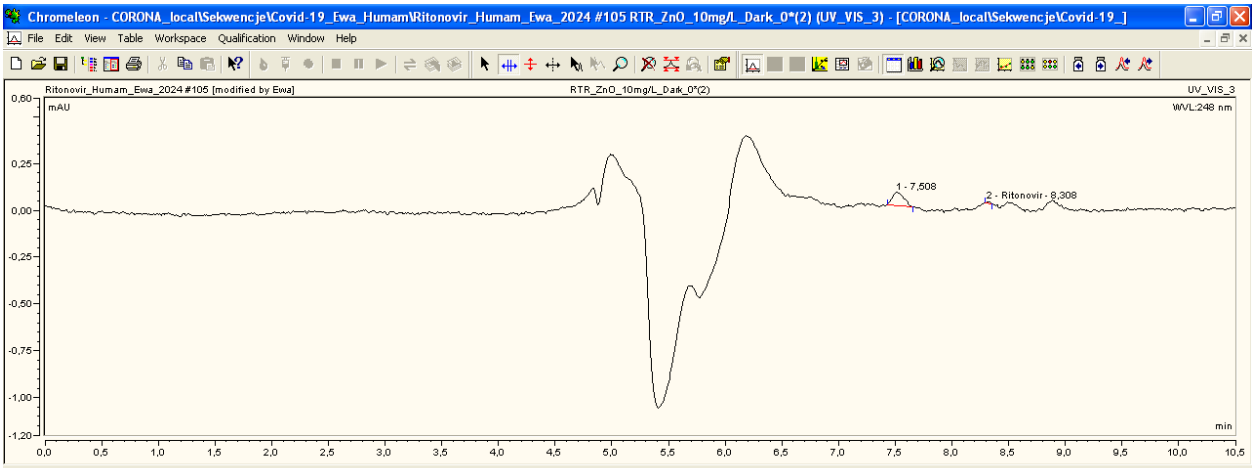

No.	Peakname	Ret.Time min	Area mAU*min	Amount	Type	Height mAU	Rel.Area %	Resolution
1	n.a.	7,508	0,0080	n.a.	BMB*	0,069	95,95	n.a.
2	Ritonovir	8,308	0,0003	0,0022	BMB	0,009	4,05	n.a.
Total:			0,0083	0,0022		0,078	100,00	

Figure S.5b. HPLC chromatogram of antiviral drug RTR after the addition of ZnO under dark conditions

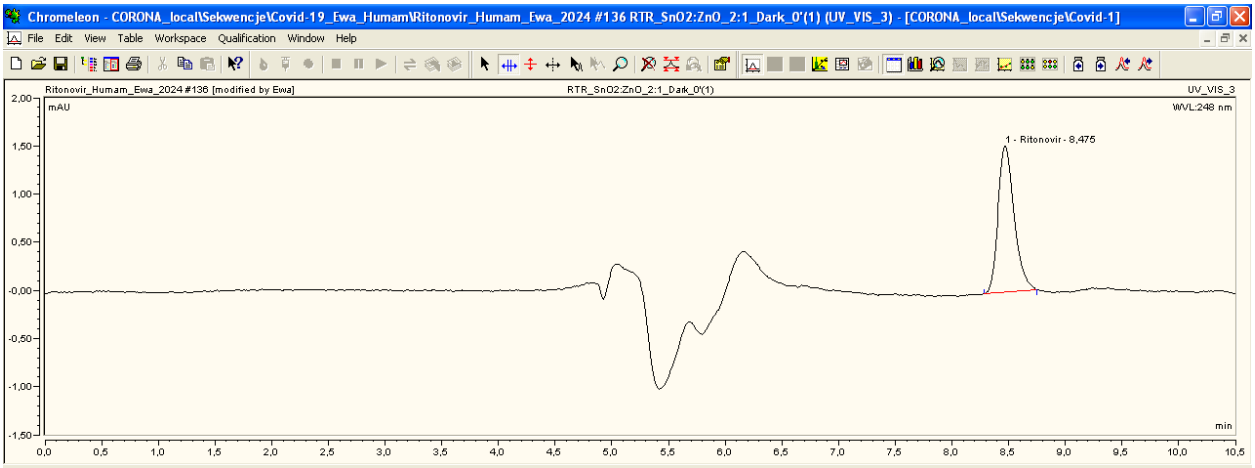

No.	Peakname	Ret.Time min	Area mAU*min	Amount	Type	Height mAU	Rel.Area %	Resolution
1	Ritonovir	8,475	0,2512	1,6229	BMB	1,522	100,00	n.a.
Total:			0,2512	1,6229		1,522	100,00	

Figure S.6a. HPLC chromatogram of antiviral drug RTR before the addition of SnO_2:ZnO (2:1) under dark conditions

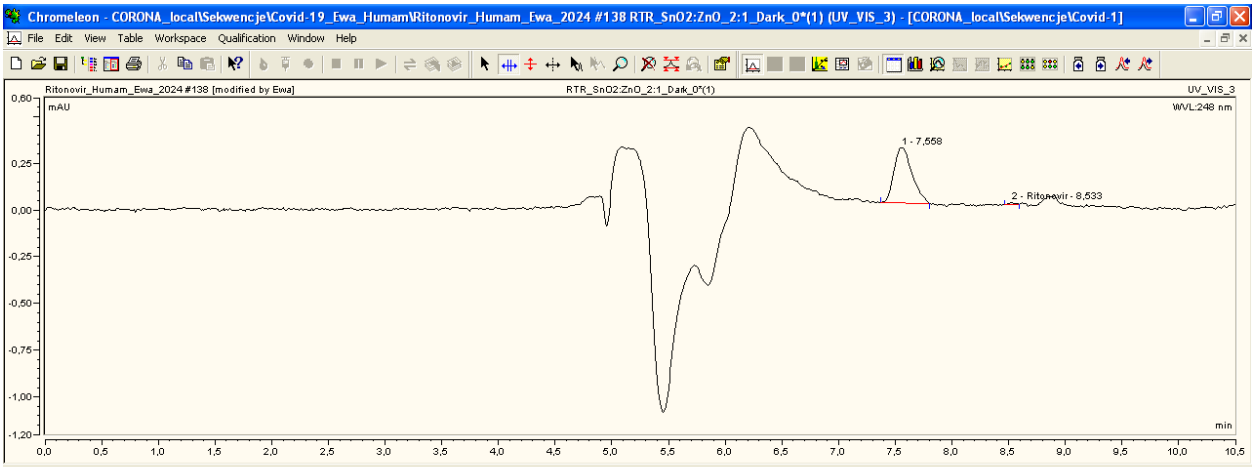

No.	Peakname	Ret.Time min	Area mAU*min	Amount	Type	Height mAU	Rel.Area %	Resolution
1	n.a.	7,558	0,0548	n.a.	BMB	0,295	98,53	4,68
2	Ritonovir	8,533	0,0008	0,0053	BMB*	0,012	1,47	n.a.
Total:			0,0556	0,0053		0,307	100,00	

Figure S.6b. HPLC chromatogram of antiviral drug RTR after the addition of SnO_2:ZnO (2:1) under dark condition

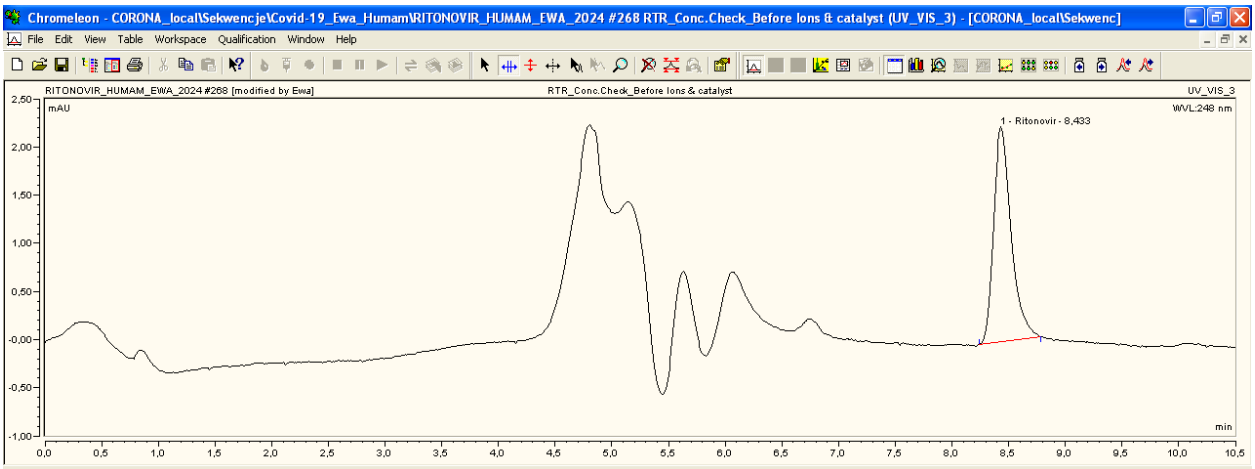

No.	Peakname	Ret.Time min	Area mAU*min	Amount	Type	Height mAU	Rel.Area %	Resolution
1	Ritonovir	8,433	0,4025	2,6005	BMB	2,230	100,00	n.a.
Total:			0,4025	2,6005		2,230	100,00	

Figure S.7a. HPLC chromatogram of antiviral drug RTR before the addition of selected photocatalyst and SO_4^{-2} ions

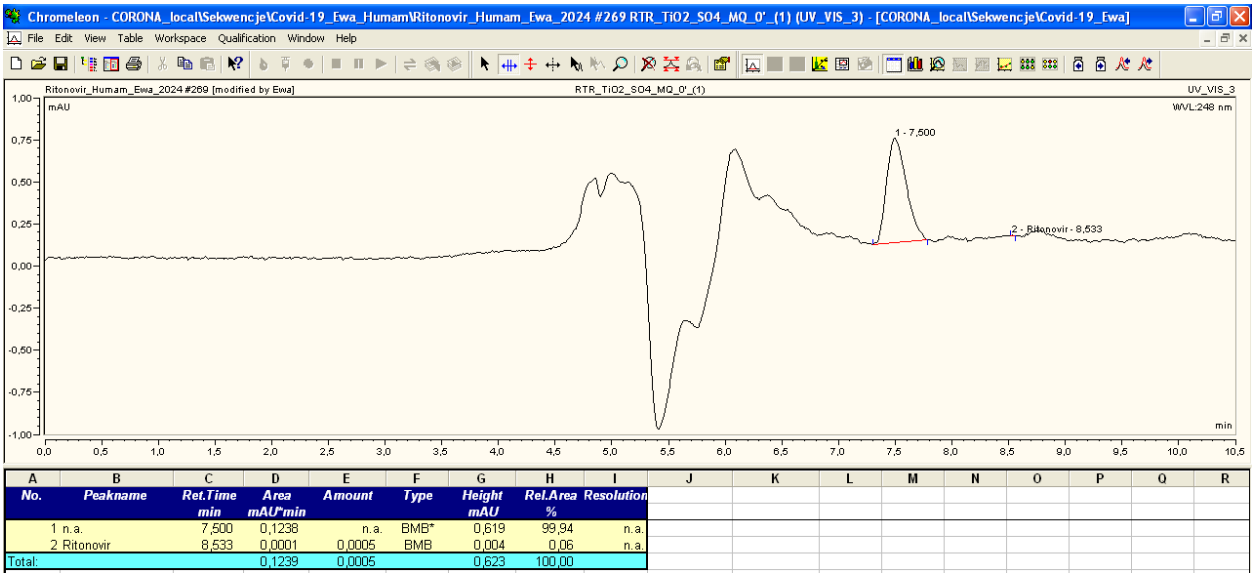

No.	Peakname	Ret.Time min	Area mAU*min	Amount	Type	Height mAU	Rel.Area %	Resolution
1	n.a.	7,500	0,1238	n.a.	BMB*	0,619	99,94	n.a.
2	Ritonovir	8,533	0,0001	0,0005	BMB	0,004	0,06	n.a.
Total:			0,1239	0,0005		0,623	100,00	

Figure S.7b. HPLC chromatogram of antiviral drug RTR after the addition of TiO_2 and SO_4^{-2} ions

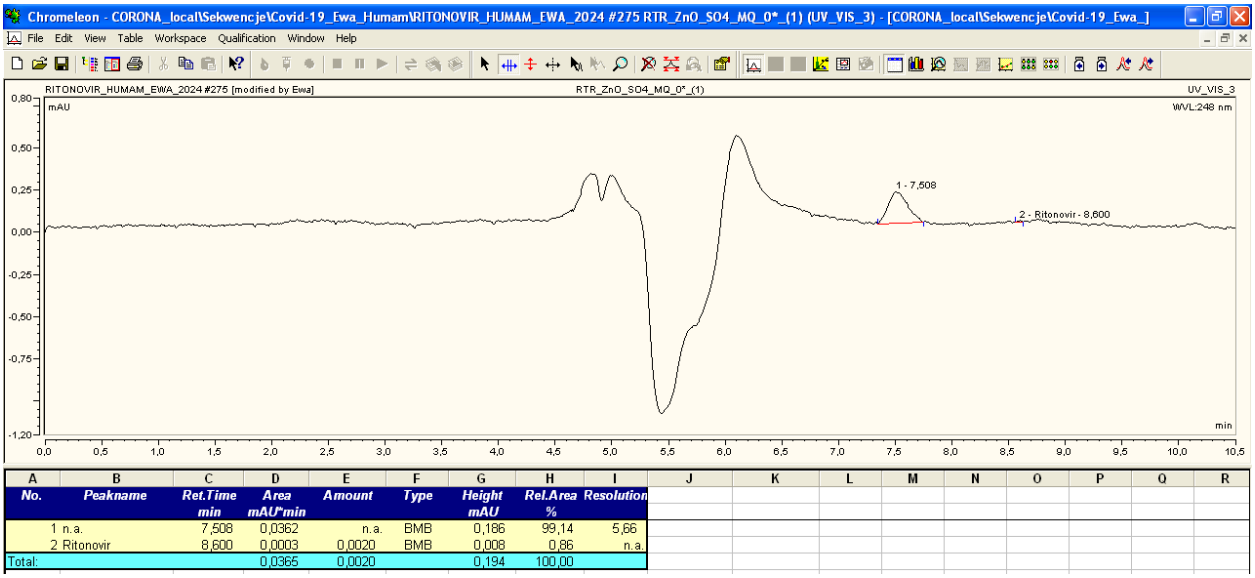

No.	Peakname	Ret.Time min	Area mAU*min	Amount	Type	Height mAU	Rel.Area %	Resolution
1	n.a.	7,508	0,0362	n.a.	BMB	0,186	99,14	5,66
2	Ritonovir	8,600	0,0003	0,0020	BMB	0,008	0,86	n.a.
Total:			0,0365	0,0020		0,194	100,00	

Figure S.7c. HPLC chromatogram of antiviral drug RTR after the addition of ZnO and SO_4^{-2} ions

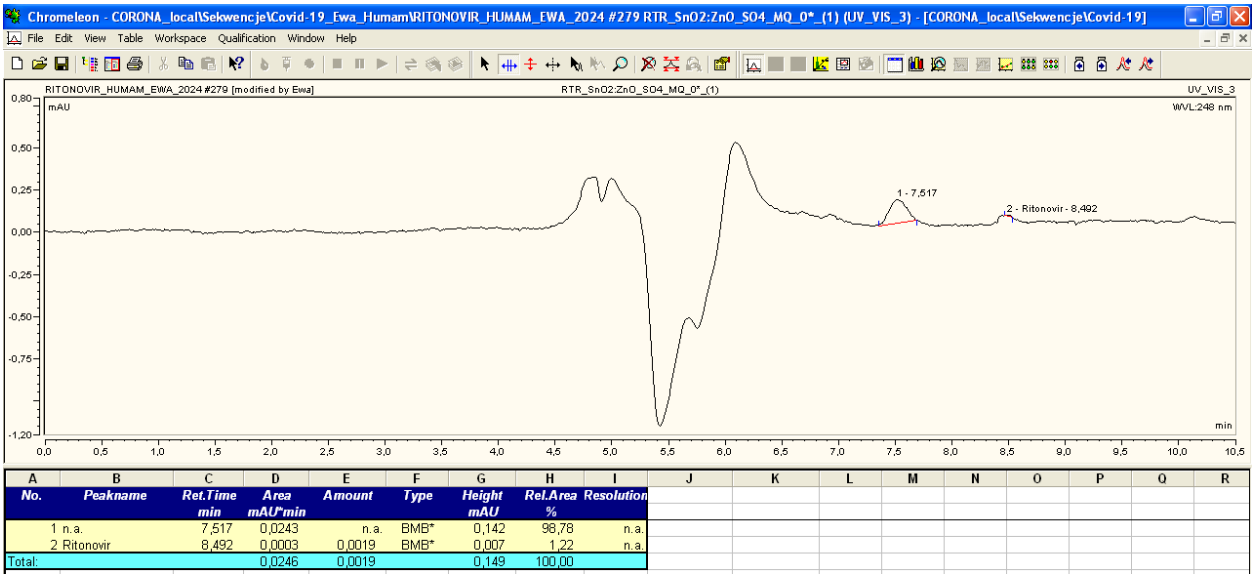

No.	Peakname	Ret.Time min	Area mAU*min	Amount	Type	Height mAU	Rel.Area %	Resolution
1	n.a.	7,517	0,0243	n.a.	BMB*	0,142	98,78	n.a.
2	Ritonovir	8,492	0,0003	0,0019	BMB*	0,007	1,22	n.a.
Total:			0,0246	0,0019		0,149	100,00	

Figure S.7d. HPLC chromatogram of antiviral drug RTR after the addition of SnO_2:ZnO and SO_4^{-2} ions

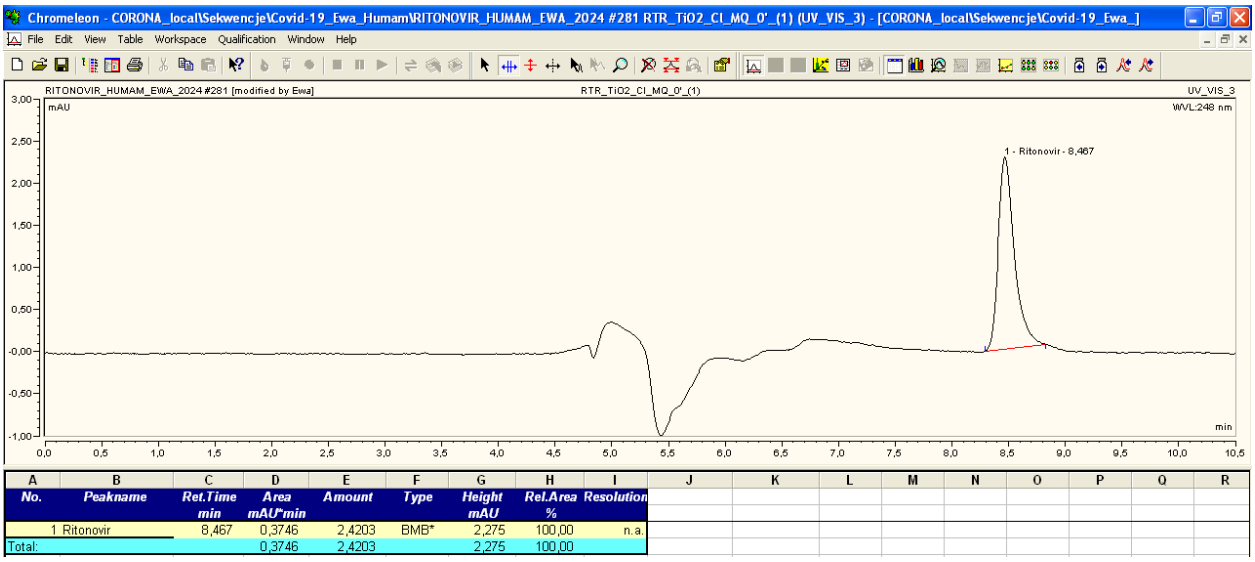

No.	Peakname	Ret.Time min	Area mAU*min	Amount	Type	Height mAU	Rel.Area %	Resolution
1	Ritonovir	8,467	0,3746	2,4203	BMB*	2,275	100,00	n.a.
Total:			0,3746	2,4203		2,275	100,00	

Figure S.8a. HPLC chromatogram of antiviral drug RTR before the addition of TiO_2 and Cl^- ions

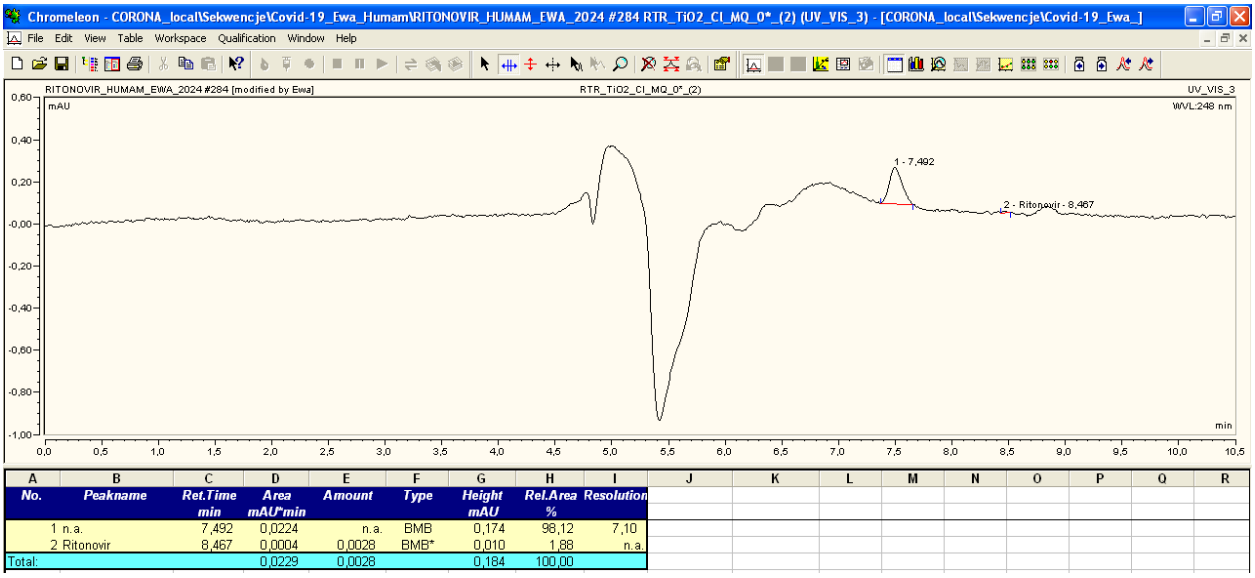

No.	Peakname	Ret.Time min	Area mAU*min	Amount	Type	Height mAU	Rel.Area %	Resolution
1	n.a.	7,492	0,0224	n.a.	BMB	0,174	98,12	7,10
2	Ritonovir	8,467	0,0004	0,0028	BMB*	0,010	1,88	n.a.
Total:			0,0229	0,0028		0,184	100,00	

Figure S.8b. HPLC chromatogram of antiviral drug RTR after the addition of TiO_2 and Cl^- ions

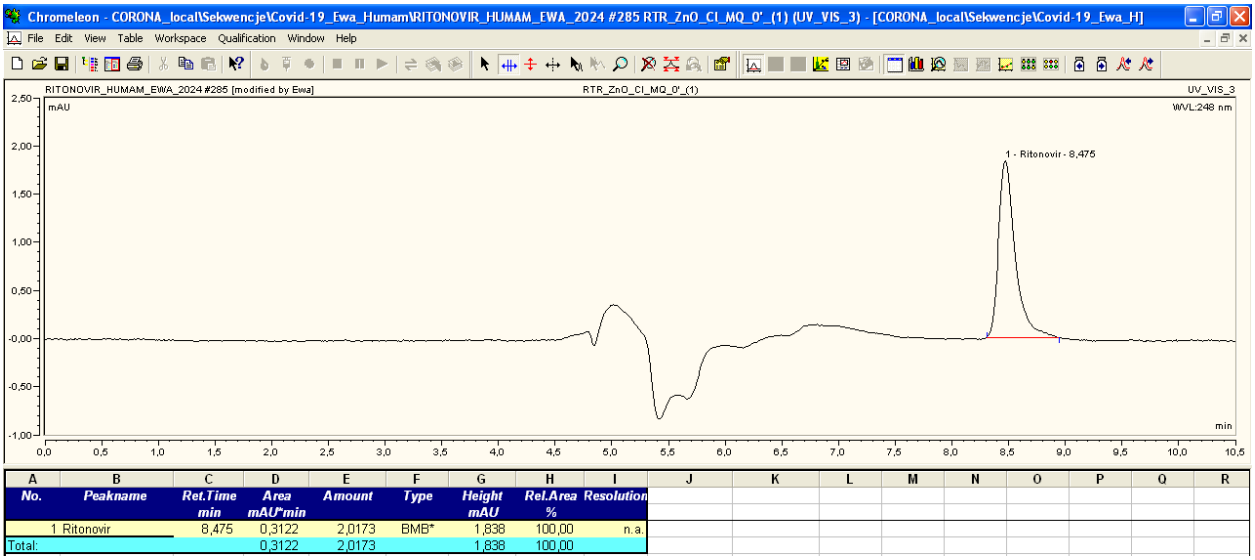

No.	Peakname	Ret.Time min	Area mAU*min	Amount	Type	Height mAU	Rel.Area %	Resolution
1	Ritonovir	8,475	0,3122	2,0173	BMB*	1,838	100,00	n.a.
Total:			0,3122	2,0173		1,838	100,00	

Figure S.9a. HPLC chromatogram of antiviral drug RTR before the addition of ZnO and Cl^- ions

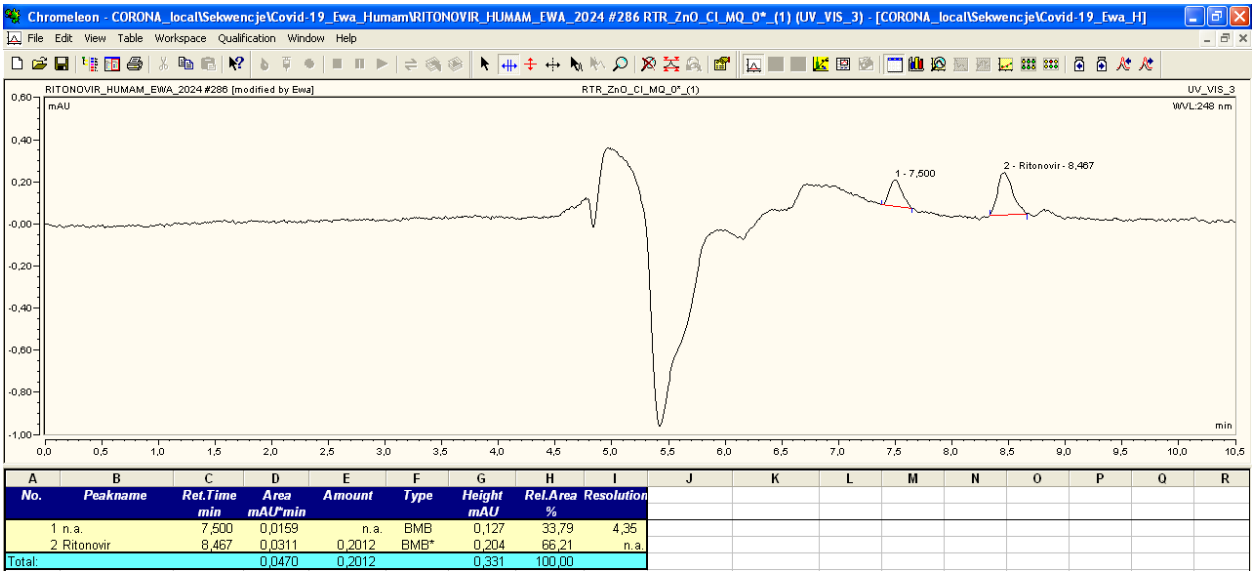

No.	Peakname	Ret.Time min	Area mAU*min	Amount	Type	Height mAU	Rel.Area %	Resolution
1	n.a.	7,500	0,0159	n.a.	BMB	0,127	33,79	4,35
2	Ritonovir	8,467	0,0311	0,2012	BMB*	0,204	66,21	n.a.
Total:			0,0470	0,2012		0,331	100,00	

Figure S.9b. HPLC chromatogram of antiviral drug RTR after the addition of ZnO and Cl ¯ions

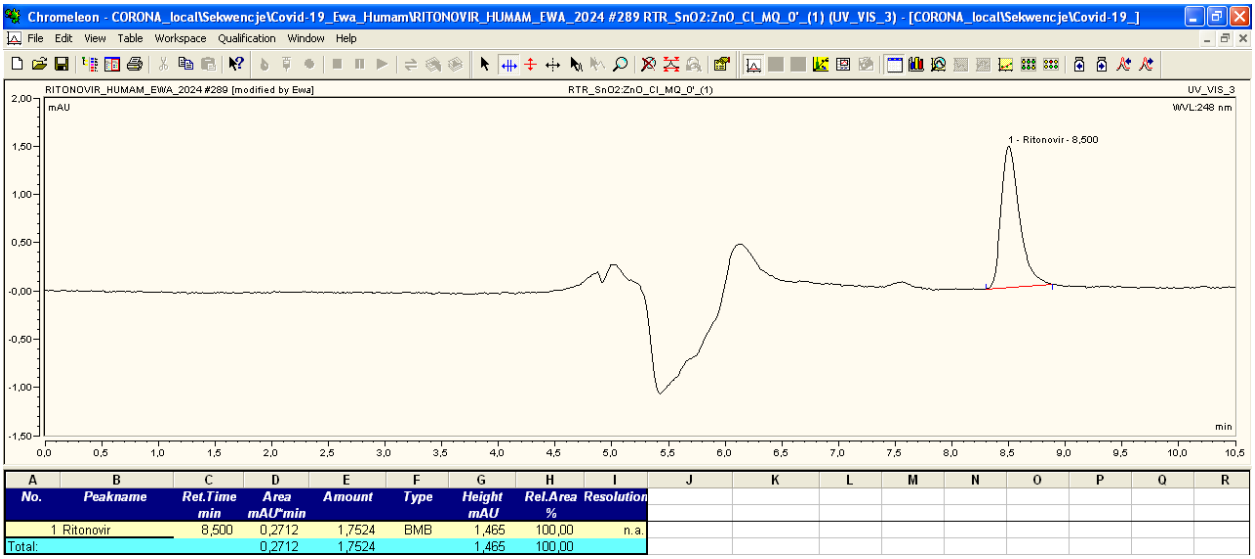

No.	Peakname	Ret.Time min	Area mAU*min	Amount	Type	Height mAU	Rel.Area %	Resolution
1	Ritonovir	8,500	0,2712	1,7524	BMB	1,465	100,00	n.a.
Total:			0,2712	1,7524		1,465	100,00	

Figure S.10a. HPLC chromatogram of antiviral drug RTR before the addition of SnO_2:ZnO and Cl ¯ions

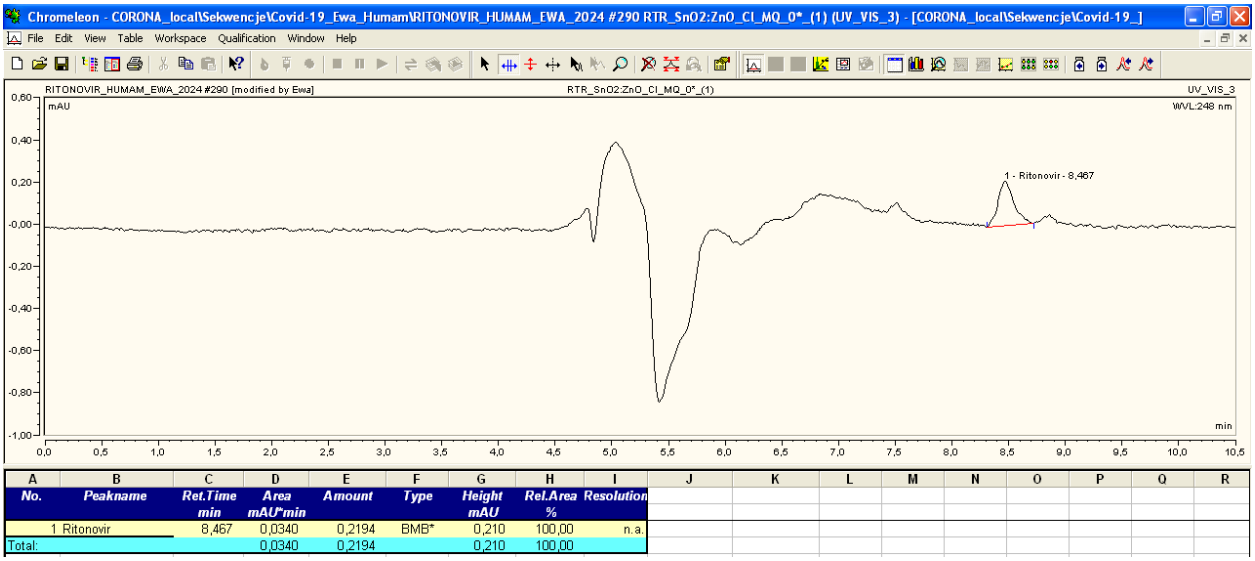

No.	Peakname	Ret.Time min	Area mAU*min	Amount	Type	Height mAU	Rel.Area %	Resolution
1	Ritonovir	8,467	0,0340	0,2194	BMB*	0,210	100,00	n.a.
Total:			0,0340	0,2194		0,210	100,00	

Figure S.10b. HPLC chromatogram of antiviral drug RTR after the addition of SnO_2:ZnO and Cl^- ions

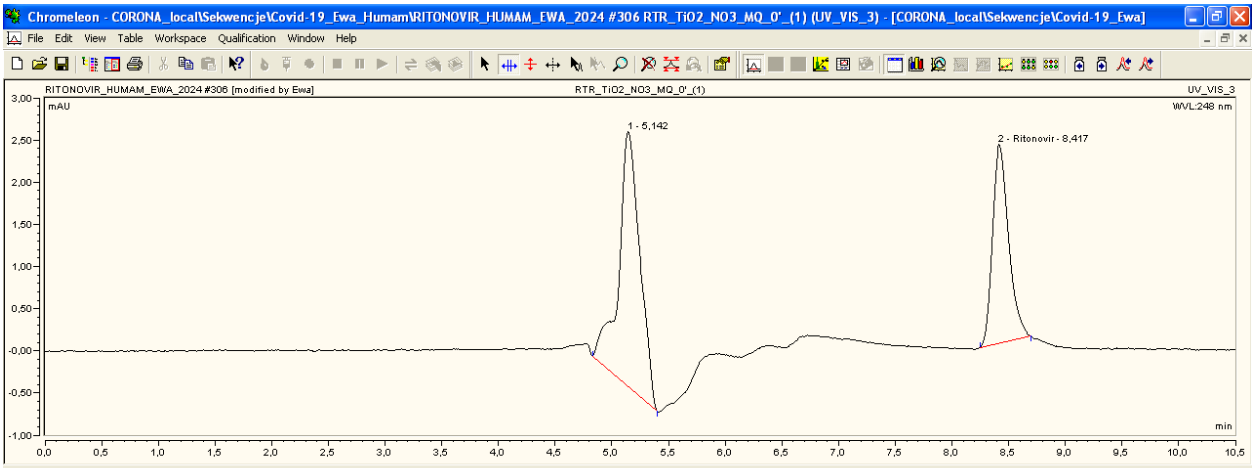

No.	Peakname	Ret.Time min	Area mAU*min	Amount	Type	Height mAU	Rel.Area %	Resolution
1	n.a.	5,142	0,6536	n.a.	BMB*	3,014	62,47	11,60
2	Ritonovir	8,417	0,3927	2,5370	BMB*	2,354	37,53	n.a.
Total:			1,0463	2,5370		5,368	100,00	

Figure S.11a. HPLC chromatogram of antiviral drug RTR before the addition of TiO_2 and NO_3^- ions

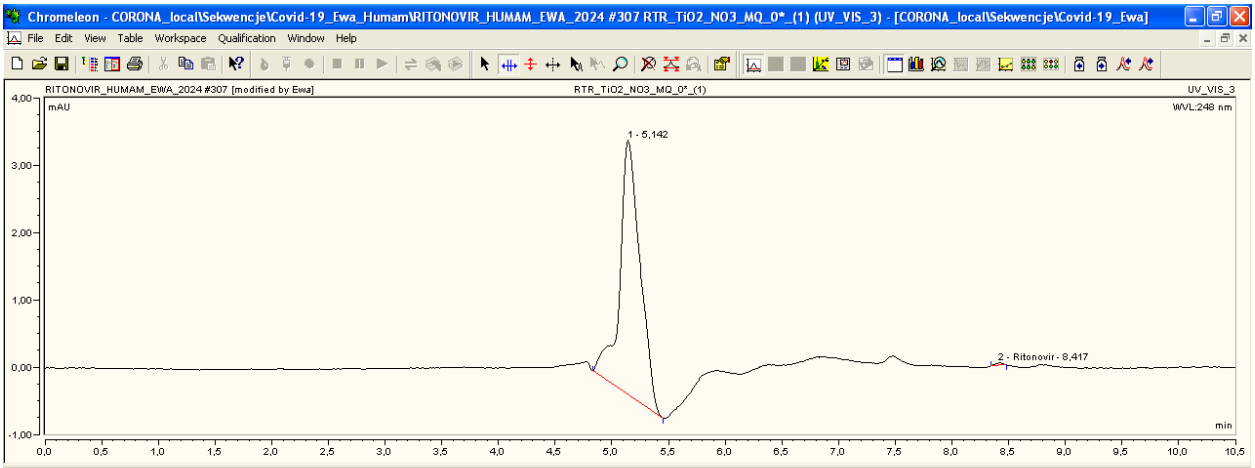

No.	Peakname	Ret.Time min	Area mAU*min	Amount	Type	Height mAU	Rel.Area %	Resolution
1	n.a.	5,142	0,7877	n.a.	BMB*	3,773	99,60	14,07
2	Ritonovir	8,417	0,0032	0,0204	BMB*	0,037	0,40	n.a.
Total:			0,7908	0,0204		3,810	100,00	

Figure S.11b. HPLC chromatogram of antiviral drug RTR after the addition of TiO_2 and NO_3^- ions

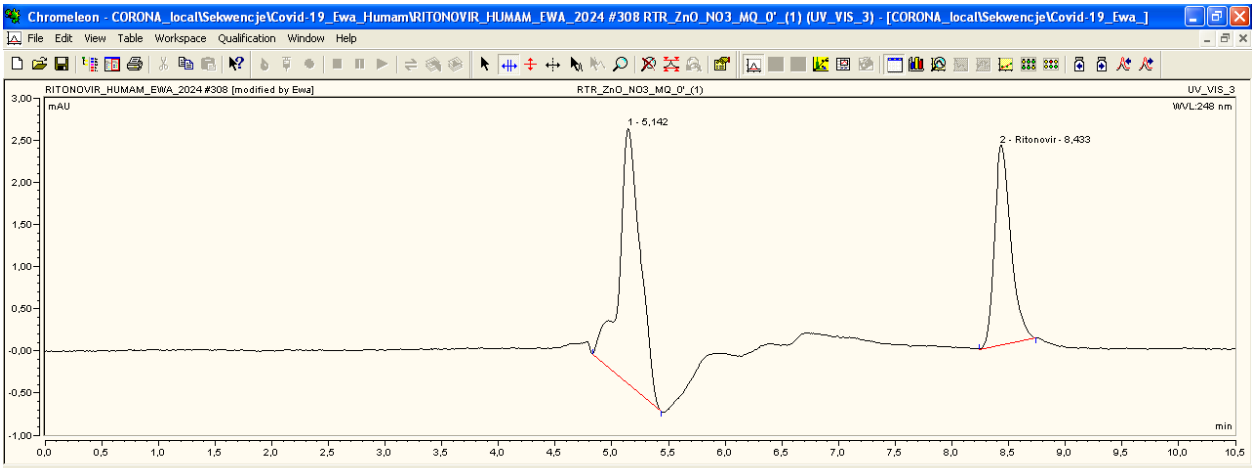

No.	Peakname	Ret.Time min	Area mAU*min	Amount	Type	Height mAU	Rel.Area %	Resolution
1	n.a.	5,142	0,6604	n.a.	BMB*	3,025	62,23	11,45
2	Ritonovir	8,433	0,4009	2,5900	BMB*	2,366	37,77	n.a.
Total:			1,0612	2,5900		5,391	100,00	

Figure S.12a. HPLC chromatogram of antiviral drug RTR before the addition of ZnO and NO_3^- ions

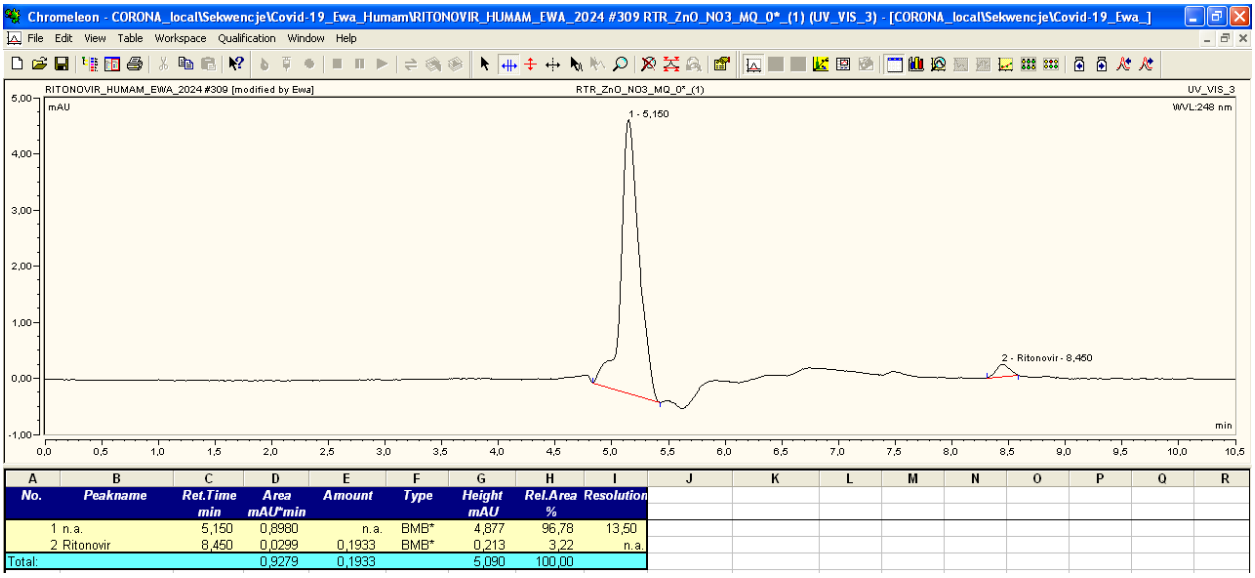

No.	Peakname	Ret.Time min	Area mAU*min	Amount	Type	Height mAU	Rel.Area %	Resolution
1	n.a.	5,150	0,8980	n.a.	BMB*	4,877	96,78	13,50
2	Ritonovir	8,450	0,0299	0,1933	BMB*	0,213	3,22	n.a.
Total:			0,9279	0,1933		5,090	100,00	

Figure S.12b. HPLC chromatogram of antiviral drug RTR after the addition of ZnO and NO_3^- ions

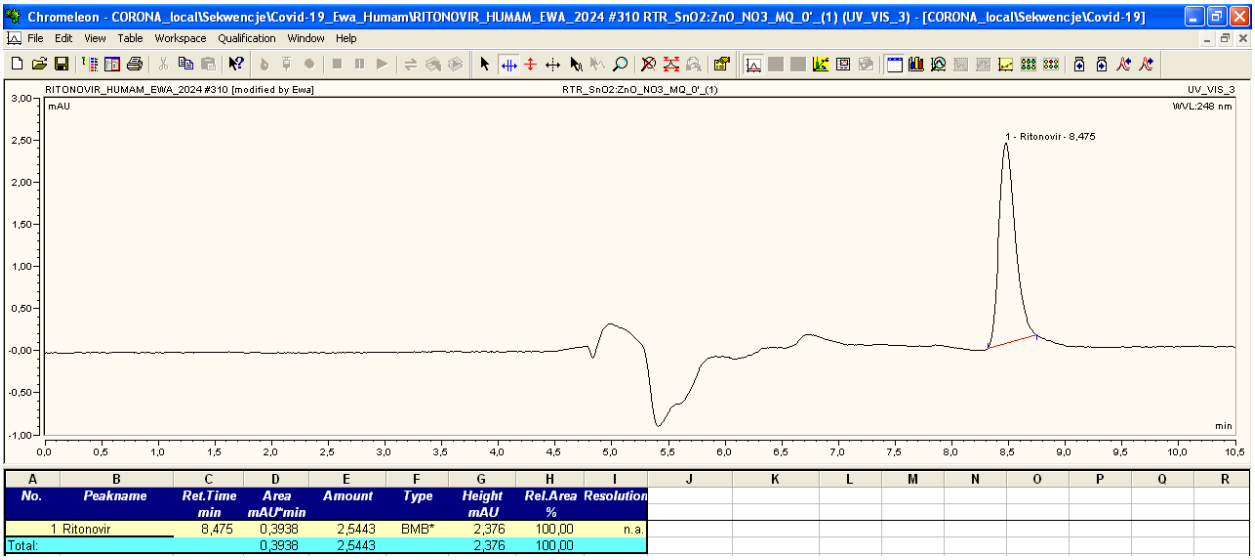

No.	Peakname	Ret.Time min	Area mAU*min	Amount	Type	Height mAU	Rel.Area %	Resolution
1	Ritonovir	8,475	0,3938	2,5443	BMB*	2,376	100,00	n.a.
Total:			0,3938	2,5443		2,376	100,00	

Figure S.13a. HPLC chromatogram of antiviral drug RTR before the addition of SnO_2:ZnO and NO_3^- ions

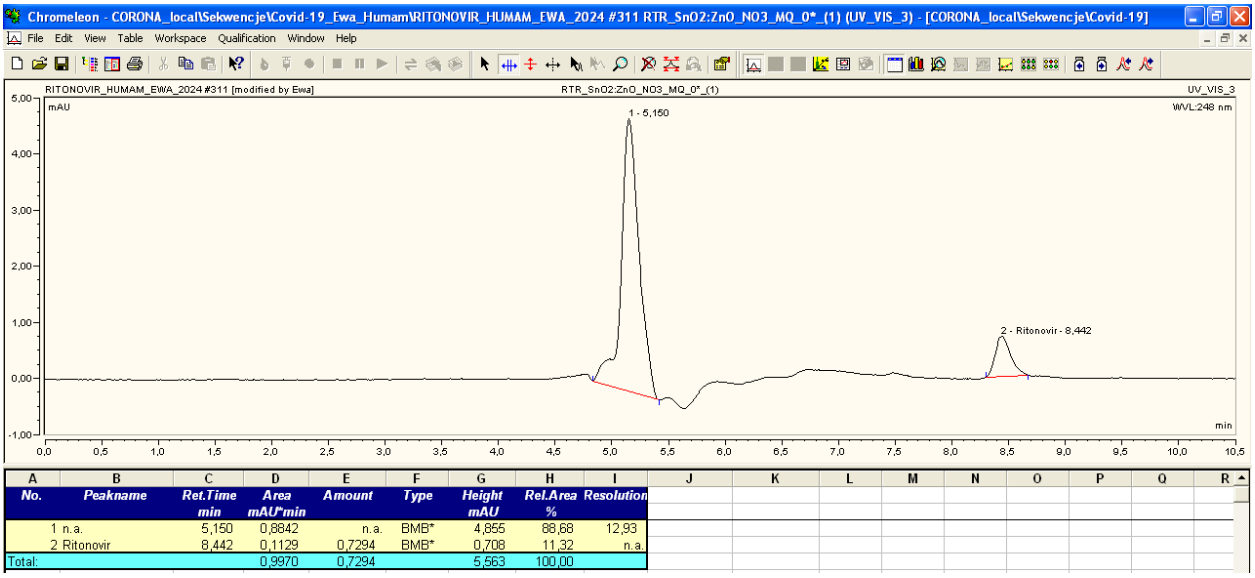

No.	Peakname	Ret.Time min	Area mAU*min	Amount	Type	Height mAU	Rel.Area %	Resolution
1	n.a.	5,150	0,8842	n.a.	BMB*	4,855	88,68	12,93
2	Ritonovir	8,442	0,1129	0,7294	BMB*	0,708	11,32	n.a.
Total:			0,9970	0,7294		5,563	100,00	

Figure S.13b. HPLC chromatogram of antiviral drug RTR after the addition of SnO_2:ZnO and NO_3^- ions

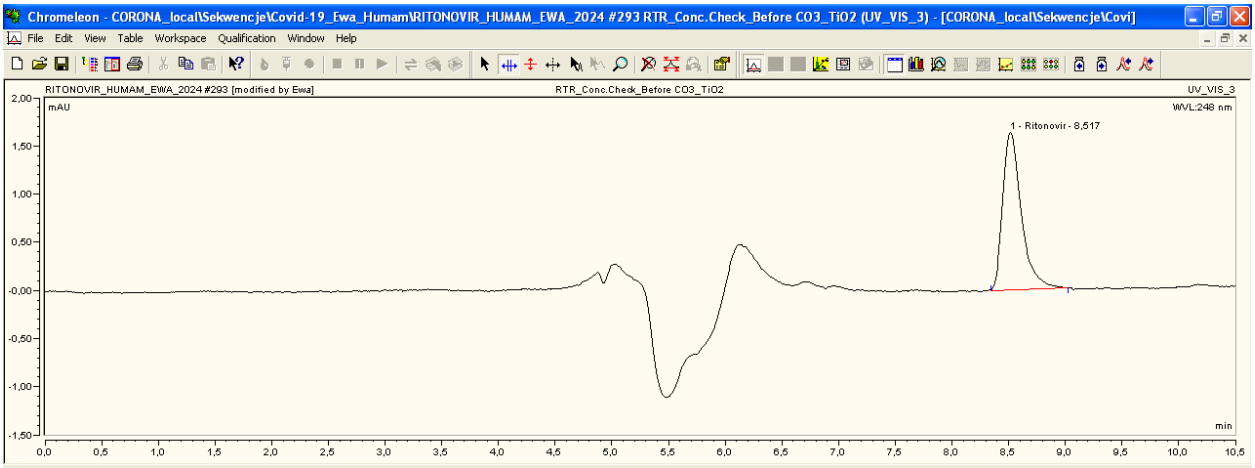

No.	Peakname	Ret.Time min	Area mAU*min	Amount	Type	Height mAU	Rel.Area %	Resolution
1	Ritonovir	8,517	0,3078	1,9885	BMB*	1,636	100,00	n.a.
Total:			0,3078	1,9885		1,636	100,00	

Figure S.14a. HPLC chromatogram of antiviral drug RTR before the addition of TiO_2 and CO_3^{-2} ions

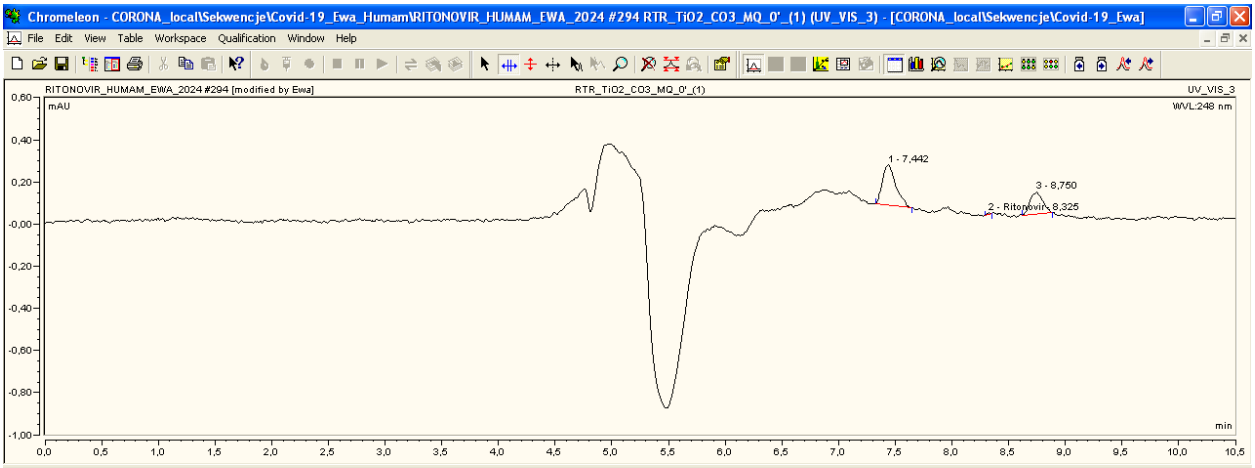

No.	Peakname	Ret.Time min	Area mAU*min	Amount	Type	Height mAU	Rel.Area %	Resolution
1	n.a.	7,442	0,0258	n.a.	BMB	0,191	65,83	7,13
2	Ritonovir	8,325	0,0002	0,0013	BMB	0,008	0,52	3,24
3	n.a.	8,750	0,0132	n.a.	BMB	0,104	33,65	n.a.
Total:			0,0391	0,0013		0,303	100,00	

Figure S.14B. HPLC chromatogram of antiviral drug RTR after the addition of TiO_2 and CO_3^{-2} ions

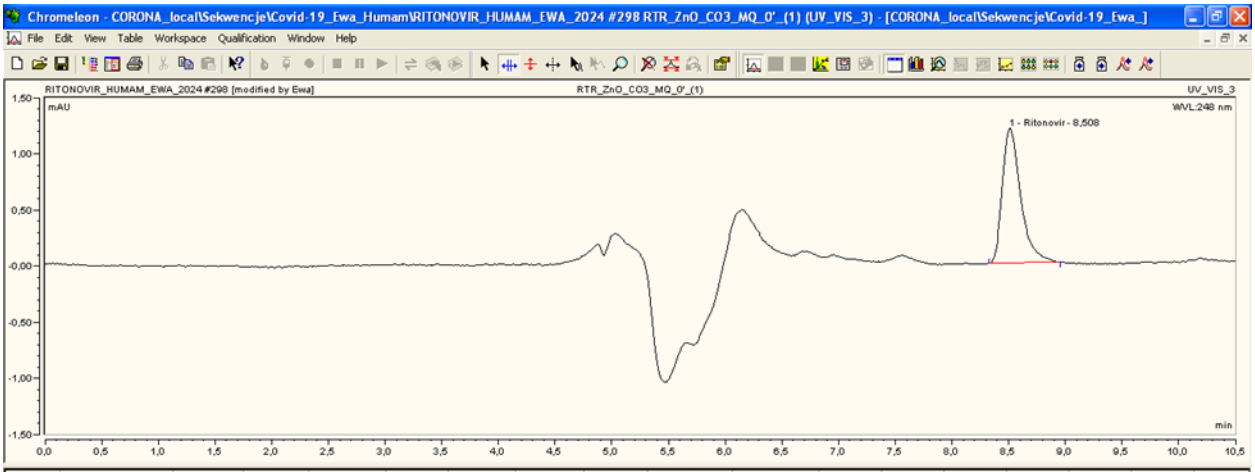

No.	Peakname	Ret.Time min	Area mAU*min	Amount	Type	Height mAU	Rel.Area %	Resolution
1	Ritonovir	8,508	0,2241	1,4483	BMB*	1,197	100,00	n.a.
Total:			0,2241	1,4483		1,197	100,00	

Figure S.15a. HPLC chromatogram of antiviral drug RTR before the addition of ZnO and CO_3^{-2} ions

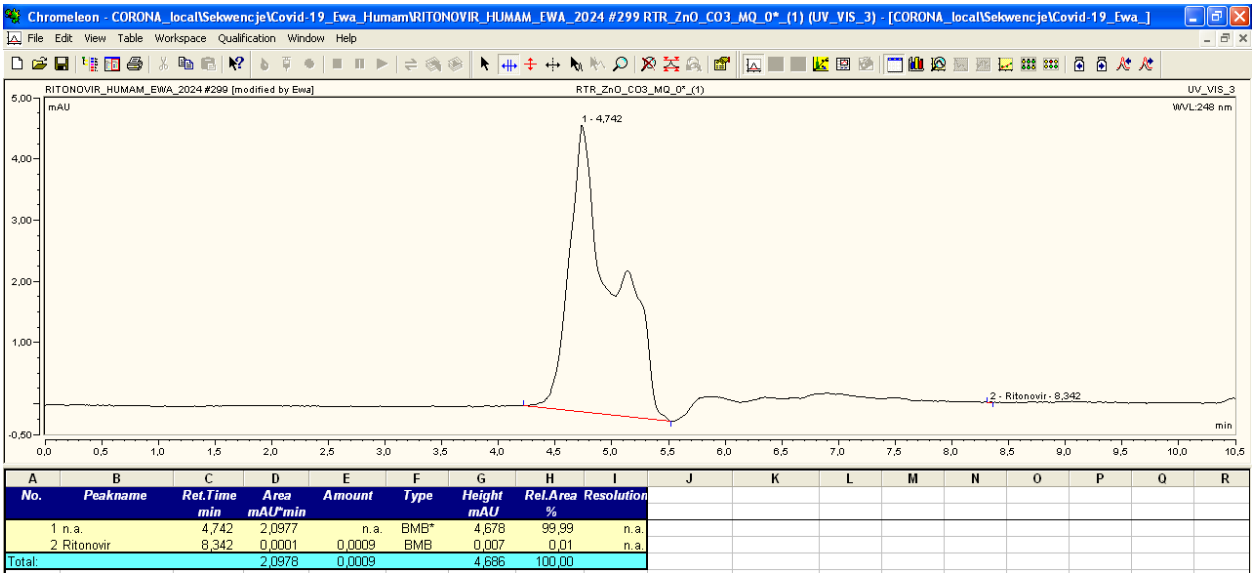

No.	Peakname	Ret.Time min	Area mAU*min	Amount	Type	Height mAU	Rel.Area %	Resolution
1	n.a.	4,742	2,0977	n.a.	BMB*	4,678	99,99	n.a.
2	Ritonovir	8,342	0,0001	0,0009	BMB	0,007	0,01	n.a.
Total:			2,0978	0,0009		4,686	100,00	

Figure S.15b. HPLC chromatogram of antiviral drug RTR after the addition of ZnO and CO_3^{-2} ions

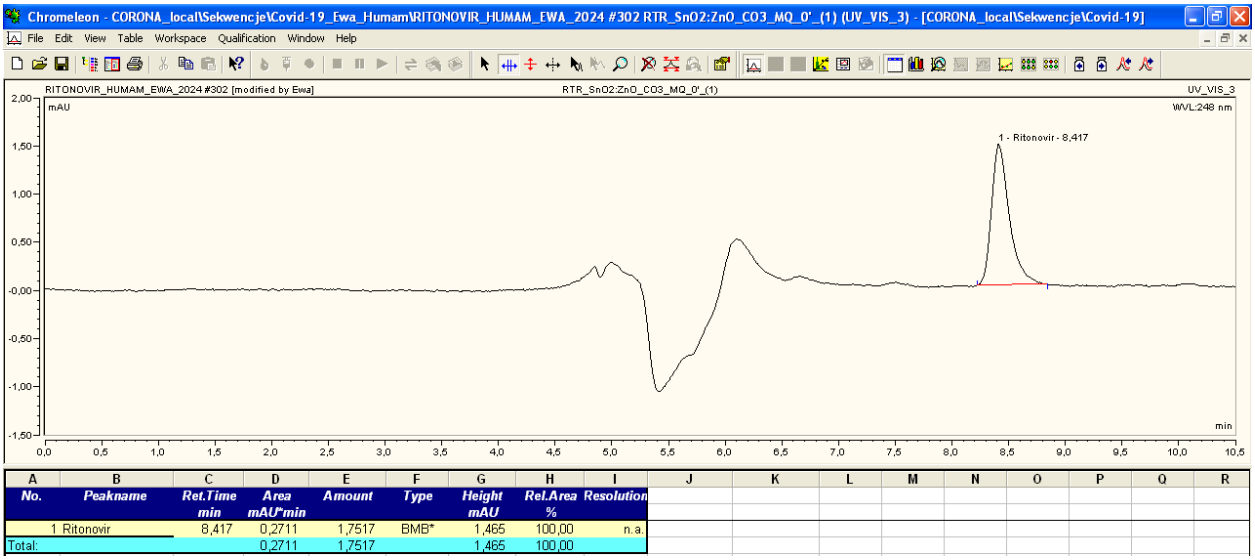

No.	Peakname	Ret.Time min	Area mAU*min	Amount	Type	Height mAU	Rel.Area %	Resolution
1	Ritonovir	8,417	0,2711	1,7517	BMB*	1,465	100,00	n.a.
Total:			0,2711	1,7517		1,465	100,00	

Figure S.16a. HPLC chromatogram of antiviral drug RTR before the addition of SnO_2:ZnO and CO_3^{-2} ions

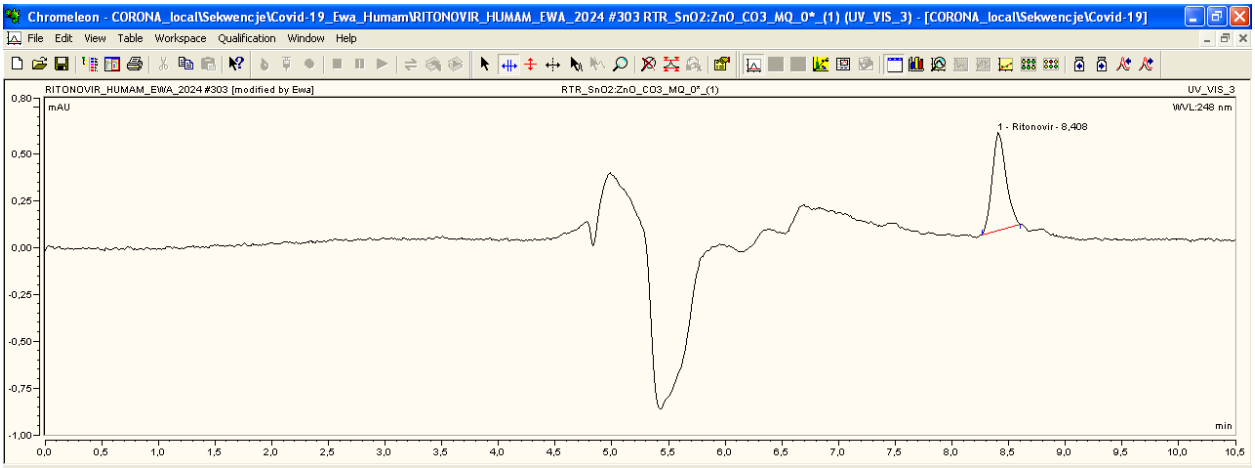

No.	Peakname	Ret.Time min	Area mAU*min	Amount	Type	Height mAU	Rel.Area %	Resolution
1	Ritonovir	8,408	0,0755	0,4879	BMB*	0,521	100,00	n.a.
Total:			0,0755	0,4879		0,521	100,00	

Figure S.16b. HPLC chromatogram of antiviral drug RTR before the addition of SnO_2:ZnO and CO_3^{-2} ions

List of Figures

Figure 1. Routes of drugs release into the aquatic environment 17

Figure 2. Types of AOPs 20

Figure 3. Mechanism of AOPs 21

Figure 4. Ostropka river, a.) winter season, b.) summer season 34

Figure 5a. Spectrum of anti- COVID drug IPN 35

Figure 5b. Spectrum of anti- COVID drug RTR 36

Figure 5c. Spectrum of anti- COVID drug REM 36

Figure. 6a. Calibration curve of isoprinosine 37

Figure. 6b. Calibration curve of ritonavir 38

Figure. 6c. Calibration curve of remdesivir 38

Figure 7. Solar box System 1500 photoreactor and xenon lamp emission spectrum at light irradiance 500 W/m^2 39

Figure. 8a. Ion profiling in MQW using ion chromatography 46

Figure. 8b. Ion profiling in TW using ion chromatography 48

Figure. 8c. Ion profiling in SW using ion chromatography 49

Figure. 9a. Photo-degradation of anti- COVID drug IPN in aquatic matrices 50

Figure. 9b. Photo-degradation of anti- COVID drug RTR in aquatic matrices 51

Figure. 9c. Photo-degradation of anti- COVID drug REM in aquatic matrices 53

Figure. 10a. Degradation of anti- COVID drug IPN in MQ-water by selected photocatalysts at dose 5.0 mg/L 55

Figure. 10b. Degradation of anti- COVID drug IPN in MQ-water by selected photocatalysts at dose 10.0 mg/L 55

Figure. 10c. Degradation of anti- COVID drug IPN in MQ-water by selected photocatalysts at dose 20.0 mg/L 57

Figure. 11a. Degradation of anti- COVID drug IPN in TW by selected photocatalysts at dose 10.0 mg/L. 58

Figure. 11b. Degradation of anti- COVID drug IPN in TW by selected photocatalysts at dose 20.0 mg/L. 58

Figure. 11c. Degradation of anti- COVID drug IPN in SW by selected photocatalysts at dose 20.0 mg/L. 59

Figure. 12. Adsorption of RTR on the surface of selected photocatalysts at dose 10.0 mg/L with solar light in MQ water 60

Figure. 13. Rapid adsorption of RTR on the surface of selected photocatalysts in a.)TW, and b). SW 61

Figure. 14. Comparison of experimental and modeled surface coverage (θ) of REM over time using a).TiO_2, b). ZnO in MQ water 64

Figure. 15. Comparison of experimental and modeled surface coverage (θ) of REM using a). TiO_2, b). ZnO in TW 66

Figure. 16. Comparison of experimental and modeled surface coverage (θ) of REM over time using a). TiO_2 P25, b). ZnO in SW 68

Figure. 17. Sorption test (dark experiments) of degradation of IPN in MQ water 70

Figure. 18. Sorption test (dark experiments) of degradation of RTR in MQ water 72

Figure. 19. Comparison of experimental and modeled surface coverage (θ) of REM over time under dark condition using a). TiO_2 P25, b). ZnO 73

Figure. 20. UV - assisted H_2O_2 degradation of a). IPN, b). RTR, and c). REM at different concentration of H_2O_2 in MQ water. 76-77

Figure. 21. Degradation of selected drugs using H_2O_2 (500 µL) under dark conditions in MQ water 78

Figure. 22. Degradation of IPN in the presence of SO_4^{-2} ions in (a) MQW (b) TW 79

Figure. 23. Degradation of IPN in the presence of Cl^- ions in (a) MQ water (b) TW 80-81

Figure. 24. Degradation of IPN in the presence of NO_3^- ions in (a) MQ water (b) TW 84

Figure. 25. Degradation of IPN in the presence of CO_3^- ions in (a) MQ water (b) TW 85-86

List of Tables

Table.1. Reported concentrations of drugs in the aquatic environment

Table.2. Physicochemical properties of Isoprinosine

Table.3. Physicochemical properties of Ritonavir

Table.4. Physicochemical properties of Remdesivir

Table.5. Physicochemical properties of selected water matrices

Table.6. Comparative anionic summary of all selected water matrices using ion chromatography

Table.7. Kinetic parameters−first-order pseudo constants of photolysis of selected drugs.

Table.8. Kinetic parameters−first-order pseudo constants of isoprinosine degradation in MQ-water

Table.9. Kinetic parameters−first-order pseudo constants of isoprinosine degradation in TW

Table.10. Kinetic parameters−first-order pseudo constants of isoprinosine degradation in SW

Table.11. Kinetic parameters−Langmuir Isotherm model for ritonavir adsorption under solar light

Table.12. Kinetic parameters−Two-phase adsorption desorption model for remdesivir under light Conditions

Table.13. Kinetic parameters−first-order pseudo constants of isoprinosine degradation in MQ-water

Table.14. Kinetic parameters−first-order pseudo constants of RTR adsorption (Langmuir Isotherm)

Table.15. Kinetic parameters−Two-phase adsorption desorption model for remdesivir under dark conditions

Table.16. Kinetic parameters−first-order pseudo drug degradation constants of selected drugs in MQ water at irradiance 500 W/m^2

Table. 17. Kinetic calculation of pseudo first order rate of degradation of IPN

Table. 18. Carbon and nitrogen parameter changes during solar photodegradation of anti-COVID-19 drugs in different water matrices

List of Publications

(Related to Thesis)

i. **Ahmed Humam**, Felis Ewa (2023): *Drugs used in COVID-19 therapy and their effects on the environment*. Desalination and Water Treatment (points of MEiN=100), Published. https://doi.org/10.5004/dwt.2023.29574

ii. **Ahmed Humam**, Felis Ewa (2024): *Solar light–driven degradation of isoprinosine – efficiency of the processes and kinetic calculations*. Journal of Ecological Engineering, (points of MEiN=70), Published. https://doi.org/10.12911/22998993/178190

iii. **Ahmed Humam**, Siddiqui Benish, Felis Ewa (2025): *Adsorption and photodegradation as processes enabling the removal of antiviral drug ritonavir from the aquatic environment.* Journal of Ecological Engineering, (points of MEiN=70), https://doi.org/10.12911/22998993/200281

iv. **Ahmed Humam**, Sunday J. Olusegun, Felis Ewa, et. al., (2025): *Solar-Light-Active Ag-TiO_2 Photocatalyst for the Degradation of Isoprinosine: Synthesis, Characterization, and Environmental Application.* (In Process).

v. **Ahmed Humam**, Felis Ewa (2025): *The influence of anions on the photodegradation of antiviral drug: Comparative analysis of photocatalysts efficiency and a kinetic study.* (Submitted to the Journal of Photochemistry & Photobiology, A: Chemistry)

List of Publications

(Unrelated to Thesis; Collaboration)

i. Uddin Jalal, **Ahmed Humam**, Asiri Yahya Ibrahim et al., (2023): *Ginger essential oil: Chemical composition, extraction, characterization, pharmacological activities, and applications.* In: Essential oils . Extraction, characterization and applications. Academic Press, Elsevier. Published. https://doi.org/10.1016/B978-0-323-91740-7.00014-1

ii. Uddin Jalal, Idrees Muhammad, **Ahmed Humam**, et al., (2024): *Biodegradation and decolourization of methylene blue, reactive Black-5, and toluidine blue-O from an aqueous solution using the polyphenol oxidase enzyme.* Frontiers in Sustainable Food Systems. Published. https://doi.org/10.3389/fsufs.2023.1320855

iii. Kowalska Katarzyna, Sowik Paulina, Bartolewski Wacław, **Ahmed Humam**, Felis Ewa, (2024): *Solar-driven photocatalytic removal of anti-microbial drugs–*

Comparison of the efficiency of selected photocatalysts. Desalination and Water Treatment. Published. https://doi.org/10.1016/j.dwt.2024.100275

Other Scientific Activities

Conferences Attended

i. **Ahmed, H.,** Felis, E. (2024): Can ZnO be viable alternative to TiO_2 for degrading antiviral drugs? **an oral** presentation at national conference, at X Scientific and Technical Conference NEW DIRECTIONS OF RESEARCH IN ENVIRONMENTAL ENGINEERING, ENERGY AND GEODSY Conference; Okuninka Lubelski, Poland held on 15-17 October 2024.

ii. **Ahmed, H.,** Felis, E. (2024): Effect of anions on the solar-light degradation of an antiviral drug used in COVID-19 therapy.; **an oral** presentation at national conference, Young Science Beyond Borders YSSB, on-line held on 24-25 October 2024.

iii. **Ahmed, H.,** Felis, E. (2024): Comparing the effectiveness of synthesized photocatalyst Ag-TiO2 with TiO2 in degradation of antiviral drug by advance oxidation process.; **a poster** presentation at national conference, at 5th International Conference Strategies toward Green Deal Implementation - Water, Raw Materials & Energy Conference; Kraków, Instytut Gospodarki Surowcami Mineralnymi i Energią Polskiej Akademii Nauk, Poland held on 27-29 November 2024.

iv. **Ahmed, H.,** Felis, E. (2023): Solar light driven degradation of isoprinosine; a poster presentation at national conference, at IX Scientific and Technical Conference NEW DIRECTIONS OF RESEARCH IN ENVIRONMENTAL ENGINEERING, ENERGY AND SURVEYING Conference; Janów Lubelski, Poland held on 06-08 September 2023.

v. **Ahmed, H.,** Felis, E. (2023): Degradation of Isoprinosine in two different water matrices by Solar-Light Driven process.; a poster presentation at national conference, at 4th International Conference Strategies toward Green Deal Implementation - Water, Raw Materials & Energy Conference; Kraków, Instytut Gospodarki Surowcami Mineralnymi i Energią Polskiej Akademii Nauk, Poland held on 14-15 December 2023.

vi. **Ahmed, H**., Felis, E. (2022): *CZY LEKI STOSOWANE W TERAPII COVID-19 STANOWIĄ PROBLEM ŚRODOWISKOWY? (Are the medicines used in COVID-19 therapy represents an environmental problem?*); an oral presentation in national conference, at XV Scientific Conference MICRO-POLLUTANTS IN THE HUMAN ENVIRONMENT; Czestochowa on 14-16 September 2022.

Conference Proceedings

i. **Ahmed H.,** Felis, E. (2024): Effect of anions on the solar-light degradation of an antiviral drug used in COVID-19 therapy.; published in conference proceedings Young Scientist Beyond Boarders. Abstract Book, 2024, pp. 09-09, ISBN 978-83-66847-97-2

ii. **Ahmed H.,** Felis, E. (2024): Comparing the effectiveness of synthesized photocatalyst Ag-TiO_2 with TiO_2 in degradation of antiviral drug by advance oxidation process.; published in conference proceedings 5th International Conference Strategies toward Green Deal Implementation - Water, Raw Materials & Energy. Abstract book / Smol Marzena (eds.), 2024, Kraków, Instytut Gospodarki Surowcami Mineralnymi i Energią Polskiej Akademii Nauk, pp. 237-237, ISBN 978-83-67606-49-3

iii. **Ahmed H.,** Felis, E. (2023): Degradation of Isoprinosine in two different water matrices by Solar-Light Driven process published in conference proceedings 4th International Conference

Strategies toward Green Deal Implementation - Water, Raw Materials & Energy. Abstract book / Smol Marzena (eds.), 2023, Kraków, Instytut Gospodarki Surowcami Mineralnymi i Energią Polskiej Akademii Nauk, pp.130-130, ISBN 978-83-67606-27-1

iv. **Ahmed, H**., Felis, E. (2022): *CZY LEKI STOSOWANE W TERAPII COVID-19 STANOWIĄ PROBLEM ŚRODOWISKOWY?* published in conference proceedings XV Scientific Conference MICRO-POLLUTANTS IN THE HUMAN ENVIRONMENT: Czestochowa on 14-16 September 2022.

Award:

i. Winner at 3-minutes thesis competition held on June 6th, 2025, at the Silesian University of Technology.

ii. Best presentation award in Environmental Sciences within Young Scientist Beyond the Boaders 2024 conference.

iii. 2024; Pro-quality award for highly-scored JCR publication in journal from TOP1 and TOP10 ranking lists (Silesian University of Technology, Poland)

Other significant achievements:

i. 2024: Selected for EURECA_PRO PhD Journey; a transformative event aimed at advancing the academic and professional growth of PhD students within the EURECA-PRO alliance. Centered around interdisciplinary research, sustainability, innovation, and the United Nations Sustainable Development Goal 12 (SDG12), it offered participants the opportunity to engage in in-depth research discussions, hands-on workshops, field excursions, and dynamic networking activities at partner universities.

ii. 2023: Mentored the Engineering Master's degree thesis. : Anna Sczasny, Direction of the study: Biotechnology.

iii. 2023: An active member of EURECA_PRO Doctoral Studies on Responsible Consumption and Production at TU Bergakademie Freiberg, Germany. I have been participating in various activities including lectures, workshops and knowledge exchange with young scientists.

iv. 2023: Attended a series of lectures and workshops (Intensive courses) in cooperation with the University of Wolverhampton, UK, during these sessions, I gained knowledge about topics such as sustainable soil management, the impact of COVID on smart cities and resilience, and knowledge management in the context of COVID.

Grants:

i. 2024: Participated in internal grant competition; BKM-Grant: BKM-717/RIE7/2024 (08/070/BKM24/0035).
Proposal Topic: *Degradation and kinetic calculation of Anti-viral drug Ritonavir in aquatic environment by solar light–driven process*.

ii. 2023: Participated in internal grant competition; BKM-Grant: BKM-664/RIE7/2023 (08/070/BKM23/0028).
Proposal Topic: *Solar light–driven degradation of isoprinosine –Efficiency of the processes and kinetic calculations.*

iii. 2022: Participated in internal grant competition; BKM-Grant: BKM-668/RIE7/2022 (08/070/BKM22/0018).
Proposal Topic: *Degradation of selected drug used in COVID-19 therapy in the aquatic environment by means of solar light driven processes*.